Mio-Pliocene erosional exhumation of the central Colorado Plateau, eastern Utah:
New insights from apatite (U-Th)/He thermochronometry

by

Markella Danielle Hoffman
B.S. Geology, California State University, Fullerton, 2006
B.S. Computer Science, California State University, Fullerton, 2006

Submitted to the Department of Geology and the
Faculty of the Graduate School of the University of Kansas
in partial fulfillment of the requirements
for the degree of Master of Science
2009

_____
Dr. Daniel F. Stockli, Chairman

_____
Dr. Diane L. Kamola

_____
Dr. Michael H. Taylor

Date Defended: July 31, 2009

The Thesis Committee for Markella Hoffman certifies
that this is the approved version of the following thesis:

Mio-Pliocene erosional exhumation of the central Colorado Plateau, eastern Utah:
New insights from apatite (U-Th)/He thermochronometry

Committee:

_____
Dr. Daniel F. Stockli, Chairman

Date Approved: August 27, 2009

ABSTRACT

Mio-Pliocene erosional exhumation of the central Colorado Plateau, eastern Utah: New insights from apatite (U-Th)/He thermochronometry

By

Markella Hoffman

Department of Geology, July 2009

University of Kansas

The landscape evolution of the Colorado Plateau has been studied for over a century, yet remains poorly understood. Several low-temperature thermochronometric studies have focused on the Grand Canyon region of the southwestern plateau to study incision and erosion of the Colorado River. This study focuses on erosion in the center of the Colorado Plateau and utilizes apatite (U-Th)/He thermochronometry to constrain the magnitude, timing, and rate of erosional exhumation in four regions of the central Colorado Plateau in eastern Utah: the Monument Uplift, Canyonlands, the Book Cliffs, and Uinta Basin. Here new thermochronometric data is presented from an integrated dataset of surface samples and core samples in order to comprehensively study erosional exhumation on the plateau. Thermochronometric data were combined with inverse thermal modeling to more quantitatively assess the timing and magnitude of erosion and test surface uplift models that make specific predictions regarding the spatial distribution of erosion in the center of the Colorado Plateau.

ACKNOWLEDGEMENTS

I would like to give special thanks to the staff at the USGS Denver Core Research Center and Canyonlands National Park for allowing the rock and core collection crucial to this project. Thank you to my invaluable research group who has helped me every step of the way with laboratory assistance, training, sample collection, writing revisions, in addition to endless support and friendship. Thank you to Melissa Wolfe and John Lee who helped lug heavy boxes of core around at the core library; Eugene Szymanski who accompanied me to Utah twice to assist with sample collection and his help with GIS; and Chris Hager for his tremendous Matlab thermal modeling program and modeling advice. Thanks to the collaborators on this project, Dr. Mousumi Roy (University of New Mexico), Dr. Joel Pederson (Utah State University), and especially to Dr. Shari Kelley (New Mexico Bureau of Geology and Mineral Resources) for providing numerous core apatite separates. Thank you to my committee members, Dr. Michael Taylor and Dr. Diane Kamola, for their insight and contribution to this work. I also thank Dr. Kamola for acquiring permission for me to conduct field work on private property in the Book Cliffs. Finally, thank you to my advisor, Dr. Danny Stockli, who has provided me with the opportunity to work in not only a fantastic laboratory, but in a spectacular field area. I am very grateful for his vast knowledge, guidance, and support. This work was made possible by NSF grant EAR-0408787 to Dr. Stockli. Additional funding was provided by ExxonMobil, GSA Grants-in-Aid, Sigma Xi, the KU Chapter of AWG, and the KU Department of Geology.

TABLE OF CONTENTS

	Page
TITLE AND SIGNATURE PAGE	ii
ABSTRACT	iii
ACKNOWLEDGMENTS	iv
TABLE OF CONTENTS	v
LIST OF TABLES	viii
LIST OF FIGURES	ix
CHAPTER SUMMARY	1
ABSTRACT	3
INTRODUCTION	4
GEOLOGIC AND TECTONIC SETTING OF THE COLORADO PLATEAU	6
General Background	6
Uplift of the Colorado Plateau	8
Uplift, exhumation, and erosion	9
Overburden estimations	10
Erosion and exhumation estimates	10
Geologic setting of study areas	12
Monument Uplift	12
Canyonlands	12
Book Cliffs and Roan Cliffs	13

Uinta Basin 14

APATITE (U-Th)/He THERMOCHRONOLOGY 15

General background 15

Apatite (U-Th)/He Analytical techniques 16

APATITE (U-Th)/He RESULTS 17

Monument Uplift 18

Canyonlands 19

Book Cliffs 21

Uinta Basin 24

APATITE (U-Th)/He SAMPLE AGE REPRODUCIBILITY 25

THERMAL MODELING OF THERMOCHRONOMETRIC DATA 27

Thermal modeling setup and constraints 29

Thermal structure of the Colorado Plateau 30

DISCUSSION OF STUDY REGIONS 31

Monument Uplift 31

Canyonlands 33

Book Cliffs 35

Uinta Basin 38

Erosional exhumation of the central Colorado Plateau 40

DRIVING FORCES FOR ACCELERATED MIO-PLIOCENE EROSIONAL EXHUMATION 42

Extensional tectonics in the Basin and Range and Gulf of California 42

Intensification of the southwest monsoon 43

Drainage integration of the Colorado Plateau 45

Interplay and feedback of driving forces: The "perfect" erosion 45

LANDSCAPE EVOLUTION 46

IMPLICATIONS FOR THE UPLIFT OF THE COLORADO PLATEAU 47

CONCLUSIONS 48

REFERENCES 52

APPENDICES 122

LIST OF TABLES

		Page
Table 1	Apatite (U-Th)/He data	63
Table 2	Core sample general information	76
Table 3	Surface sample general information	78

LIST OF FIGURES

		Page
Figure 1	Sample location map	80
Figure 2	Monument Uplift map and cross-section	82
Figure 3	Canyonlands map and cross-section	84
Figure 4	Book Cliffs map and cross-sections	86
Figure 5	Regional cross-section	88
Figure 6	Monument Uplift age-elevation plots, thermal history plots	90
Figure 7	Regional samples age-elevation, age-distance plots	93
Figure 8	Canyonlands age-elevation plots, thermal history plots	95
Figure 9	Hay Canyon age-elevation plots, thermal history plots	98
Figure 10	Sego Canyon age-elevation plots, thermal history plots	101
Figure 11	Blaze Canyon age-elevation plots, thermal history plots	104
Figure 12	Uinta Basin age-elevation plots, thermal history plots	107
Figure 13	Grain size vs. Apatite (U-Th)/He age plot	110
Figure 14	Effective Uranium concentration vs. (U-Th)/He age plots	112
Figure 15	Exhumation summary plot	114
Figure 16	Exhumation age probability density plot	116
Figure 17	Regional erosion estimations	118
Figure 18	Erosion summary map	120

CHAPTER SUMMARY

The research presented below, proposed by Dr. Daniel Stockli, is one portion of an interdisciplinary NSF funded research investigation of erosion and uplift of the Colorado Plateau. This portion of the project utilizes apatite (U-Th)/He thermochronometry to examine erosional exhumation in the central Colorado Plateau. Other portions of the investigation include apatite fission-track thermochronometry and sonic velocity studies by Dr. Shari Kelly (New Mexico Bureau of Geology and Mineral Resources), Graphical Information System (GIS) geomorphic reconstructions by Dr. Joel Pederson (Utah State University), and numerical modeling of surface uplift of the plateau by Dr. Mousumi Roy (University of New Mexico).

This chapter, entitled *Mio-Pliocene erosional exhumation of the central Colorado Plateau, eastern Utah: New insights from apatite (U-Th)/He thermochronometry,* is a manuscript intended for the submission to the journal *Geological Society of America Bulletin* with coauthors Dr. Daniel Stockli and Dr. Shari Kelley. The study utilizes a combination of surface samples and core samples to constrain the magnitude, timing, and rate of erosional exhumation on the central Colorado Plateau. The four study regions in eastern Utah include Monument Uplift, Canyonlands, Book Cliffs, and Uinta Basin. Some core samples were collected by Dr. Stockli, Dr. Kelley, and John Lee from both the USGS Denver Core Research Center and the Utah Core Research Center. Apatite mineral fractions of these core samples were provided by Dr. Kelley. In addition, core samples were collected at the USGS Denver Core Research Center in January, 2007 by Markella Hoffman, Melissa

Wolfe, and John Lee. Surface samples for this research were collected from the Canyonlands and Book Cliffs regions in May 2007 and May 2008 by Markella Hoffman, Eugene Szymanski, and Dr. Daniel Stockli. Mineral separation of these core and surface samples was performed by Markella Hoffman at the Isotope Geochemistry Laboratory at the University of Kansas. The integration of these core samples and surface samples has proved critical to the success of this research project. Apatite (U-Th)/He results are combined with the inverse thermal modeling program written by Christian Hager from the University of Kansas. The combination of thermochronometric data with thermal modeling has proven to be a powerful tool to more quantitatively constrain the magnitude and timing of erosional exhumation on the Colorado Plateau. The results from this study provide further constraints on the magnitude and spatial distribution of erosion and provide critical temporal constraints on the accelerated pulse of erosion in the late Miocene to early Pliocene. In addition, these results provide important implications for surface uplift models for the Colorado Plateau.

ABSTRACT

The landscape evolution of the Colorado Plateau has been studied by scientists for over a century, yet its late Cenozoic erosional and geomorphic history remains poorly understood. This study investigates the temporal and spatial distribution, magnitude, and rate of erosional exhumation that has carved the spectacular modern landscape of the central Colorado Plateau. New thermochronometric data are presented from a swath of four regions in eastern Utah, namely the Monument Uplift, Canyonlands, Book Cliffs, and Uinta Basin, to establish the thermal and erosional history and reconstruct the long-term landscape evolution of the central Colorado Plateau. This thermochronometric study utilizes an integrated sampling approach which combines surface samples and cores in order to increase the vertical sampling window to more comprehensively quantify erosional exhumation. All apatite (U-Th)/He (AHe) ages from surface and core samples are younger than stratigraphic ages, suggesting complete or partial thermal resetting after deposition and burial. Core samples (depths >1 km) have proven critical to this study and indicate significant Mio-Pliocene cooling and exhumation at 6 Ma. Shallower cores and surface samples have a broad spread of Eocene to late Miocene ages (5–55 Ma), and indicate residence in the helium partial retention zone (HePRZ). Furthermore, AHe ages suggest a south to north progression in erosion on the Colorado Plateau. In Monument Uplift, 1.5–2 km of erosion is calculated, 2–3 km in Canyonlands, 0.9–2.2 km in the Book Cliffs, and 0.2–1.2 km in Uinta Basin. Accelerated erosional exhumation of the central Colorado Plateau in the late Miocene to early Pliocene is attributed to a combination of geologic events, including drainage integration of the Colorado River off the southwest Colorado Plateau, the opening of the Gulf of California, and the intensification of a southwest monsoon climate.

INTRODUCTION

The Colorado Plateau physiographic province of the western United States encompasses the four corners region of Utah, Colorado, Arizona, and New Mexico (Figure 1). Situated between the Uinta and Rocky Mountains, the extensional Basin and Range Province, and Rio Grande Rift, this tectonically enigmatic crustal block has remained relatively undeformed since the late Cretaceous and stands at an anomalously high elevation of ~2 km. Numerous hypotheses exist to explain these high elevations and the uplift history of the Colorado Plateau (e.g., Bird, 1984; Humphreys, 1995; Spencer, 1996; McQuarrie and Chase, 2000; Pederson et al., 2002b; Humphreys et al., 2003; Roy et al., 2009), however the timing and causes of surface uplift continue to be a topic of debate.

The Colorado Plateau is drained by the Colorado River and its major tributaries, the Green River, San Juan River, and Little Colorado River, and these rivers are responsible for a variety of unique landforms and deeply incised canyons. The long-term landscape evolution of the Colorado Plateau, including drainage evolution of the Colorado River and its sediment discharge, has been the subject of much investigation. The highly-debated evolution of the lower Colorado River is thought to be the result of either headward erosion and stream capture (e.g., Lucchitta, 1989; Lucchitta et al., 2001) or propagating lake-spillover events (e.g., Meek and Douglass, 2001; House et al., 2005; Dorsey et al., 2007). Other studies have focused on the origin of early Colorado River deposits in the lower Colorado River trough (e.g., Hualapai Limestone and Bouse Formation) and their implications

for the surface uplift of the plateau (e.g., Spencer and Patchett, 1997; Faulds, 2001; Lucchitta et al., 2001, Poulson and John, 2003). While these studies have provided much insight to the history of the Colorado River, fundamental questions about the long-term geomorphic evolution of the Colorado Plateau remain including the timing, magnitude, and spatial distribution of erosion on the plateau. Several landscape evolution studies have concentrated on the southwestern region of the Colorado Plateau, particularly around the Mogollon Rim and Grand Canyon areas. Along the southern boundary of the plateau, Paleocene and Eocene Mogollon "rim gravels" have undergone extensive erosion in the late Oligocene (Cooley and Davidson, 1963; Elston and Young, 1991; Holm, 2001; Potochnik, 2001) with little reburial (Flowers et al., 2008). In the Grand Canyon region, thermochronometric studies show two main phases of erosion: Laramide unroofing and another cooling event in the late Cenozoic (e.g., Dumitru et al., 1994; Kelley et al., 2001; Naeser et al., 2001; Lee, 2007; Flowers et al., 2008). Far less is known, however, about the erosional history of the central plateau, an area with dramatic incision and significant overburden removal in the late Cenozoic (Pederson et al., 2002b; Stockli et al., 2002; Pederson et al., 2007).

This study uses apatite (U-Th)/He thermochronometry to investigate Neogene erosional exhumation in the center of the Colorado Plateau in eastern Utah (Figure 1). Apatite (U-Th)/He thermochronometry has been shown to be a powerful tool to reconstruct long-term thermal histories (e.g., House et al., 1997; Wolf et al., 1997; Farley, 2000; Stockli et al., 2000; Reiners et al., 2000; Farley and Stockli, 2002;

Ehlers and Farley, 2003) and its low-temperature sensitivity is ideally suited to constrain the magnitude, timing, and spatial patterns of erosion in this area. This study presents new thermochronometric data (93 samples, 517 aliquot ages) from a combination of cores and surface samples from the Monument Uplift, Canyonlands, Book Cliffs, and Uinta Basin regions that enable us to elucidate the thermal and erosional history of the central Colorado Plateau and to reconstruct the long-term landscape evolution of this region (<10 Ma). These data allow us to test recent geomorphic and geodynamic models for the uplift of the central Colorado Plateau in response to the flexural isostatic rebound from erosion in the late Cenozoic (e.g., Pederson et al., 2002b; Callahan et al., 2006) and determine the implications for these models to shed light on the highly debated uplift history of the Colorado Plateau.

GEOLOGIC AND TECTONIC EVOLUTION OF THE COLORADO PLATEAU

General background

The Colorado Plateau physiographic province is a 340,000 km^2 region in the western United States (Figure 1) and has remained relatively undeformed internally since the latest Cretaceous. The plateau is flanked by Basin and Range extension to the west and south, the Rio Grande Rift Valley to the southeast, the Rocky Mountains to the east, and the Uinta Mountains to the north. Its Paleozoic and Mesozoic history was a period of relative quiescence and stability, punctuated by the Ancestral Rocky Mountain, Sevier, and Laramide orogenic events (e.g., Hunt, 1956; Stokes, 1986;

Barnes, 1993; Hintze, 1993). Paleozoic strata on the Colorado Plateau are largely associated with the development of a long-lived passive continental margin and only briefly interrupted by the Pennsylvanian Ancestral Rocky Mountain orogeny, resulting in local uplifts (e.g. the Uncompahgre Uplift) and dramatic subsidence in the Paradox Basin (Stokes, 1986; Barnes, 1993; Condon, 1997; Huntoon et al., 2002). In the early Cretaceous, the Sevier orogeny caused subsidence and the formation of the broad Cretaceous Western Interior foreland basin (Beaumont, 1981; Jordan, 1981; Pang and Nummedal, 1995; DeCelles and Mitra, 1995; DeCelles and Coogan, 2006), resulting in the accumulation of nearly 1000 m of deep marine mudstone (Fisher et al., 1960; Stokes, 1986; Hettinger and Kirschbaum, 2003). The late Cretaceous to early Cenozoic Laramide orogeny, characterized by the transition between thin-skinned to thick-skinned deformation (Tikoff and Maxson, 2001), resulted in several basement-cored uplifts and the subsidence of intramontane basins (Dickinson et al., 1988; Bird, 1998). The Oligocene marked a period of magmatism, with laccolith emplacement in central Utah (e.g., Henry, La Sal, and Abajo Mountains) (Nelson et al., 1992; Nelson, 1997) and extensive volcanism along the periphery of the plateau associated with ignimbrite flare-up (e.g. Lipman and Glazner, 1991).

In contrast to the deposition and deformation in the early history of the Colorado Plateau, its Neogene history is dominated by dramatic erosion and incision, with few Neogene strata present on the plateau. Thermochronometric studies in the region have shown recent erosion in the Grand Canyon (e.g., Flowers et al., 2008; Lee, 2007) and also further north in the Waterpocket Fold area of Utah (Dumitru et

al., 1994). In addition, chronostratigraphic records of terrace formation indicate rapid incision along the trunk of the Colorado River in the Canyonlands region post 6 Ma (Pederson, 2006).

Uplift of the Colorado Plateau

A multitude of hypotheses for surface uplift and interplay with erosional exhumation of the Colorado Plateau exist, each having distinct temporal and spatial characteristics. Recent hypotheses and mechanisms for uplift include (1) late Cretaceous to early Cenozoic mid-crustal flow (McQuarrie and Chase, 2000); (2) middle Cenozoic flat-slab subduction (Spencer, 1996); (3) Laramide crustal thickening followed by late Cenozoic erosional isostatic rebound (Pederson et al., 2002b; Callahan et al., 2006); and (4) middle to late Cenozoic epeirogeny associated with anomalous mantle conditions (Bird, 1984; Humphreys, 1995; Humphreys et al., 2003; Roy et al., 2009).

Laramide deformation has been attributed to the uplift of the Colorado Plateau from the late Cretaceous to the middle Cenozoic. McQuarrie and Chase (2000) suggest late Cretaceous to early Cenozoic mid-crustal flow, from west to east, has resulted in preferential thickening of the lower crust. In contrast, Spencer (1996) argues for post-Laramide uplift when a thinned lithosphere is heated from the underlying asthenosphere in the mid Cenozoic.

Other uplift mechanisms involve a combination of Laramide deformation with late Cenozoic flexural isostatic uplift in response to erosional unroofing (Pederson et al., 2002b). Callahan et al. (2006) test this hypothesis with a 3-D flexural rock uplift

model and predict concentric patterns of increasing rock uplift in response to this erosional unloading, with less than one km of recent epeirogenic uplift in the central Colorado Plateau and tapering to zero at its margins. Thus, maximum erosion is predicted to occur in the center of the plateau: a prediction tentatively supported by erosion estimates from geomorphic surface reconstructions (e.g., Pederson et al., 2002b; Pederson, 2006). In addition, this erosion-driven flexural rebound in the center of the plateau could also account for higher Pleistocene river incision rates seen in the same area (Pederson, 2006; Pederson et al., 2007). Callahan et al. (2006), using 3-D flexural models, concluded that erosional rebound cannot explain the total observed rock uplift and an additional form of uplift is required. Post-Laramide mechanisms for uplift include middle to late Cenozoic epeirogeny, usually associated with anomalous mantle composition or temperature (e.g., Bird, 1988; Humphreys, 1995; Humphreys et al., 2003). Roy et al. (2009) propose that 1.6–2.0 km uplift of the Colorado Plateau is triggered by thermal perturbation and reequilibriation of the mantle underneath the Colorado Plateau, in addition to a small component of erosional rebound.

Uplift, exhumation, and erosion

The relationship between surface uplift and exhumation is summarized by England and Molnar (1990), where surface uplift = rock uplift – exhumation, with surface uplift being the change in surface elevation with respect to sea level, rock uplift is the displacement of rocks relative to sea level, and exhumation as the displacement of rocks with respect to the surface. Thermochronometric studies

measure exhumation, and based on the relationship defined by England and Molnar (1990), this study tests the timing and spatial patterns of surface uplift predicted by Roy et al. (2009). Cooling in the southwest region of the plateau primarily occurred in the early Cenozoic (Flowers et al., 2008; Lee, 2007), and is possibly associated with uplift and erosion of the plateau. In the central plateau, however, erosion and incision are more recent (<10 Ma) (Stockli et al., 2002; Pederson et al., 2002b), which suggests cooling in the central Colorado Plateau could be related to the inward encroachment of thermally-driven rock uplift (20–40 Ma; Roy et al., 2009).

Overburden estimations

Nuccio and Condon (1996) evaluated the petroleum potential of the Paradox Basin in eastern Utah and determined maximum overburden for their thermal and burial models. The magnitude of erosion for several locations in the Paradox Basin region since 25 Ma was estimated at 2 km near Monument Uplift and the confluence of the Green and Colorado Rivers. Approximately 2.4 km of overburden removal is estimated near the Green River east of Canyonlands, however in the structurally deepest parts of the Paradox Basin, near Moab, Utah, removal of overburden is estimated at 3.5–4 km.

Erosion and exhumation estimates

Geomorphic landscape reconstructions of the Eocene-Oligocene stratigraphic boundary on the Colorado Plateau by Pederson et al. (2002b) indicate "post-Laramide" erosion is spatially variable, with a mean erosion estimate of approximately 800 m across the plateau. The greatest exhumation of 1.5–4 km is

centered over the Canyonlands and Glen Canyons region, along the trunk of the Colorado River system, and diminishes drastically towards the plateau edge (Pederson, 2006). These estimations, although not spatially coincident, are similar to overburden estimations by Nuccio and Condon (1996).

Previous low-temperature thermochronometric studies on the Colorado Plateau have focused on the Grand Canyon region to quantify the timing and rate of incision along the Colorado River and exhumation of the plateau. Apatite fission-track (AFT) ages from the Grand Canyon area predominately record Laramide exhumation and minor cooling related to Cenozoic river incision since <6 Ma (e.g., Dumitru et al., 1994; Kelley et al., 2001; Naeser et al., 2001) but shed little light on the erosional history of the central Colorado Plateau. However, apatite (U-Th)/He (AHe) results from the Grand Canyon by Flowers et al. (2007, 2008) and Lee (2007) indicate an overall southwest to northeast progression of erosion and overburden removal, with at least 1.5 km of erosion since the late Cretaceous. Post-Laramide 30–18 Ma, a second phase of unroofing continued in the Kaibab Uplift region, whereas toward the interior of the Colorado Plateau, another pulse of erosion was found in the late Cenozoic 5–18 Ma (Stockli et al., 2002; Flowers et al., 2007, 2008; Lee, 2007). In the Waterpocket Fold region of southern Utah, late Cretaceous AFT ages indicate Laramide cooling (Dumitru et al., 1994). Shorter fission-track lengths, however, suggest 2–3 km of burial in the early to mid Cenozoic, followed by late Cenozoic exhumation.

This thermochronometric study focuses on a north-south swath of four areas in eastern Utah: the Monument Uplift, Canyonlands, Book Cliffs and Roan Cliffs, and the Uinta Basin (Figure 1). The following sections briefly summarize the geology of these regions from south to north.

Geologic setting of study areas

Monument Uplift

The basement-cored Laramide-age north-trending Monument Uplift extends approximately 210 km from northeastern Arizona to southern Utah (Figure 1). The core of the Monument Uplift exposes Pennsylvanian and Permian strata (Figure 2), while across the Comb Ridge Monocline, the Triassic Moenkopi and Chinle Fms. and the Jurassic Glen Canyon Group form steeply-dipping hogbacks (Stokes, 1986; Huntoon et al., 2002; Bump and Davis, 2003). The Monument Uplift has also been bisected by the San Juan River, forming goosenecks and exposing the Pennsylvanian Hermosa Formation at the base of its canyons.

Canyonlands

Canyonlands National Park is located north of Monument Uplift in eastern Utah (Figure 1) and its geology is dominated by gently north-dipping late Paleozoic and Mesozoic strata (Figure 3). Minor structural deformation of the region is associated with salt movement and dissolution in the underlying Pennsylvanian Paradox Formation (Foxford et al., 1998; Walsh and Schultz-Ela, 2003). At the base of the Green and Colorado River canyons are the Pennsylvanian Honaker Trail limestone and Permian Cutler limestone and sandstone (Huntoon et al., 2002). The

Permian White Rim Sandstone forms a prominent bench throughout the northern region of Canyonlands. The Triassic and Jurassic strata (i.e., Moenkopi and Chinle Formations, Wingate Sandstone, Kayenta Formation, Navajo and Entrada Sandstones) comprise the majority of the steep red walls seen in Canyonlands (Stokes, 1986; Barnes, 1993). Canyonlands National Park is divided into three districts by the Green and Colorado Rivers, each with distinct erosional characteristics (Figure 3). This study focuses on the Island in the Sky District, flanked by the Green and Colorado Rivers and dominated by deep and dramatic incision. North of Canyonlands, the Jurassic Morisson Formation and Cretaceous Mancos Shale form mudstone lowlands.

Book Cliffs and Roan Cliffs

The Book and Roan Cliffs are stacked east-west trending escarpments located north of Canyonlands (Figure 1). These south-facing cliffs have no major structural deformation and consist of gently northeast-dipping Cretaceous and early Cenozoic strata (Figure 4). The Book Cliffs, the southern and most pronounced escarpment, are comprised of shallow marine sandstones of the late Cretaceous Mesaverde Group (e.g., Blackhawk Formation, Castlegate Sandstone, Sego Sandstone, Neslen, Farrer, and Tuscher Formations) deposited in the eastward prograding Cretaceous Western Interior foreland basin (Fouch et al., 1983). To the north, the Roan Cliffs are primarily comprised of the fluvial Paleocene Wasatch Formation and the Eocene Green River Formation (Stokes, 1986). With nearly one kilometer of total vertical relief, the combined Book and Roan Cliffs escarpment separates the low-relief

badlands of the Mancos Shale from the Uinta Basin to the north. The cliffs are dissected by numerous canyons, including the Green River's Desolation Canyon. For simplicity, the Book Cliffs and Roan Cliffs are referred to as only the Book Cliffs region in subsequent sections.

Uinta Basin

North of the Book Cliffs and Roan Plateau lies the Uinta Basin, the northernmost extent of the study region (Figure 1). The Uinta Basin is a Laramide-age intramontane basin, formed from flexural effects of the tectonic load in the Uinta Mountains to the north (Dickinson et al., 1988). Episodic subsidence and sedimentation has resulted in alternating fluvial and lacustrine sediments up to 5 km thick during the latest Cretaceous to Oligocene times (Hunt, 1956). The Green River, Uinta, and Duchesne Fms. are the dominant Cenozoic strata in the basin (Hintze, 1988). This region's topography is relatively flat in the center with sloping edges, similar to its synclinal structure. Although several rivers flow across the basin from the mountains to the north (e.g., Green, Duchesne, and White Rivers), there is little incision or relief (Stokes, 1986).

A combination of core and surface samples have been collected from these four regions of the central Colorado Plateau for apatite (U-Th)/He thermochronometric analyses. A background of thermochronology and analytical methods are discussed below.

APATITE (U-Th)/He THERMOCHRONOLOGY

General background

Apatite (U-Th)/He (AHe) thermochronometry is a powerful tool to constrain rates and timing of exhumation in various tectonic and geomorphic settings (e.g., House et al., 1997; Wolf et al., 1997; Farley, 2000; Stockli et al., 2000; Reiners et al., 2000; Farley and Stockli, 2002; Ehlers and Farley, 2003). Helium produced by U, Th, and Sm α-decay is almost completely retained at temperatures less than ~40^{o}C and nearly totally expelled out of the crystal structure at temperatures above ~80^{o}C, where (U-Th)/He ages are reset. Assuming typical geothermal gradients (25^{o}C/km) and a mean surface temperature of 10^{o}C, this corresponds to a depth interval between ~1–3 km; a region termed the Helium Partial Retention Zone (HePRZ) (Wolf et al., 1996, 1998; Stockli et al., 2000). AHe ages, therefore, are able to record the temperature evolution of rocks in the upper 3 km of the crust and can be used to estimate the timing and magnitude of erosional exhumation. Furthermore, the shape of the HePRZ recovered from vertical sample arrays is a function of the thermal history and, therefore, can be used to recover a detailed thermal history through numerical modeling (e.g., Wolfe et al., 1998; Stockli et al., 2000; Ketcham, 2005).

He diffusion kinetic studies indicate radiation damage enhances He retentivity (Shuster et al., 2006). The amount of radiation damage in an apatite grain is partially controlled by the total concentration of α-producing parents, or effective U concentration ([eU]) where [eU] = [U] + .2302[Th] + 0.005[Sm]. AHe ages having a wide range of [eU] are known to exhibit significant scatter (e.g., Shuster et al., 2006;

Flowers et al., 2007; Biswas et al., 2007; Flowers et al., 2008). Shuster et al. (2006) have proposed a helium trapping model (HeTM) which incorporates diffusion kinetics as a function of time and He concentration (a proxy for radiation damage). However radiation damage only completely anneals at higher temperatures (Shuster and Farley, 2009) while He is expelled at temperatures well below 100^{o}C, therefore for geologic settings where samples undergo burial and reheating to temperatures below 150^{o}C (e.g., Biswas et al., 2007; Flowers et al., 2008), the HeTM may not be the most accurate. An updated HeTM by Flowers et al. (2009), called the radiation damage accumulation and annealing model (RDAAM), use the effective fission-track density as a better proxy for accumulated radiation damage. Since Colorado Plateau detrital apatite exhibit a range of [eU] and therefore different diffusion kinetics, it is expected that radiation damage is very important and applicable to this study and this new RDAAM is incorporated into the thermal modeling of AHe ages from this study.

Apatite (U-Th)/He Analytical Techniques

All thermochronometric analyses and mineral separation were performed in the Isotope Geochemistry Laboratory at the University of Kansas. Apatite was separated using standard heavy mineral separation techniques, including a Jawcrusher, Pyramid water table, heavy liquids, and Frantz Magnetic Separator (Appendix A). If possible, euhedral apatite grains greater than 70 μm in diameter where chosen, in order to decrease the uncertainty associated with the F_T correction (Farley, 2002; Farley et al., 1996). However due to mechanical abrasion and

hydrodynamic sorting of detrital apatite, occasionally selected grains were slightly rounded or less than 70 μm.

For each sample, six single grains (aliquots) were selected, photographed, measured, and individually loaded into platinum foil packets. The ^{4}He concentration of apatite is measured in an ultra-high vacuum line by heating grains for five minutes at ~1080^{o}C using the Nd-YAG laser method as described by House et al. (2000). The presence of inclusions may be detected by a second lasing, or reextract. Aliquots are spiked with a HNO_3-based solution containing a ^{235}U- ^{230}Th-^{149}Sm tracer, and heated to ensure complete dissolution. U, Th, and Sm contents are measured by isotope dilution on an inductively coupled plasma mass spectrometer (ICP-MS). Reported analytical uncertainties in AHe ages are ~6% (2σ) based on the reproducibility of laboratory standards.

APATITE (U-Th)/He RESULTS

As mentioned previously, apatite (U-Th)/He ages are sensitive to temperature changes and therefore depth changes in the upper 3 km of the crust. To better understand the cooling of the upper crust in response to erosion, samples should be collected with the largest possible vertical elevation spread. Previous AHe studies on surface samples from Laramide monoclines in Utah show ages with broad age spreads and strong elevation correlation suggestive of protracted residence in the apatite HePRZ (Stockli et al., 2002; Stockli, 2005). Those data loosely constrain the

timing of erosional exhumation on the central Colorado Plateau to <10 Ma. Limited relief in the region only allows access to a small vertical exposure window (~1.5 km) for the collection of surface samples. To more comprehensively quantify the thermal and erosional exhumation history of the region, this study systematically integrates 50 surface samples in addition to 43 core samples (517 aliquots total, Table 1). Erroneous ages, those outside typical 6% analytical error (2σ), may be associated with numerous factors. In this study, outliers having high He reextracts, indicating the possible presence of high U- or Th- bearing inclusions, or those with very small U or He concentrations (<1ppm), anomalous Th/U ratios, or unusual rare earth element (REE) concentrations were excluded from the results discussed below (see Table 1 for all (U-Th)/He data).

Monument Uplift

Surface samples for the Monument Uplift region were analyzed by Stockli et al. (2002). These samples (MU-) were collected from the eastern flank of the Monument Uplift and span 400 m vertical elevation (Figure 2). Stockli et al. (2002) reported AHe results from these surface samples that range from 13–45 Ma (Figure 6A). These data generally correlate with elevation and the wide spread of ages has been attributed to a protracted residence in an exhumed HePRZ.

Six core samples were collected from the Monument Uplift region from wells DC-411811-1/Dolores, DC-411828-1/Dolores, and DC-411824-2/Dolores (DC-11-, DC-28-, DC-24-) from depths of 60–600 m (Table 2). The core samples collected were fine-grained sandstone from the Permian Cutler Formation (Figure 2). Since

these wells were close together, the samples were combined into one composite "core". This composite core yielded AHe ages between 3.2 ± 0.1 and 12.6 ± 0.8 Ma (n= 28) (Figure 6A). The ages vary little with elevation, however the shallowest core sample (DC-212) has the oldest ages 6.4 ± 0.4 – 12.6 ± 0.8 Ma and is similar to surface sample ages with a minimum age of 13 Ma (Stockli et al., 2002). The [eU] of these samples range from 5–80 ppm.

Canyonlands

In the southern Canyonlands region, two samples were taken north of the confluence of the Green and Colorado Rivers for regional thermochronometric studies. At the southernmost extent of the Island in the Sky, the Kayenta Formation was sampled (08CP66), and a sample from the Triassic Moenkopi Formation was collected on the White Rim Road north of the confluence (08CP72) (Figure 5 and Table 3). The two samples yielded ages between 10.5 ± 0.8 and 25.0 ± 1.8 Ma (n=11). These results, combined with other regional samples discussed later, are shown in Figure 7A.

North of this region, one vertical transect was collected along the Shafter Trail from the top of the Island in the Sky District to the White Rim Sandstone bench (07CP53–07CP62). An extension of this vertical transect was collected in Lathrop Canyon (08CP69–08CP71), slightly south of Shafer Trail, from the White Rim Sandstone to the Colorado River level. These 13 samples had a combined vertical relief of about 700 m and were collected from the Cutler Formation, the White Rim Sandstone, Moenkopi and Chinle Formations and the Wingate, Kayenta, and Navajo

Sandstones (Figure 3). In the Shafer Trail portion of the transect, 10 samples yielded a broad spread of Neogene to late Paleogene ages between 5.4 ± 0.5 and 37.8 ± 2.3 (n=47), shown in Figure 8A. In Lathrop Canyon, sample ages were remarkably similar, between 4.5 ± 0.4 and 41.5 ± 3.3 Ma (n=14). Overall, ages from the Canyonlands vertical transect increase with increasing elevation. The [eU] varies from 4–148 ppm.

The Canyonlands region is protected by the National Park Service and no wells are located within the park, however two boreholes were sampled immediately north of Canyonlands National Park, near the Moab Fault and salt anticline region of Moab, Utah. Wells 24-20-26-2 (LLE-) and 24-20-35-2 Seven Mile (SM-) were fairly deep at approximately 800-950 m (Table 2, Figure 5), however the lithology of most of the core was mainly non-apatite bearing evaporates and carbonates of the Paradox Formation, and the core yielded only three samples. These samples are treated as a single composite well due to the proximity of the two wells and combined with the Canyonlands vertical transect. The three core samples analyzed from the Canyonlands region (LLE-2656, LLE-2797, SM-3032) generated mid to late Miocene AHe ages ranging from 4.4 ± 0.3 to 11.0 ± 0.2 Ma (n=11) (Figure 8A). AHe ages from these core samples show no correlation with elevation and have [eU] varying between 5–94 ppm.

An additional four surface samples were gathered for regional thermochronometric studies in the lowlands region between the Canyonlands and the Book Cliffs (07CP40, 07CP42, 07CP48, 07CP51) (Figure 5). Samples were obtained

from the Jurassic Cedar Mountain Formation, Salt Wash Member of the Morrison Formation, and the Navajo Sandstone, yielding AHe ages between 4.5 ± 0.3 and 32.0 ± 1.9 Ma (n=19) (Figure 7A). The [eU] has a slightly smaller range from 4–47 ppm. Despite intense hydrocarbon exploration, attempts to locate core from this region proved unsuccessful.

Book Cliffs

In the Book Cliffs region, a total of 34 samples were gathered along three transects: (1) a transect across the Book Cliffs and Roan Cliffs in Hay Canyon near the Utah-Colorado border, (2) a transect of the central Book Cliffs in Sego Canyon, and (3) a vertical transect in the Blaze Canyon area of the central Book Cliffs. At Hay Canyon (Figure 4), 12 samples (07CP02–07CP14) were collected from the top of the Roan Cliffs to the base of the Book Cliffs escarpment, with about 900 m of vertical elevation spread over 21 km horizontal distance. Stratigraphy sampled is shown in Figure 4 and in Table 3. The surface samples from this transect have a wide range of Eocene to early Pliocene ages. AHe ages of samples 07CP02–07CP14 ranged from 5.5 ± 0.6 – 29.1 ± 4.3 Ma (n=63) (Figure 9A). This transect shows a correlation between age and elevation and a wide span of [eU] between 5–175 ppm.

A majority of the cores collected are from the Book Cliffs, especially the eastern Book Cliffs near Hay Canyon, an intensely explored region with many old oil exploration wells. Cores from wells GC-1 (GC-1), 2 Book Cliffs (2BC-), 3 Book Cliffs (3BC-), 4 Book Cliffs (4BC-) (Table 2) were sampled from 20–300 m depths, and due to their proximity to each other and to Hay Canyon, can be combined into a

composite core with the Hay Canyon traverse of surface samples (Figure 4). Seven samples from the Mesaverde Group and the Wasatch Formation were collected from 2BC and GC-1, which had 200–300 m of core available. Wells 3BC and 4BC had less than 100 m of core to sample, so only 1–3 very fine-grained Mesaverde sandstone samples were collected from each core. Only one sample (~1200 m depth) was collected from well 1-A Federal 258 (1AFED258) in the Hay Canyon region due to an abundance of Paradox halite and carbonate. Twenty shallow core samples (<300 m depth) generated a broad span of AHe ages 1.2 ± 0.1 – 55.8 ± 5.2 Ma (n=101) (Figure 9A) which also correlated with [eU] of 4–300 ppm. The deeper 1AFED258 sample yielded ages 4.7 ± 0.3 and 5.0 ± 0.3 (n=2).

In Sego Canyon, 13 surface samples were taken from the central Book Cliffs (07CP15-07CP25, 07CP35 (Figure 4). This transect also spanned about 900 m of vertical elevation over 25 km horizontal distance. Samples were from the same stratigraphic units as Hay Canyon. In Sego Canyon, surface samples 07CP15–07CP25 and 07CP35 spanned from 8.1 ± 0.5 – 51.8 ± 3.1 Ma (n=59) (Figure 10A). Also showing a correlation between age and elevation, [eU] in Sego Canyon has a similar range from 5–140 ppm.

Fewer wells are located near Sego Canyon, 5 Book Cliffs (5BC-) and 3 Federal 335 (3FED335), and samples from both were combined with the Sego Canyon transect (Figure 4). Two samples from the Mesaverde Group were collected from 5BC at depths of approximately 300 and 500 m yielding ages ranging from 5.5 ± 0.3 –14.0 ± 0.4 (n=10). Deeper core samples (900 m) from 3FED335 gave AHe

ages ranging from 4.9 ± 0.3 – 6.0 ± 0.4 (n=2) (Figure 10A), similar to 1AFED258 in Hay Canyon.

In the region between Blaze Canyon and Crescent Canyon (deemed the Blaze Canyon region), seven surface samples were collected up the front of the Book Cliffs escarpment (07CP26–07CP32), totaling 400 m of relief. Detailed sample stratigraphy and locations can be found in Table 3. These samples yielded AHe ages ranging from 2.1 ± 0.1 – 35.7 ± 2.1 Ma (n=29) (Figure 11A) and show a clear positive correlation between age and elevation and a span of [eU] between 7–195 ppm. One sample collected from a nearby well, Blaze C 1 (PH) from a depth of about 1400 m, was combined with the Blaze Canyon vertical transect. AHe ages from this core were similar to other deep cores in the Book Cliffs region and ranged from 2.4 ± 0.3 – 7.4 ± 0.2 Ma (n=4).

A few samples were collected from cores to the west of the Green River in the Book Cliffs at depths between 500–800 m. The Green River Formation was sampled from the Peters Point 1 core (Ppt) and the Ferron Sandstone was sampled from core State of Utah RGU-1 (RGU). These deeper cores yielded AHe ages between 3.2 ± 0.1 – 11.1 ± 0.3 Ma (n=10).

In Tusher Canyon, just east of the Green River, the last two samples were collected for regional thermochronometric studies (07CP63 and 07CP65). These samples were collected from the Blackhawk Formation and the Castlegate Sandstone. AHe ages of these samples are between 3.7 ± 0.2 – 19.9 ± 1.2 Ma (n=10) (Figure 7A).

Uinta Basin

Wells from the Uinta Basin targeted early Cretaceous strata and thus these wells commonly were very deep (~1300–2700 m). Several core samples were collected from wells 21-15-10-22 Natural Buttes (NB), 2-7 Flat Mesa Federal (FMF), 13-25-14-23 Trap Spring (TS), and So Ouray Unit 1 (SO) (Table 2). Three to four very fine-grained sandstone samples were collected from the Cedar Mountain Formation, Dakota Sandstone, and Mesaverde Group in cores NB and FMF. One sample was collected from the Cedar Mountain Formation in the TS core. In the SO core, one sample from the Mesaverde Group was collected from a depth of about 1400 m.

Approximately half of the aliquots from Uinta Basin samples yielded ages between 1.0 ± 0.1 – 4.2 ± 0.6 Ma (n=21) (Figure 12A). The shallowest core sample (NB-4412 at ~250 m elevation) returned ages 3.4 ± 0.2 – 6.9 ± 0.4 Ma (n=3). The remaining aliquots (n=22) had very low amounts of He (<0.1 nmol/μg) and AHe ages <1 Ma. Based on modern geothermal gradients of 30 ^{o}C/km in the Uinta Basin discussed previously and a mean surface temperature of 10 ^{o}C, current temperatures at the depth of most of these samples (>2000 m) range from 70–90 ^{o}C. At these temperatures, AHe ages should be completely reset and AHe ages <1 Ma are consistent with this assessment. This indicates the depth to the base of the modern HePRZ in the Uinta Basin is approximately 2300 m.

APATITE (U-Th)/He SAMPLE AGE REPRODUCIBILITY

There are several explanations for poor reproducibility in AHe ages compared to typical 6% analytical errors including U- and Th- rich inclusions, grain size variability, mechanical abrasion, zoning, He implantation and inheritance, and variations in [eU]. High U-,Th- mineral inclusions are common in apatite and known to cause anomalously old AHe ages (e.g., House et al., 1997, 1999). Inclusions were frequently encountered and difficult to detect due to the slightly abraded and pitted nature of detrital apatite, and despite much scrutiny high He reextracts were detected (Table 1). Although He inclusions do cause clear age variations, they are easily identified and discarded.

Grain size may also play a role in the scatter of AHe ages since closure temperature and diffusivity of apatite are known to vary with grain size (Farley, 2000; Farley, 2002; Reiners and Farley, 2001). However Figure 13 shows no correlation between the total distribution of grain radii and AHe ages, thus grain size does not appear to be controlling the spread in ages.

Increased error may also stem from rounding due to mechanical abrasion since the exterior of the grain is removed and an F_T correction would result in an overly old age. To avoid these complications, only the least abraded grains were chosen for analysis. However, both clear euhedral grains and rounded grains had large variations in AHe ages for the same sample, thus a non-euhedral morphology is not the dominant source of scatter.

Zoning and He implantation can result in a disproportionate amount of He lost at the edge of a grain (Farley et al., 1996; Farley, 2002), but apatite fission-track studies show only about 5–10% of apatite from this region exhibit zoning (S. Kelley, personal commun.) and suggests zoning is unlikely to cause this age variation. Grains adjacent to apatite having significantly higher concentrations of U or Th, could result in He implantation along the edges of apatite grains. Since the distance between U-rich phases in most rocks is usually large, in general He implantation can be ignored (Farley et al., 1996; Farley, 2002; Ehlers and Farley, 2003).

The poor reproducibility seen in AHe ages from the central Colorado Plateau stems mainly from varying [eU] and He inheritance in detrital apatite. Detrital apatite grains are deposited from regions with different provenance He ages and varying U and Th parent concentrations. For samples with ages that are only partially reset, He inheritance can cause significant spread in AHe ages among aliquots of the same sample (e.g., House et al., 1999). Therefore He inheritance is very applicable to this study and a viable explanation for the significant age variation seen. Recent studies on the influence of radiation damage and [eU] on AHe ages indicate these factors are important in the interpretation of AHe data (Shuster et al., 2006; Flowers et al., 2007; Flowers et al., 2008, 2009; Flowers, 2009). Figure 14 shows plots of [eU] and AHe ages for each study region. The results fall into three general categories: (1) low [eU] samples, (2) quickly cooled samples, and (3) samples with a positive correlation with [eU]. For low [eU] grains (< 20 ppm), radiation damage is minimal and no relationship between [eU] and AHe ages is seen. Deep core samples in all regions

had AHe ages invariant of [eU], due to relatively quick cooling and a short residence in the HePRZ. The surface samples and shallow cores that experienced protracted residence in the HePRZ display a positive correlation between [eU] and AHe age. This correlation is not linear due to other factors that can contribute to AHe age scatter (e.g., He inheritance), however, a relationship exists showing a general increasing trend in [eU] for older AHe ages. Thus variations in [eU] and associated radiation damage can certainly contribute to the observed scatter in AHe ages.

THERMAL HISTORY MODELING OF THERMOCHRONOMETRIC DATA

Inverse modeling of thermochronometric ages is an excellent method to constrain the thermal history of a region and commonly used in association with fission-track thermochronology (e.g., Monte Trax (Gallagher, 1995), AFTSolve (Ketcham et al., 2000), HeFTy (Ketcham, 2005)). Inverse modeling software for AHe ages is available (e.g., DECOMP (Meesters and Dunai (2002a, 2002b), HeFTy (Ketcham, 2005)), but can only be utilized for individual samples rather than multiple sample suites. The modeling of combined surface samples and cores in a vertical transect provides a much more quantitative method to more accurately constrain thermal histories by incorporating both multiple grain and kinetic parameters.

The thermal modeling program employed in this study was written by C. Hager at the University of Kansas using Matlab® software and allows the inverse modeling of multiple (U-Th)/He samples from vertical arrays to reconstruct thermal histories. The following section describes the modeling approach employed.

Random thermal histories with monotonic heating or cooling paths between user-defined constraints are generated in a Monte Carlo simulation, similar to HeFTy (Ketcham, 2005). AHe ages are computed using standard helium production and finite difference diffusion equations (i.e., Crank-Nicolson solution, Thomas Algorithm) as summarized in Ketcham (2005) and references therein. Given the large [eU] variations encountered in apatite samples from the central Colorado Plateau, all inversely modeled ages incorporate radiation damage He diffusivity kinetics according to the RDAAM model, which uses the effective fission-track density as a proxy for radiation damage and its annealing behavior (Flowers et al., 2009). To model a vertical array of samples, a thermal offset for each aliquot is calculated from the highest aliquot in the array, using a range of specified geothermal gradients. Modeled AHe ages for each random thermal history and the calculated offset histories should match each aliquot in an array. Since this data exhibits much spread, possibly attributed to factors such as radiation damage or He inheritance, aliquots are modeled that define the lower and upper bounds of AHe ages (e.g., Flowers et al., 2007). Other variations such as parent nuclide concentrations, grain dimensions, and kinetic parameters can be specified for each dataset. Thermal histories that match the observed ages of each aliquot in a vertical array are plotted based on 1σ or 2σ accuracy, however one outlier is commonly allowed in each vertical array.

Thermal modeling setup and constraints

The thermal models in this study utilize the trapping model diffusion parameters as summarized by Shuster et al. (2006) and all grain parameters are user-defined. The aliquots chosen for modeling are those that define the boundaries of the cooling envelopes for each region. The thermal history of an area is determined by modeling 3–5 single grain ages on either side of the cooling envelope. In general 4–5 AHe ages are modeled and usually one non-matching outlier, determined by the program, is allowed to account for some scatter seen in AHe ages. The youngest and oldest edges of these envelopes are modeled using 10,000 randomly generated thermal histories each.

All thermal histories begin at 400 Ma and 200°C to ensure initial He concentration is 0. A wide range of cooling paths are deliberately generated between these constraints and the sample stratigraphic age in order to generate a spread of He concentrations and ages to account for the unknown provenance age of each grain. Other constraints include the stratigraphic age of the uppermost sample in each vertical transect since the thermal history path must be at surface temperatures (10–15°C) during deposition of the geologic formation. AHe results show all samples have been at least partially reset during burial (>40°C), yet fission-track lengths from southern Utah (Dumitru et al., 1994) suggest temperatures did not exceed 95°C. Therefore thermal histories must pass through this 40–100°C window between 3–13 Ma, as evidenced by the timing of exhumation in AHe ages. Finally, the thermal history path ends at the present time (0 Ma) and average annual surface

temperature for the Colorado Plateau of 10°C. These user-defined constraints are shown as red boxes in each thermal history plot, however usually the earliest portion of the thermal histories (>200 Ma) are not shown to emphasize more detail in the late Cenozoic history of the central Colorado Plateau.

Thermal structure of the central Colorado Plateau

Quantifying the thermal structure of the crust on the Colorado Plateau is essential when using thermochronometers that are sensitive to low temperatures (< 80°C), such as apatite, since temperature is used to calculate the magnitude of erosion. The effects of western North American tectonics have changed the thermal structure of the Colorado Plateau over time. During the Sevier orogeny and subduction of the Farallon plate, the transfer of heat from the hot underlying asthenospheric wedge increased heat flow and geothermal gradients were moderately high 25–50°C/km (Barton and Hanson, 1989). However in Laramide times, hot asthenosphere was replaced by a cold slab during the change from normal to shallow angle subduction, resulting in widespread refridgeration and decreased geothermal gradients (<20°C/km) in the western Cordillera and possibly in the Colorado Plateau (Dumitru et al., 1991). Subsequently, the influx of heat associated with magmatism and laccolith emplacement in Utah during the Oligocene and early Miocene (Nelson et al., 1992) may have caused another rise in the geothermal gradient at this time.

Blackett (2004) compiled geothermal information from temperature-depth data in Utah boreholes. In the Monument Uplift region, these boreholes show geothermal gradients range from 29–34°C/km. In the Canyonlands area, geothermal

gradients are slightly lower, ranging from 21–24°C/km. Geothermal gradients in the Book Cliffs range from 27–35°C/km. No data was available for the Uinta Basin, however in the northernmost Book Cliffs, gradients are 28–31°C/km. These data are similar to geothermal gradient estimates of 20–30°C/km used by previous thermochronometric studies on the Colorado Plateau (e.g., Dumitru et al., 1994; Flowers et al., 2008; Lee, 2007). For this study, the modern range of geothermal gradient for each specific area are utilized to translate cooling into exhumation and quantify the magnitude of erosion in the central Colorado Plateau region.

DISCUSSION OF STUDY REGIONS

Monument Uplift

AHe results from core samples and surface samples in the Monument Uplift feature two different trends. Figure 6A depicts surface sample ages from the Monument Uplift exhibit much scatter over similar elevations between 13–50 Ma (Stockli et al., 2002), yet core ages change little with depth or elevation 3–12 Ma. On this age-elevation plot, the inflection point between these two age populations marks the change from relatively slow to fast cooling. The surface sample ages reveal slower cooling in the HePRZ for at least 40 M.y., between 10–50 Ma. Similar core ages at varying elevations indicate significant late Miocene to Pliocene cooling and exhumation. The inflection point marks the base of a fossil HePRZ and the 80°C paleoisotherm. Based on a geothermal gradient of 30°C/km for the Monument Uplift (Blackett, 2004) and mean annual surface temperature of 10°C, the range of HePRZ

temperatures corresponds to 1–2.3 km of overburden removal in the Monument Uplift region since the late Miocene. Erosion rates are estimated to be 0.15–0.36 mm/yr since the latest Miocene during this period of rapid cooling and exhumation.

AHe ages that define the boundaries of the cooling envelope of Monument Uplift (Figure 6A) were selected for thermal modeling. Figure 6B shows the observed aliquot ages on an age-elevation plot, combined with paths of the matching modeled ages. Only modeled ages that fit the data within 1 or 2σ are shown. A range of geothermal gradients between 20–30°C/km are applied to calculate all the AHe ages in a transect. Gradients that best fit the Monument Uplift data were 30°C/km, and agree remarkably well with estimates by Blackett (2004). Figure 6C shows modeled thermal histories for the Monument Uplift AHe ages. After deposition of Permian strata 250–290 Ma most of the thermal histories show either (1) gradual reheating until the late Miocene erosional cooling event or (2) slower reheating after deposition until about 90 or 30 Ma, followed by temperatures that increase more rapidly, and finally rapid erosional cooling during the late Miocene. This reheating is caused by either constant sedimentation rates during sample burial or slow sedimentation followed by rapid sedimentation in the late Cretaceous (e.g., Mancos shale). Increased temperatures approximately 30 Ma may also be attributed to reheating from adjacent laccolith intrusion (Nelson et al., 1992; Nelson, 1997). Other thermal histories that have very rapid reheating shortly after deposition have matched observed AHe ages but make little geologic sense. Figure 6D is a close-up of the most recent portion of the thermal histories. Most thermal histories for Monument

Uplift show maximum reheating temperatures of the uppermost modeled sample that range between 55–70°C. The onset of rapid cooling occurs between 4–10 Ma. By utilizing the best-fit geothermal gradient for the region, 30°C/km, and more precise reheating temperatures found by the model, estimates of the magnitude of erosion in this area can be further constrained. About 1.5–2.0 km of sediment in the Monument Uplift region has been removed since the late Miocene with rates of 0.23–0.3 mm/yr.

Canyonlands

The AHe results from the Canyonlands vertical transect and cores are very similar to results from samples in the Monument Uplift region. Surface sample ages range from 5–38 Ma with poor reproducibility (Figure 8A), whereas the deep cores (SM-, LLE-) in the Canyonlands region are much younger 4–11 Ma and exhibit less scatter. Again the inflection point between the two populations indicates a transition from slow cooling in the HePRZ for at least 30 M.y., from 38 Ma to 5 Ma, to fast cooling in the late Miocene to early Pliocene. Based on an average geothermal gradient in the Canyonlands region range of 22°C/km (Blackett, 2004), this corresponds to 1.4–3.2 km of erosion and erosion rates of 0.21–0.52 mm/yr.

The aliquots model ages for the two envelopes of the Canyonlands vertical transect are depicted in Figure 8B. Since the Canyonlands data exhibited more age spread, one model age outlier for each boundary of the envelope is permitted. Although the model used a range of geothermal gradients between 20–30°C/km, the geothermal gradients that best fit the Canyonlands data were similar to those observed by Blackett (2004), at 20°C/km. Modeling results from the Canyonlands area show

reheating through the early Mesozoic and accelerated reheating after 75 Ma, possibly due to increased sedimentation rates in the late Cretaceous (Figure 8C). Some histories show reheating more recently around 20 Ma, which may be caused by laccolith emplacement around this time. Figure 8D focuses on the details of the more recent thermal histories. Maximum reheating temperatures span from 50–100°C, however the 1σ fit temperatures are between 50–70°C and show cooling at 4–5 Ma. Using the best-fit geothermal gradient of 20°C/km and this range of maximum temperatures, 2–3 km of erosion is calculated for the Canyonlands region since the late Miocene and erosion rates of 0.3–0.45 mm/yr.

Samples in between Canyonlands and the Book Cliffs, collected for regional thermochronometric studies, are combined with other regional samples from near the confluence of the Green and the Colorado Rivers and those collected in Tusher Canyon in the Book Cliffs. AHe ages, shown in Figure 7A, span from 4–32 Ma and increase slightly with increasing elevation. The spread in sample ages suggest these samples resided in the HePRZ for an extended period of time prior to erosional exhumation.

These regional samples were collected to determine spatial variations in erosion on the central Colorado Plateau. Figure 7B shows these regional AHe ages plotted against each sample's latitude to determine spatial exhumation trends. Regional samples from further south (around the confluence) are slightly older than samples from the north (Tusher Canyon, Book Cliffs), suggesting exhumation started in the south central Colorado Plateau and continued towards the north central plateau.

However, these samples were collected at different elevations, with as much as 500 m elevation spread, which makes it difficult to differentiate between lateral cooling and vertical cooling. More samples from similar elevations, or cores which were unobtainable, must be analyzed from a broader area to confidently state whether this south to north erosional progression is present.

Book Cliffs

AHe results from the three transects in the Book Cliffs are very similar. In Hay Canyon, surface samples range from 5–30 Ma with a generally positive correlation between age and elevation (Figure 9A), despite significant aliquot AHe age scatter. A reoccurring relationship between surface samples/shallow cores and deep cores is observed. The surface samples and shallow cores resided within the before early Pliocene exhumation at 5 Ma. Based on an average geothermal gradient for the Book Cliffs of 32^{o}C/km (Blackett, 2004), this corresponds to 0.9–2.2 km of overburden removal. Erosion rates for Hay Canyon range from 0.14–0.33 mm/yr.

Figure 9B shows the modeled AHe ages for the two boundaries of the cooling envelope in Hay Canyon. Some model age outliers were allowed to account for the wide spread in observed ages. In Hay Canyon, the thermal histories used geothermal gradients between 20–34^{o}C/km, and the best fit geothermal gradient was 20^{o}C/km, lower than 32^{o}C/km previously observed by Blackett (2004). This gradient is also lower than modeled geothermal gradients for the central Book Cliffs discussed next. An average geothermal gradient between the observed gradients and the best-fit modeled gradients is used, 26^{o}C/km. Figure 9C shows the thermal histories that fit

the observed Hay Canyon data. After early Eocene deposition of the uppermost transect sample, 49–57 Ma, the thermal histories experienced three types of reheating during burial. The first type, immediate rapid reheating after Eocene deposition, appears inconsistent with independent geological evidence of depositional rates. Either reheating occurred gradually during relatively constant sedimentation rates or slow initially followed by more rapid heating around 25 Ma, possibly associated with laccolith emplacement. Figure 9D highlights the recent portion of the thermal histories. Maximum burial temperatures for surface samples range from 40–60^{o}C in Hay Canyon and erosional cooling took place 5–10 Ma. Using the average gradient of 26^{o}C/km, 1.2–1.9 km of erosion has been calculated for the Hay Canyon region of the Book Cliffs since the late Miocene. Erosion rates range from 0.18–0.29 mm/yr, but likely represent minimum erosion rates given the average geothermal gradient used.

In Sego Canyon, the results are similar to Hay Canyon. Surface sample AHe ages increase with elevation from 8–52 Ma (Figure 10A). Shallow cores (5BC-) overlap with the surface samples from 6–20 Ma. The single deep core sample (3FED335) produced ages 5–6 Ma. The Sego Canyon surface samples and shallow cores also resided in the HePRZ for around 50 M.y., between 6–52 Ma, before erosional exhumation 5–6 Ma in the late Miocene to early Pliocene. Using an average geothermal gradient of 32^{o}C/km for the Book Cliffs from Blackett (2004),

0.9–2.2 km of overburden has been removed from the Sego Canyon region. Since 6 Ma, erosion rates are 0.14–0.33 mm/yr.

Thermal modeling results from Sego Canyon are shown in Figure 10B. One model outlier was permitted to account for some of the spread in AHe ages. Geothermal gradients utilized by this model range from 20–32°C/km and the best-fit for Sego Canyon samples was 32°C/km. Thermal histories that match observed ages at this geothermal gradient are seen in Figure 10C. Samples at the top of the transect in Sego Canyon have late Eocene depositional ages. After deposition, samples experienced mainly constant sedimentation rates and gradual reheating. Figure 10D shows maximum burial temperatures of 45–65°C for this region, and erosional exhumation between 5–8 Ma. Using a geothermal gradient of 32°C/km, 1.1–1.7 km of erosion is determined in the Sego Canyon area, with erosion rates of 0.17–0.26 mm/yr.

In the Blaze Canyon area of the central Book Cliffs, AHe results are expected to be similar to the adjacent Sego Canyon. AHe ages from this vertical transect ranged from 2–36 Ma (Figure 11A). Ages also generally increase with increasing elevation. The core samples show less age variation from 3–11 Ma, with the deepest core (PH-) having ages from 3–7 Ma. The change from slow cooling in the HePRZ for at least 25 M.y., to rapid exhumation occurs approximately 11 Ma in Blaze Canyon during the late Miocene. Using the average geothermal gradient for the Book Cliffs, 32°C/km (Blackett, 2004), the magnitude of erosion in Blaze Canyon is 0.9–2.2 km. Erosion rates since about 6 Ma are 0.14–0.33 mm/yr.

Figure 11B shows the results of modeled aliquot ages for the two sides of the cooling envelope in Blaze Canyon. No model outliers were allowed for these three aliquots. Geothermal gradients ranged from 20–34°C/km. However the younger envelope of AHe ages had better matches with a geothermal gradient of 34°C/km, whereas the older envelope ages matched a lower gradient of 20°C/km. In all other models, both the young and older envelopes of AHe ages each had matching best-fit geothermal gradients. Since Blaze Canyon is adjacent to Sego Canyon and Blackett (2004) estimated higher gradients here, 34°C/km is selected as the best-fit geothermal gradient for Blaze Canyon. Figure 11C reveals the matching thermal histories for the modeled ages, characterized by slow reheating consistent with gradual sedimentation and burial. Figure 11D shows the most recent portion of thermal histories for the past 15 M.y. Maximum reheating temperatures range from 50–70°C prior to rapid erosional exhumation at 5 Ma. These maximum temperatures with a geothermal gradient of 34°C/km constrain erosion in central Book Cliffs to 1.2–1.8 km and a post 6 Ma average erosion rate 0.17–0.27 mm/yr.

Uinta Basin

The AHe results for Uinta Basin are significantly younger than ages from the previous three regions. Here, cores were sampled from depths of 1.4–2.6 km and ages ranged from about 7 to nearly 0 Ma (Figure 12A). Nearly half of the aliquots from Uinta Basin have been excluded due to low He concentrations. Based on geothermal gradients of 34°C/km from Blackett (2004), the samples from these cores had resided in temperatures typical of the modern HePRZ and greater, between

60–100°C. Due to these high temperatures in the Uinta Basin, AHe ages of these deep cores have been partially to completely reset since erosional exhumation in the late Miocene to early Pliocene.

Figure 12B shows the modeled ages from selected aliquots in Uinta Basin. Geothermal gradients ranged from 20–34°C/km and similar to Blackett (2004) and the Sego and Blaze Canyon gradients, the highest gradient of 34°C/km best matched the AHe data. In Figure 12C the thermal histories are plotted that match the observed ages. After deposition of these late Cretaceous strata 65–85 Ma, most 1σ fits show either gradual reheating or rapid early Miocene reheating, possibly due to laccolith intrusions. Figure 12D focuses on the more recent portion of the thermal histories since 15 Ma. Here the uppermost core sample from the Uinta Basin (NB-4412) undergoes a range of maximum burial temperatures between 60–95°C with the onset of erosional exhumation occurring 5–9 Ma. This sample has been at least partially reset, and deeper samples collected have been completely reset at higher temperatures. Using a geothermal gradient of 34°C/km, the uppermost Uinta Basin core sample was at maximum depths of 1.5–2.5 km. Since this sample was collected from a depth of about 1300 m, the magnitude of erosion in the Uinta Basin is estimated at 0.2–1.2 km.

In summary, AHe results from the central Colorado Plateau exhibit remarkably similar trends, with the exception of the young, reset Uinta Basin ages. Surface samples and shallow cores from Monument Uplift, Canyonlands, and the Book Cliffs all have a broad spread of Paleocene to early Pliocene ages 2–56 Ma.

This is indicative of slow cooling during a protracted residence in the lower portion of the HePRZ for at least 50 M.y., between 5–56 Ma. Deeper cores have relatively little age spread and AHe ages that are invariant of elevation. On a summary age-elevation plot (Figure 15) the inflection point in the cooling history of these samples marks the change from a period of slow cooling to an onset of rapid erosional cooling. The deep core ages show significant late Miocene to Pliocene cooling associated with erosional exhumation 3–11 Ma (Figure 15), with an average exhumation age 6.6 ± 0.3 Ma (average error is standard deviation of the mean (SDOM)), if Uinta Basin young ages are excluded. Figure 16 shows greatest number of AHe exhumation ages from deep cores range from 4.3–7.7 Ma, with the greatest probability of exhumation age occurring 5.0–6.3 Ma. AHe results show that the central Colorado Plateau experienced a period of rapid erosional exhumation at 5–7 Ma.

Erosional exhumation of central Colorado Plateau

AHe data combined with thermal modeling provide powerful constraints for erosion of the central Colorado Plateau. Erosional exhumation has occurred during the latest Miocene to early Pliocene around 6 Ma. The magnitude of erosion is substantial and results indicate 1–3 km of overburden has been removed from the center of the Colorado Plateau since only 6 Ma, confirming a predicted bull's eye trend in the spatial distribution of erosion (Pederson et al., 2007). These estimates are consistent with many other erosion estimates for the region (e.g., Dumitru et al., 1994; Nuccio and Condon, 1996; Stockli et al., 2002; Pederson et al., 2002b; 2007). Figure 17 shows erosion results compared with other studies. From south to north,

Monument Uplift results of 1.5–2 km are nearly the same as the 2 km estimation by Nuccio and Condon (1996). Pederson et al. (2002b) found a slightly larger range of erosion in Monument Uplift of 1–2 km. In the Canyonlands region of the central Colorado Plateau, this study finds the greatest amount of erosion is 2–3 km. Nuccio and Condon's estimations (1996) in the Moab region of Canyonlands are higher at 3.4–4 km. Pederson et al. (2002b) used geomorphic reconstructions to predict a larger range in erosion in Canyonlands between 1.5–4 km. Estimates of 2–3 km by Dumitru et al. (1994) in the Waterpocket Fold region of the central Colorado Plateau are consistent with this study. This study estimates erosion in the Book Cliffs ranges from 0.9–2.2 km, slightly less than the 2 km determined by Nuccio and Condon (1996), and more than the 0.2–1.2 km of erosion found in the Uinta Basin. Figure 18 shows a map of erosion estimates in the central Plateau, combined with estimates from other studies on the Colorado Plateau. The spatial distribution of erosion appears to have a concentric pattern, with the greatest amount of erosion in the Canyonlands region, slightly less in Monument Uplift and Book Cliffs region, and far less in the Uinta Basin. Overall these estimates further constrain previous erosion estimates for the central Colorado Plateau, but also add important temporal constraints to the landscape evolution of this region.

DRIVING FORCES FOR ACCELERATED MIO-PLIOCENE EROSIONAL EXHUMATION

AHe results provide substantial evidence for the prominent Neogene erosion of the central Colorado Plateau, which thermochronometric studies in the southwest plateau region have suggested. Other erosion studies, such as geomorphic reconstructions and petroleum generation models, focus on the magnitude and spatial distribution of erosion. This study further constrains erosion rates and patterns and also adds temporal constraints. Results show late Miocene to early Pliocene erosional exhumation in the central Colorado Plateau and these temporal constraints can help spotlight certain mechanisms for erosion. Below the causes for the Mio-Pliocene erosion seen in the central Colorado Plateau are discussed.

Extensional tectonics in the Basin and Range and the Gulf of California

Basin and Range extension at 18 Ma began to delineate the western and southern borders of the Colorado Plateau. In the mid Miocene, a once northeast flowing Colorado River (McKee and McKee, 1972) reversed its course to the southwest as a result of extension and change in base level (Pierce et al, 1979). The onset of Basin and Range faulting coincides with a period of unroofing between 28–16 Ma in the southwest region of the Colorado Plateau (Flowers et al., 2008). This phase of mid Cenozoic unroofing in the southwest plateau is presumed to be associated with Basin and Range extension and the subsequent Colorado River drainage reversal. However, this study finds more recent cooling at about 6 Ma,

which suggests Basin and Range extension has had little effect on erosion on the central plateau.

Other regional tectonic controls may be more applicable to erosion in the central Colorado Plateau. The opening of the Gulf of California at 6 Ma (Oskin and Stock, 2003), a result of transform movement and extension between the North American Plate and the Pacific Plate (Atwater, 1970), temporally coincides with the Mio-Pliocene cooling in the central plateau. While it is unlikely the opening of the Gulf of California was the direct cause for rapid Mio-Pliocene erosion, it provided a location for the deposition of large volumes of sediment eventually carried by the Colorado River from the Colorado Plateau (Merriam and Bandy, 1965; Lucchitta, 1972). In the Gulf of California, five kilometers of marine, deltaic, and fluvial sediment have accumulated and sedimentation rates varied from 5.5–0.5 mm/yr (Johnson et al, 1983). Today, as a result of the anthropogenic impact on the Colorado River and dam construction in the past century, the sediment supply in the Colorado River has drastically declined and caused sediment starvation in the northern Gulf of California (Carriquiry et al., 2001).

Intensification of southwest monsoon

Several studies suggest the presence of a wetter Pliocene climate in the western United States and Colorado Plateau for a wide variety of reasons (e.g., Remeika et al., 1988; Ruddiman and Kutzbach, 1989; Molnar and England, 1990; Thompson, 1991; Hay et al., 2002). Increased sediment accumulation rates during the Late Cenozoic from all over the world have also been attributed to changes in

climate during this time (Molnar, 2004). It is possible a wetter climate during the Pliocene could be responsible for this pulse of erosion of the Colorado Plateau.

The Anza-Borrego region of the Salton Trough, the landward extension of the Gulf of California, includes over six kilometers of Late Cenozoic sediment deposited by the Colorado River (Kerr and Kidwell, 1991). The Imperial and Palm Springs Formations in this region contain reworked Cretaceous foraminifera and pollen, originating from the Upper Cretaceous Mancos Shale on the Colorado Plateau (Merriam and Bandy, 1965; Fleming, 1994). The stratigraphic distribution of pollen suggests erosion of the southern Colorado plateau began by at least 4.5 Ma, and 3.9 Ma sediment from the northern plateau was deposited in the Salton Trough (Fleming, 1994). Rapid removal of large quantities of sediment by the Colorado River from an area as vast as the central Colorado Plateau could indicate significantly more precipitation and an overall wetter climate in the Pliocene (Fleming, 1994).

In addition, climate changes associated with the opening of the Gulf of California have affected the late Miocene to early Pliocene history of the Colorado River (Hunt and Elders, 2001). Increased summer rainfall, associated with new moisture and monsoons brought by the newly formed Gulf of California may have enhanced headward erosion along the Colorado River. The acceleration in the development of the Colorado River drainage, in addition to increased stream incision and erosion rates on the Colorado Plateau, may have been enhanced by the change in climate during the latest Miocene to Pliocene times (Hunt and Elders, 2001).

Drainage integration of the Colorado Plateau

In the central Colorado Plateau, widespread erosional exhumation at 6 Ma also temporally corresponds with the regional drainage integration of the Colorado River system. Once integrated off the plateau, the lower Colorado River extended into the Lake Mead region, the Salton Trough, and eventually to the Gulf of California. The 4–6 Ma age of a throughflowing Colorado River is constrained by $^{40}Ar/^{39}Ar$ ages (e.g., Faulds et al., 2001; Spencer et al., 2001) from formations bracketing the first Colorado River sediments in the Bouse Formation (Buising, 1990). Regional incision of the Grand Canyon at 6 Ma was induced by drainage integration (Lucchitta, 1972; McKee and McKee, 1972). Pederson et al. (2002a) indicates the 1500 m dropping of base level after the integration off the Grand Wash Cliffs has driven incision further upstream. It is suspected the rapid and substantial erosion of the central Colorado Plateau is largely driven by this newly integrated Colorado River.

Interplay and feedback of driving forces: The "perfect" erosion

No single event is likely to be the sole source of erosion seen in the central Colorado Plateau. A combination of well-timed events in latest Miocene and early Pliocene have resulted in between 1–3 km of erosion across the current landscape of the central Colorado Plateau. The combination of drainage integration, climate, and the opening of the Gulf of California is a powerful sequence of events, all temporally coinciding with this pulse of erosion at 6 Ma. While the integration of the Colorado River off the southwest Colorado Plateau may be responsible for much of the incision

seen on the plateau, a wetter climate can greatly increase erosion also. The newly opened Gulf of California around the same time provides a location for the vast quantity of sediment removed.

LANDSCAPE EVOLUTION

Landscape evolution studies on the southwest plateau have shown a progression of overburden removal from southwest to northeast beginning in the late Cretaceous at the edges of the plateau, with more recent erosion towards the interior (i.e. Lee, 2008; Flowers et al., 2008). This erosional trend appears to have continued into the center of the Colorado Plateau, perhaps controlled by lithology. Once erosion-resistant limestone was exposed in the southwest plateau (e.g. Kaibab Limestone), erosion continued north into the plateau interior. Here, the easily erodible bedrock in the central Colorado Plateau, including the mudstones of the Jurassic Morrison Formation and Cretaceous Mancos Shale, may have contributed to the vast quantity of erosion seen in the central Colorado Plateau. This period of Mio-Pliocene erosion in the central plateau region has transformed the landscape of the Colorado Plateau to its present state.

Erosion estimates calculated by Pederson et al. (2002b) since 30 Ma and Nuccio and Condon (1996) at 25 Ma were very similar to erosion estimates from this study, suggesting most of the erosion since 25–30 Ma has primarily occurred in the last 6 M.y. The Pliocene landscape was greatly impacted by the evolution of the modern Colorado River drainage system. Sometime after 7 Ma, the Green River

traveled around the Uinta Mountains and integrated with the Colorado River in the Canyonlands region (Winkler, 1970; Pederson and Hadder, 1995). More recently in the latest Pliocene, incision in the southwest region of the plateau began at the Mogollon Slope as the Little Colorado River integrated with the Colorado River in the Grand Canyon (Holm, 2001). Finally, the Colorado River drainage integration off the southwest plateau and subsequent erosion also had a dramatic effect on the morphology of the modern landscape of the Colorado Plateau.

After the integration of the Colorado River system and lowering of base level at 6 Ma, erosion rates likely peaked shortly after this 1500 m base-level decrease and over time gradually subsided, similar to reported rates of incision. Quaternary incision rates in the Grand Canyon cannot account for the magnitude of incision observed, and thus rates are expected to be higher during initial canyon-cutting 5–6 Ma and have decreased since (Pederson et al., 2002a; Karlstrom et al., 2007). These reported Quaternary incision rates are similar to the low range of observed erosion rates from this study (0.03–0.15 mm/yr), yet much less than the maximum erosion rates seen in the Canyonlands region (0.3–0.45 mm/yr). A decrease in erosion and incision rates since 6 Ma suggests that landscape evolution primarily occurred closer to 6 Ma and the modern landscape of the Colorado Plateau is indeed Pliocene in age.

IMPLICATIONS FOR THE UPLIFT OF THE COLORADO PLATEAU

AHe thermochronometric results and thermal modeling show erosional exhumation of the central Colorado Plateau occurred at 6 Ma. A maximum of 2–3

km of sediment has been removed from the central Colorado Plateau at this time. These results, combined with other thermochronometric studies, give some support to the surface uplift mechanism proposed by Pederson et al. (2002b) and tested by Callahan et al. (2006), claiming surface uplift can be explained by isostatic response to erosional unroofing. 3-D flexural uplift models by Callahan et al. (2006) predict higher quantities of erosion in the center of the plateau, with little erosional rebound around the flanks. This study finds erosion of up to 3 km in the center of the plateau, whereas other studies have shown little to no unroofing at the edges during the Late Cenozoic (e.g., Flowers et al., 2008; Lee, 2007). However, Roy et al. (2009) found erosion could not explain the total rock uplift observed and the residual uplift must be caused by a tectonic process, such as thermal reequilibriation associated with the removal of the Farallon slab. This study has implications for Laramide or post-Laramide tectonically-driven surface uplift mechanisms. Rapid erosion in the Mio-Pliocene is temporally decoupled from these tectonic processes responsible for surface uplift. While surface uplift mechanisms of the Colorado Plateau may remain a topic of debate, rapid erosional exhumation of the central Colorado Plateau at 6 Ma cannot be attributed to surface uplift.

CONCLUSIONS

This thermochronometric study integrates core and surface samples to comprehensively quantify erosional exhumation and elucidate the landscape evolution in the central Colorado Plateau. This combination of cores and surface

samples for four regions of the central Colorado Plateau has generated over 500 single grain detrital AHe ages. Thermochronometric data and thermal modeling are used to constrain the timing, magnitude, and spatial distribution of erosion in the central Colorado Plateau. Deep cores from Monument Uplift, Canyonlands, Book Cliffs, and the Uinta Basin are key for determining temporal constraints on erosional exhumation of the central plateau. AHe results from these cores show erosional exhumation 3–11 Ma during the late Miocene to early Pliocene. Thermal modeling results indicate cooling between two modeled AHe age envelopes occurred 5–10 Ma. Probability plots of all exhumation ages suggest erosional exhumation occurred 6.6 Ma. However, surface samples from these regions show a wide variation in ages from 5–56 Ma and represent slow cooling in the HePRZ. The depth to the base of the HePRZ (80^{o}C) can be used to estimate the magnitude of erosion, however thermal modeling more precisely determines maximum reheating temperatures for thermal histories and best-fitting geothermal gradients for specific regions to better constrain erosion in four main study regions.

The erosional exhumation history of the central Colorado Plateau varies from that of the surrounding edges of the plateau. Significant rapid erosion has dominated in the eastern Utah area of the central plateau since 6 Ma. Since the latest Miocene to early Pliocene, as much as 3 km of sediment overburden has been removed from the central plateau, whereas relatively little erosion has occurred along the periphery. In Monument Uplift, 1.5–2 km of overburden has been removed. Like many studies predicted, the Canyonlands region has experienced the most erosion, 2–3 km. In the

Hay Canyon, Sego Canyon, and Blaze Canyon, 0.9–2.2 km of erosion has been determined. In the Uinta Basin, only 0.2–1.2 km of overburden removal is predicted. The Book Cliffs and Uinta Basin regions have experienced the least amount of erosion and also have preserved Cenozoic strata, not common on most of the plateau. Regional AHe ages hint at a south to north progression of erosion, however the timing of erosional exhumation in each region at 4–10 Ma does not have significant spatial variation.

The landscape of the Colorado Plateau is remarkably young and has taken its present shape only in the last 6 M.y. Erosion estimates since 30 Ma are dominated by accelerated erosion in the Mio-Pliocene. During the Pliocene, the Colorado River drainage system developed its modern course and erosion and incision rates were higher than today. Higher incision rates around 6 Ma, suggests the modern Colorado Plateau landscape formed at this time.

Finally, the Mio-Pliocene erosional exhumation results from this study, combined with other thermochronometric studies in the southwest plateau, support the erosional isostatic rebound mechanism for a portion of surface uplift in the center of the Colorado Plateau. These thermochronometric results provide evidence that the center of the plateau has undergone significantly more erosion when compared to the edges. The flexural isostatic rebound in response to erosional unloading can be responsible for a portion of surface uplift in the center of the plateau. However, this study also shows erosional exhumation is temporally decoupled with either Laramide or post-Laramide tectonic mechanisms responsible for the majority of surface uplift

of the Colorado Plateau. Erosion is not a direct result of surface uplift, but rather a combination of unique events at 6 Ma. Erosion in the central Colorado Plateau has occurred due to the "perfect" combination of driving forces: drainage integration of the Colorado River off the plateau, the southwest monsoon climate, and the opening of the Gulf of California. These events have combined to produce up to 3 km of erosion in the central plateau, a quantity that rivals the amount of sediment removed from the Grand Canyon's gorge. Such dramatic erosion has resulted in the evolution of the spectacular and remarkably young, central Colorado Plateau landscape; a region containing the country's greatest abundance of national parks with unique erosional landforms of mesas, monuments, arches, and deeply incised canyons that attract visitors from all over the world.

REFERENCES

Atwater, T., 1970, Implications of plate tectonics for the Cenozoic evolution of western North America: Geological Society of America Bulletin, v. 81, p. 3,513–3,536.

Barnes, F.A., 1993, Geology of the Moab Area: Moab, Utah, Canyon Country Publications, 264 p.

Barton, M.D., and Hanson, R.B., 1989, Magmatism and the development of low-pressure metamorphic belts: Implication for the western United States and thermal modeling: Geological Society of America Bulletin, v. 101, p. 1,051–1,065.

Beaumont, C., 1981, Foreland basins: Royal Astronomical Society Geophysical Journal, v. 65, p. 291–329.

Bird, P., 1984, Laramide crustal thickening event in the Rocky Mountains foreland and Great Plains: Tectonics, v. 3, p. 741–758.

Bird, P., 1998, Kinematic history of the Laramide orogeny in latitudes 35^{o}–49^{o}N, western United States: Tectonics, v. 17, p. 780–801.

Biswas, S., Coutand, I., Grujic, D., Hager, C., and Stockli, D., 2007, Exhumation uplift of the Shillong plateau and its influence on the eastern Himalayas: New constraints from apatite and zircon (U-Th-[Sm])/He and apatite fission track analyses: Tectonics, v. 26, TC6013.

Blackett, R.E., 2004, Geothermal gradient data for Utah, Utah Geological Survey, p. 1–8.

Buising, A.V., 1990, The Bouse Formation and bracketing units, Southeastern California and Western Arizona: Implications for the evolution of the proto-Gulf of California and the lower Colorado River: Journal of Geophysical Research, v. 95, p. 20111–20132.

Bump, A.P., and Davis, G.H., 2003, Late Cretaceous-early Tertiary Laramide deformation of the northern Colorado Plateau, Utah and Colorado: Journal of Structural Geology, v. 25, p. 421–440.

Callahan, C.N., Roy, M., and Pederson, J. L., 2006, Modeled flexural response to

erosion in the Colorado Plateau: Implications for Laramide and post-Laramide rock uplift processes: EOS, American Geophysical Union, v. 87, no. 52, Fall Meet. Suppl., Abstract S43A-1374.

Carriquiry, J.D., Sanchez, A., and Camancho-Ibar, V.F., 2001, Sedimentation in the northern Gulf of California after cessation of the Colorado River discharge: Sedimentary Geology, v. 144, p. 37–62.

Condon, S.M., 1997, Geology of the Pennsylvanian and Permian Cutler Group and Permian Kaibab Limestone in the Paradox Basin, Southeastern Utah and Southwestern Colorado: U.S. Geological Survey Bulletin 2000-P, p. P1–P46.

Cooley, M.E., and Davidson, E.S., 1963, The Mogollon Highlands– Their influence on Mesozoic and Cenozoic erosion and sedimentation: Arizona Geological Society Digest, v. 6, p. 7–35.

DeCelles, P.G., and Coogan, J.C., 2006, Regional structure and kinematic history of the Sevier fold-and-thrust belt, central Utah: Geological Society of America Bulletin, v. 118, p. 841–864.

DeCelles, P.G., and Mitra, G., 1995, History of the Sevier orogenic wedge in terms critical taper models, northeast Utah and southwest Wyoming: Geological Society of America Bulletin, v. 107, p. 454–462.

Dickinson, W.R., Klute, M.A., Hayes, M.J., Janecke, S.U., Lundin, E.R., McKittrick, M.A., and Olivares, M.D., 1988, Paleogeographic and paleotectonic setting of Laramide sedimentary basins in the central Rocky Mountain region: Geological Society of America Bulletin, v. 100, p. 1,023–1,039.

Dorsey, R.J., Fluette, A., McDougall, K., Housen, B.A., Janecke, S.U., Axen, G.J., and Shirvell, C.R., 2007, Chronology of Miocene-Pliocene deposits at Split Mountain Gorge, Southern California: A record of regional tectonics and Colorado River evolution: Geology, v. 35, p. 57–60.

Dumitru, T.A., Gans, P.B., Foster, D.A., and Miller, E.L., 1991, Refridgeration of the western Cordilleran lithosphere during Laramide shallow-angle subduction: Geology, v. 19, p. 1145–1148.

Dumitru, T.A., Duddy, I.R., and Green, P.F., 1994, Mesozoic-Cenozoic burial, uplift, and erosion history of the west-central Colorado: Geology, v. 22, p. 499–502.

Ehlers, T.A., and Farley, K.A., 2003, Apatite (U-Th)/He thermochronometry: methods and applications to problems in tectonic and surface processes: Earth

and Planetary Science Letters, v. 206, p. 1–14.

Elston, D.P., and Young, R.A., 1991, Cretaceous-Eocene (Laramide) Landscape Development and Oligocene-Pliocene Drainage Reorganization of Transition Zone and Colorado Plateau, Arizona: Journal of Geophysical Research, v. 96, p. 12,389–12,406.

England, P., and Molnar, P., 1990, Surface uplift, uplift of rocks, and exhumation of rocks: Geology, v. 18, p. 1,173–1,177.

Farley, K.A., 2000, Helium diffusion from apatite: general behavior as illustrated by Durango fluorapatite, Journal of Geophysical Research, v. 105, p. 2903–2914.

Farley, K.A., 2002, (U-Th)/He dating: Techniques, calibrations, and applications, *in* Porcelli, D., Ballentine, C.J., and Wieler, R., eds., Noble Gases in Geochemistry and Cosmochemistry, Mineral Society of America: Washington D.C., p. 819–844.

Farley, K.A., Wolf, R.A., and Silver, L.T., 1996, The effects of long alpha-stopping distances on (U-Th)/He ages: Geochimica et Cosmochimica Acta, v. 60, p. 4223–4229.

Farley, K.A., and Stockli, D.F., 2002, (U-Th)/He dating of Phosphates: Apatite, Monazite, and Xenotime, *in* Kohn, M., Rakovan, M.K., and Hughes, J.M., eds., Phosphates: Mineral Society of America: Washington D.C., p. 559–578.

Faulds, J.E., Wallace, M.A., Gonzalez, L.A., and Heizler, M.T., 2001, Depositional Environment and Paleogeographic Implications of the Late Miocene Hualapai Limestone, Northwestern Arizona and Southern Nevada, *in* Young, R.A., and Spamer, E.E., eds., The Colorado River Origin and Evolution: Grand Canyon, Arizona, Grand Canyon Association Monograph No. 12, p. 81–87.

Fisher, D.J., Erdmann, C.E., and Reeside, J.B., Jr., 1960, Cretaceous and Tertiary Formations of the Book Cliffs, Carbon, Emery, and Grand Counties, Utah, and Garfield and Mesa Counties, Colorado: U.S., Geological Survey Professional Paper 332, 80 p.

Fleming, R.F., 1994, Cretaceous pollen in Pliocene rocks: Implications for Pliocene climate in the southwestern United States: Geology, v. 22, p. 787–790.

Flowers, R.M., Shuster, D.L., Wernicke, B.P., and Farley, K.A., 2007, Radiation damage control on apatite (U-Th)/He dates from the Grand Canyon region, Colorado Plateau: Geology, v. 35, p. 447–450.

Flowers, R.M., Wernicke, B.P., and Farley, K.A., 2008, Unroofing, incision, and uplift history of the southwestern Colorado Plateau from apatite (U-Th)/He thermochronology: Geological Society of America Bulletin, v. 120, p. 571–587.

Flowers, R.M., 2009, Exploiting radiation damage control on apatite (U-Th)/He dates in cratonic regions: Earth and Planetary Science Letters, v. 277, p. 148–155.

Flowers, R.M., Ketcham, R.A., Shuster, D.L., and Farley, K.A., 2009, Apatite (U-Th)/He thermochronometry using a radiation damage accumulation and annealing model: Geochimica et Cosmochimica Acta, v. 73, p. 2,347–2,365.

Fouch, T.D., Lawton, T.F., Nichols, D.J., Cashion, W.B., and Cobban, W.A., 1983, Patterns and timing of synorogenic sedimentation *in* Upper Cretaceous rocks of central and northeast Utah, in Reynolds, M.W., and Dolly, E.D., eds., Mesozoic paleography of the west-central United States: Denver, Colo., Rocky Mountain Paleogeography Symposium 2, p. 305–336.

Foxford, K.A., Walsh, J.J., Watterson, J., Garden, I.R., Guscott, S.C., and Burley, S.D., 1998, Structure and content of the Moab Fault Zone, Utah, USA, and its implications for fault seal prediction: Geological Society, London, Special Publications, v. 147, p. 87–103.

Gallagher, K., 1995, Evolving temperature histories from apatite fission-track data: Earth and Planetary Science Letters, v. 136, p. 421–435.

Hay, W.W., Soeding., E., DeConto, R.M., and Wold, C.N., 2002, The Late Cenozoic uplift – climate change paradox: International Journal of Earth Sciences, v. 91, p. 746–774.

Hettinger, R.D., and Kirschbaum, M.A., 2003, Stratigraphy of Upper Cretaceous Mancos Shale (upper part) and Mesaverde Group in the southern part of the Uinta and Piceance Basins, Utah and Colorado, *in* Petroleum Systems and Geologic Assessment of Oil and Gas in the Uinta-Piceance Province, Utah and Colorado, p. 1–21.

Hintze, L.F., 1993, Geologic History of Utah: Brigham Young University Geology Studies Special Publication, 202 p.

Holm, R.F., 2001, Cenozoic paleogeography of the central Mogollon Rim– southern Colorado Plateau region, Arizona, revealed by Tertiary gravel deposits, Oligocene to Pliestocene lava flows, and incised streams: Geological Society

of America Bulletin, v. 113, p. 1467–1485.

House, M.A., Wernicke, B.P., Farley, K.A., and Dumitru, T.A., 1997, Cenozoic thermal evolution of the central Sierra Nevada, California, from (U-Th)/He thermochronometry: Earth and Planetary Science Letters, v. 151, p. 167–179.

House, M.A., Farley, K.A., and Kohn, B.P., 1999, An empirical test of helium diffusion in apatite: borehole data from the Otway basin, Australia: Earth and Planetary Science Letters, v. 170, p. 463–474.

House, M.A., Farley, K.A., and Stockli, D., 2000, Helium chronometry of apatite and titanite using Nd-YAG laser heating: Earth and Planetary Science Letters, v. 183, p. 365–368.

House, P.K., Pearthree, P.A., Howard, K.A., Bell, J.W., Perkins, M.E., Faulds, J.E., and Brock, A.L., 2005, Birth of the lower Colorado River—Stratigraphic and geomorphic evidence for its inception near the conjunction of Nevada, Arizona, and California, *in* Pederson, J., and Dehler, C.M., eds., Interior western United States: Geological Society of America Field Guide 6, p. 357–387.

Humphreys, E.D., 1995, Post-Laramide removal of the Farallon slab, western United States: Geology, v. 23, p. 987–990.

Humphreys, E.D., Hessler, E., Dueker, K., Farmer, C., Erslev, E., and Atwater, T., 2003, How Laramide-age hydration of North American lithosphere by the Farallon slab controlled subsequent activity in the western United States: International Geological Review, v. 45, p. 575–595.

Hunt, C.B., 1956, Cenozoic geology of the Colorado Plateau: U.S. Geological Survey Professional Paper 279, 99 p.

Hunt, A.G., and Elders, W.A., 2001, Climate Change and the Evolution of Grand Canyon and the Colorado River Delta, *in* Young, R.A. and Spammer, E.E., eds., Colorado River: Origin and Evolution, Grand Canyon Association, p. 191–194.

Huntoon, J.E., Dubiel, R.F., Stanesco, J.D., Mickelson, D.L., and Condon, S.M., 2002, Permian-Triassic depositional systems, paleogeography, paleoclimate, and hydrocarbon resources in Canyonlands and Monument Valley, Utah: Geological Society of America Field Guide 3: Science at the Highest Level, p. 33–58.

Johnson, N.M., Officer, C.B., Opdyke, N.D., Woodard, G.D., Zeitler, P.K., and Lindsay, E.H., 1983, Rates of Cenozoic tectonism in the Vallecito-Fish Creek basin, western Imperial Valley, California: Geology, v. 11, p. 664–667.

Jordan, T.E., 1981, Thrust loads and Foreland Basin Evolution, Cretaceous, Western United States: American Association of Petroleum Geologists Bulletin, v. 65, p. 2,506–2,520.

Karlstrom, K.A., Crow, R.S., Peters, L., McIntosh, W., Raucci, J., Crossey, L.J., Umhoefer, P., and Dunbar, N., 2007, $^{40}Ar/^{39}Ar$ and field studies of Quaternary basalts in Grand Canyon and model for carving Grand Canyon: Quantifying the interaction of river incision and normal faulting across the western edge of the Colorado Plateau: Geological Society of America Bulletin, v. 119, p. 1283–1312.

Kelley, S.A., Chapin, C.E., and Karlstrom, K.E., 2001, Laramide cooling histories of the Grand Canyon, Arizona and the Front Range, Colorado, determined from apatite fission-track thermochronology, *in* Young, R.A. and Spammer, E.E. eds., Colorado River: Origin and Evolution, Grand Canyon Association, p. 37–42.

Kerr, D.R., and Kidwell, S.M., 1991, Late Cenozoic sedimentation and tectonics, western Salton Trough, California, *in* Walawender, M.J., and Hanan, B.B., eds., Geological excursions in southern California and Mexico: Geological Society of America, National Meeting Guidebook: San Diego, San Diego State University, Department of Geological Sciences, p. 137–416.

Ketcham, R.A., 2005, Forward and Inverse Modeling of Low-Temperature Thermochronometry Data, *in* Reiners, P.W., and Ehlers, T.A., eds., Low-Temperature Thermochronology: Techniques, Interpretations, and Applications: Reviews in Mineralogy and Geochemistry, v. 58, p. 275–314.

Ketcham, R.A., Donelick, R.A., and Donelick, M.B., 2000, AFTSolve: A program for multi-kinetic modeling of apatite fission-track data: Geologic Materials Research 2, p. 1–32.

Lee, J.P., 2007, Cenozoic unroofing of the Grand Canyon region, Arizona [M.S. Thesis]: Lawrence, University of Kansas, 119 p.

Lipman, P.W., and Glazner, A.F., 1991, Introduction to middle Tertiary Cordilleran volcanism – Magma sources and relations to regional tectonics: Journal of Geophysical Research, v. 96, p. 13,193–13,199.

Lucchitta, I., 1972, Early History of the Colorado River in the Basin and Range Province: Geological Society of America Bulletin, v. 83, p. 1933–1948.

Lucchitta, I., 1989, History of the Grand Canyon and of the Colorado River in Arizona: Arizona Geological Society Digest, v. 17, p. 701–715.

Lucchitta, I., McDougall, K., Metzger, D.G., Morgan, P., Smith, G.R., and Chernoff, B., 2001, The Bouse Formation and Post-Miocene Uplift of the Colorado Plateau, *in* Young, R.A., and Spamer, E.E., eds., The Colorado River Origin and Evolution: Grand Canyon, Arizona, Grand Canyon Association Monograph No. 12, p. 173–179.

Ludwig, K.R., Isoplot/Ex 3.00. A geochronological toolkit for Microsoft Excel, Berkley Geochronological Center, Special Publication no. 4.

Meek, N., and Douglass, J., 2001, Lake Overflow: An Alternative Hypothesis for Grand Canyon Incision and Development of the Colorado River, *in* Young, R.A., and Spamer, E.E., eds., The Colorado River Origin and Evolution: Grand Canyon, Arizona, Grand Canyon Association Monograph No. 12, p. 199–204.

Meesters, AGCA, and Dunai, T.J., 2002a, Solving the production-diffusion for finite diffusion domains of various shapes Part I. Implications for low-temperature (U-Th)/He thermochronology: Chemical Geology, v. 186, p. 333–344.

Meesters, AGCA, and Dunai, T.J., 2002b, Solving the production-diffusion for finite diffusion domains of various shapes Part II. Application to cases with α-ejection and nonhomogeneous distribution of source: Chemical Geology, v. 186, p. 347–363.

Merriam, R., and Bandy, O.L., 1965, Source of upper Cenozoic sediments in Colorado Delta region: Journal of Sedimentary Petrology, v. 35, p. 911–916.

McKee, E.D., and McKee, E.H., 1972, Pliocene Uplift of the Grand Canyon Region—Time of Drainage Adjustment: Geological Society of America Bulletin, v. 83, p. 1,923–1,932.

McQuarrie, N., and Chase, C.G., 2000, Raising the Colorado Plateau: Geology, v. 28, p. 91–94.

Molnar, P., 2004, Late Cenozoic increase in accumulation rates of terrestrial sediment: How might climate change have affected erosion rates?: Annual Review of Earth and Planetary Science, v. 32, p. 67–80.

Molnar, P., and England, P., 1990, Late Cenozoic uplift of mountain ranges and global climate change: chicken or egg?: Nature, v. 346, p. 29–34.

Naeser, C.W., Duddy, I.R., Elston, D.P., Dumitru, T.A., and Green P.F., 2001, Fission-track analysis of apatite and zircon from Grand Canyon, Arizona, *in* Young, R.A., and Spamer, E.E., eds., The Colorado River Origin and Evolution: Grand Canyon, Arizona, Grand Canyon Association Monograph No. 12, p. 31–36.

Nelson, S.T., 1997, Reevaluation of the Central Colorado Plateau Laccoliths in the Light of New Age Determinations, *in* Friedman, J.D., and Huffman, A.C., eds., Laccolith Complexes of Southeastern Utah: Time of Emplacement and Tectonic Setting– Workshop Proceedings: U.S. Geological Survey Bulletin 2158, p. 37–39.

Nelson, S.T., Davidson, J.P., and Sullivan, K.R., 1992, New age determinations of central Colorado Plateau laccoliths, Utah: Recognizing disturbed K-Ar systematics and re-evaluating tectonomagmatic relationships: Geological Society of America Bulletin, v. 104, p. 1547–1560.

Nuccio, V.F., and Condon, S.M., 1996, Burial and Thermal History of the Paradox Basin, Utah and Colorado, and Petroleum Potential of the Middle Pennsylvanian Paradox Formation, Reston, Virginia: U.S. Geological Survey Bulletin 2000-O, p. O1–O41.

Oskin, M., and Stock, J., 2003, Pacific-North America Plate motion and opening of the Upper Delfin basin, northern Gulf of California, Mexico: Geological Society of America Bulletin, v. 115, p. 1,173–1,190.

Pang, M., and Nummedal, D., 1995, Flexural subsidence and basement tectonics of the Cretaceous Western Interior basin, United States: Geology, v. 23, p. 173–176.

Pederson, J.L., 2006, Weak bedrock, fast incision, deep exhumation, and flexural rebound in the central Colorado Plateau: A confluence of new datasets: Geological Society of America Abstracts with Programs, v. 38, no. 7, p. 282.

Pederson, J.L., Karlstrom, K., Sharp, W., and McIntosh, W., 2002a, Differential incision of the Grand Canyon related to Quaternary faulting – Constraints from U-series and Ar/Ar dating: Geology, v. 30, p. 739–742.

Pederson, J.L., Mackley, R.D., Eddleman, J.L., 2002b, Colorado Plateau uplift and

erosion – evaluated using GIS: GSA Today, v. 12, p. 4–10.

Pederson, J.L., and Hadder, K.W., 2005, Revisiting the Classic Conundrum of the Green River's Integration through the Uinta Uplift, *in* Dehler, C.M., Pederson, J.L., Sprinkel, D.A., and Kowallis, B.J., eds., Uinta Mountain geology: Utah Geologic Association Publication 33, p. 1–6.

Pederson, J.L., Callahan, C.N. and Roy, M., 2007, The central Colorado Plateau bullseye – linking patterns of quantified incision, exhumation, and flexure: Geological Society of America Abstracts with Programs, v. 39, no. 6, p. 184.

Pierce, H.W., Damon, P.E., and Shafiqullah, M., 1979, An Oligocene(?) Colorado Plateau edge in Arizona: Tectonophysics, v. 61, p. 1–24.

Potochnik, A.R., 2001, Paleogeomorphic evolution of the Salt River Region: Implications for Cretaceous-Laramide inheritance for ancestral Colorado River Drainage, *in* Young, R.A., and Spamer, E.E., eds., The Colorado River Origin and Evolution: Grand Canyon, Arizona, Grand Canyon Association Monograph No. 12, p. 17–24.

Poulson, S.R., and John, B.E., 2003, Stable isotope and trace element geochemistry of the basal Bouse Formation carbonate, southwestern United States: Implications for the Pliocene uplift history of the Colorado Plateau: Geological Society of America Bulletin, v. 115, p. 434–444.

Reiners, P.W., 2005, Zircon (U-Th)/He Thermochronometry: *in* Reiners, P.W., and Ehlers, T.A., eds., Low-Temperature Thermochronology: Techniques, Interpretations, and Applications: Reviews in Mineralogy and Geochemistry, v. 58, p. 151–176.

Reiners, P.W., Brady, R., Farley, K.A., Fryxell, J.E., Wernicke, B.P., and Lux, D., 2000, Helium and argon thermochronometry of the Gold Butte block, Virgin Mountains, Nevada: Earth and Planetary Science Letters, v. 178, p. 315–326.

Reiners, P.W., and Farley, K.A., 2001, Influence of crystal size on apatite (U-Th)/He thermochronology: an example from the Bighorn Mountains, Wyoming: Earth and Planetary Science Letters, v. 188, p. 413–420.

Remeika, P., Fischbein, I.W., and Fischbein, S.A., 1988, Lower Pliocene petrified wood from the Palm Springs Formation, Anza Borrego Desert State Park, California: Review of Palaeobotany and Palynology, v. 56, p. 183–198.

Roy, M., Jordan, T.H., and Pederson, J., 2009, Colorado Plateau magmatism and

uplift by warming of heterogeneous lithosphere: Nature (in press).

Ruddiman, W.F., and Kutzbach, J.E., 1989, Forcing of Late Cenozoic Northern Hemisphere climate by plateau uplift in southern Asia and the American West: Journal of Geophysical Research, v. 94, p. 18,379–18,391.

Shuster, D.L., and Farley, K.A., 2009, The influence of artificial radiation damage and thermal annealing on helium diffusion kinetics in apatite: Geochimica et Cosmochimica Acta, v. 73, p. 183–196.

Shuster, D.L., Flowers, R.M., and Farley, K.A., 2006, The influence of natural radiation damage on helium diffusion kinetics in apatite: Earth and Planetary Science Letters, v. 249, p. 148–161.

Spencer, J.E., 1996, Uplift of the Colorado Plateau due to lithospheric attenuation during Laramide low-angle subduction: Journal of Geophysical Research, v. 101, p. 13,595–13,609.

Spencer, J.E., and Patchett, P.J., 1997, Sr isotope evidence for a lacustrine origin for the upper Miocene to Pliocene Bouse Formation, lower Colorado River trough, and implications for timing of Colorado Plateau uplift: Geological Society of America Bulletin, v. 109, p. 767–778.

Spencer, J.E., Peters, L., McIntosh, W.C., and Patchett, P.J., 2001, 40Ar/39Ar Geochronology of the Hualapai Limestone and Bouse Formation and Implications for the Age of the Lower Colorado River, *in* Young, R.A., and Spamer, E.E., eds., The Colorado River Origin and Evolution: Grand Canyon, Arizona, Grand Canyon Association Monograph No. 12, p. 89–92.

Stockli D.F., 2005, Thermochronometric constraints on Tertiary erosional exhumation and incision of the Colorado Plateau− A progress report: Geological Society of America Abstracts with Programs, v. 37, no. 7, p. 109.

Stockli, D.F., Farley, K.A., and Dumitru, T.A., 2000, Calibration of the apatite (U-Th)/He thermochronometer on an exhumed fault block, White Mountains, California: Geology, v. 28, p. 983–986.

Stockli D.F., Bump, A.P., Davis, G., and Farley, K.A., 2002, Preliminary (U-Th)/He thermochronological constraints on timing and magnitude of Tertiary denudation of the Colorado Plateau, Utah: Geological Society of America Abstracts with Programs, v. 34, no. 6, p. 321.

Stokes, W.L., 1986, Geology of Utah: Salt Lake City, Occasional Paper Number 6 of

the Utah Museum of Natural History, 280 p.

Thompson, R.S., 1991, Pliocene environments and climates in the western United States: Quaternary Science Reviews, v. 10, p. 115–132.

Tikoff, B. and Maxson, J., 2001, Lithospheric buckling of the Laramide foreland during late Cretaceous and Paleogene, western United States: Rocky Mountain Geology, v. 36, p. 13–35.

Vermeesch, P., Seward, D., Latkoczy, C., Wipf, M., Gunther, D., and Baur, H., 2007, α -emitting mineral inclusions in apatite, their effect on (U-Th)/He ages, and how to reduce it: Geochimica et Cosmochimica Acta, v. 71, p. 1,737–1,746.

Winkler, G.R., 1970, Sedimentology and geomorphic significance of the Bishop Conglomerate and the Brown's Park Formation, Eastern Uinta Mountains, Utah, Colorado, and Wyoming [M.S. thesis], Salt Lake City, University of Utah, 115 p.

Walsh, P., and Schultz-Ela, D.D., 2003, Mechanics of graben evolution in Canyonlands National Park, Utah: Geological Society of America Bulletin, v. 115, p. 259–270.

Wolf, R.A., Farley, K.A., and Silver, L.T., 1996, Helium diffusion and low temperature thermochronometry of apatite: Geochimica et Cosmochimica Acta, v. 60, p. 4,231–4,240.

Wolf, R.A., Farley, K.A., and Silver, L.T., 1997, Assessment of (U-Th)/He thermochronometry: The low temperature history of the San Jacinto mountains, California: Geology, v. 25, p. 65–68.

Wolf, R.A., Farley, K.A., and Kass, D.M., 1998, Modeling of the low temperature sensitivity of the apatite (U-Th)/He thermochronometer: Chemical Geology, v. 148, p. 105–114.

Table 1. Apatite (U-Th)/He data

Sample	Age (Ma)	± 2σ (My)	U (ppm)	Th (ppm)	Sm (ppm)	eU (ppm)	Th/U	He (nmol/g)	Mass (µg)	Equiv. Sphere radius (µm)	Ft
Book Cliffs, Hay Canyon Vertical Transect											
07CP02-1	16.2	1.3	14.3	53.6	40.7	26.8	3.8	1.12	0.45	27.06	0.47
07CP02-2	13.4	1.1	5.7	43.0	27.1	15.7	7.6	0.58	0.59	29.13	0.49
07CP02-3*	41.0	3.3	45.8	67.9	49.8	61.7	1.5	7.71	0.97	33.05	0.56
07CP02-4	15.2	1.2	12.6	39.5	42.7	21.9	3.1	0.97	0.76	31.28	0.53
07CP02-5	20.6	1.6	11.7	37.8	38.5	20.6	3.2	1.18	0.59	29.54	0.51
07CP02-6	24.5	2.0	14.3	34.0	50.5	22.4	2.4	1.54	0.69	29.52	0.51
07CP03-1	22.4	1.8	17.6	30.1	37.9	24.7	1.7	1.97	2.32	43.56	0.65
07CP03-2	17.5	1.4	7.1	22.3	72.3	12.6	3.1	0.77	1.72	41.26	0.63
07CP03-3*	19.6	1.6	11.5	48.9	33.7	22.9	4.3	1.56	1.93	41.95	0.63
07CP03-4*	28.9	2.3	13.2	29.9	154.2	20.8	2.3	2.04	1.42	38.49	0.61
07CP03-5*	61.4	4.9	23.5	28.8	26.5	30.3	1.2	6.55	1.94	42.31	0.65
07CP03-6	26.8	2.1	54.5	149.2	313.0	90.4	2.7	9.22	3.47	50.24	0.69
07CP04-1	18.2	1.5	9.4	36.6	69.6	18.2	3.9	1.22	2.79	46.54	0.67
07CP04-2	21.9	1.8	30.2	202.9	184.9	77.8	6.7	6.34	2.83	48.14	0.67
07CP04-3	21.0	1.7	107.3	294.6	88.6	175.5	2.7	13.86	3.22	49.92	0.69
07CP04-4	15.4	1.2	5.8	23.9	38.8	11.5	4.1	0.66	2.70	47.52	0.67
07CP04-5	23.0	1.8	23.2	123.4	55.8	51.9	5.3	4.42	2.94	48.03	0.67
07CP04-6	18.3	1.5	11.4	27.0	29.0	17.7	2.4	1.19	2.38	46.50	0.67
07CP05-1	15.1	1.2	4.3	37.0	37.1	12.9	8.7	0.62	1.11	35.80	0.57
07CP05-2	20.4	1.6	7.5	30.5	46.5	14.7	4.1	1.04	1.72	41.71	0.63
07CP05-3	15.1	1.2	7.6	39.5	58.2	17.0	5.2	0.83	1.17	36.46	0.58
07CP05-4*	56.1	4.5	2.5	18.4	53.0	7.0	7.3	1.44	2.44	44.65	0.65
07CP05-5	25.8	0.2	103.8	302.0	85.5	173.8	2.9	15.57	1.90	41.88	0.63
07CP05-6	16.6	0.6	19.3	37.9	110.2	28.6	2.0	1.79	2.99	48.44	0.68
07CP06-1	23.9	0.8	12.9	20.0	58.8	17.8	1.5	1.56	2.43	45.89	0.67
07CP06-2*	43.4	0.9	34.6	87.2	119.4	55.3	2.5	8.45	1.87	42.63	0.64
07CP06-3	23.6	0.3	36.8	74.8	67.0	54.3	2.0	4.61	2.47	44.80	0.66
07CP06-4	22.3	0.6	12.7	24.0	20.4	18.3	1.9	1.43	1.79	42.21	0.64
07CP06-5	17.3	0.8	14.2	11.9	39.1	17.1	0.8	0.96	1.15	35.82	0.60
07CP06-6	11.2	0.5	4.1	30.7	48.1	11.4	7.4	0.46	2.04	44.37	0.65
07CP07-1	6.9	0.1	14.0	41.5	15.6	23.6	3.0	0.55	1.68	39.97	0.62
07CP07-2	29.1	4.3	2.0	12.0	75.3	5.1	6.1	0.52	1.59	39.02	0.61
07CP07-3	18.5	0.2	32.6	166.8	60.0	71.3	5.1	4.95	2.87	49.39	0.68
07CP07-4	18.9	0.1	81.1	276.1	36.6	144.8	3.4	8.71	1.12	36.05	0.58
07CP07-5	19.4	0.1	68.5	269.8	37.7	130.8	3.9	9.18	2.49	45.99	0.66
07CP07-6	13.1	0.1	92.6	78.7	77.8	111.1	0.9	4.74	1.19	36.16	0.60
07CP08-1	11.3	1.1	1.9	11.5	23.7	4.7	6.0	0.19	1.75	42.11	0.63
07CP08-2	11.8	0.2	25.8	56.2	55.7	39.1	2.2	1.55	1.54	39.06	0.61
07CP08-3	12.0	0.2	25.4	177.6	131.1	66.9	7.0	2.73	1.49	40.14	0.61
07CP08-4	10.2	0.1	24.8	106.5	60.8	49.6	4.3	1.80	2.33	44.14	0.65
07CP08-5	17.4	0.6	36.5	88.5	234.1	58.0	2.4	3.65	1.97	44.38	0.65
07CP08-6	20.8	0.3	28.1	32.8	24.5	35.8	1.2	2.53	1.70	39.48	0.62
07CP09-1	14.5	0.4	12.5	61.3	75.9	27.0	4.9	1.43	2.44	46.44	0.66

Table 1 cont.

Sample	Age (Ma)	± 2σ (My)	U (ppm)	Th (ppm)	Sm (ppm)	eU (ppm)	Th/U	He (nmol/g)	Mass (µg)	Equiv. Sphere radius (µm)	Ft
Book Cliffs, Hay Canyon Vertical Transect cont.											
07CP09-2	12.1	0.1	52.2	162.4	117.0	90.1	3.1	4.11	3.38	50.41	0.69
07CP09-3	1.5	0.0	77.3	228.8	195.3	130.9	3.0	0.69	2.40	43.83	0.65
07CP09-4	9.4	0.2	7.8	44.2	15.1	18.0	5.7	0.61	2.32	44.47	0.65
07CP09-5	22.6	1.7	4.5	24.5	100.3	10.7	5.4	0.97	4.29	55.60	0.71
07CP09-6	11.3	0.3	14.1	34.3	51.9	22.3	2.4	0.92	2.52	46.80	0.67
07CP10-1	18.3	0.6	28.0	93.0	145.3	50.2	3.3	2.58	0.70	29.74	0.51
07CP10-2	7.2	0.1	61.6	119.7	121.9	89.7	1.9	2.09	1.17	36.37	0.59
07CP10-3	5.5	0.6	3.4	24.7	21.8	9.2	7.2	0.14	0.72	30.63	0.51
07CP10-4*	961.6	190.7	1.6	18.6	23.1	6.0	11.6	16.69	0.65	30.21	0.51
07CP10-5	12.0	1.5	1.8	22.2	24.3	7.0	12.2	0.24	0.78	31.31	0.52
07CP10-6*	23.5	0.3	221.4	410.1	370.6	317.7	1.9	22.47	0.85	32.67	0.55
07CP11-1	12.8	0.2	7.9	44.9	25.7	18.4	5.7	0.87	2.64	48.48	0.67
07CP11-2	11.2	0.2	21.8	55.6	34.2	34.8	2.6	1.30	1.38	38.83	0.61
07CP11-3	10.8	0.7	13.5	42.1	92.1	23.7	3.1	0.91	1.89	42.97	0.64
07CP11-4	9.6	0.6	25.1	54.7	105.6	38.2	2.2	1.25	1.49	39.76	0.62
07CP11-5	14.3	0.9	4.9	25.9	32.6	11.1	5.2	0.50	0.99	34.76	0.57
07CP11-6	16.9	1.0	25.8	104.8	35.7	50.1	4.1	3.01	2.15	43.89	0.65
07CP13-1	6.7	0.4	18.7	78.9	54.4	37.2	4.2	0.76	0.94	33.86	0.56
07CP13-2	6.4	0.4	20.7	78.8	54.4	39.1	3.8	0.77	1.01	34.37	0.56
07CP13-3	12.1	0.7	9.4	86.4	80.2	29.7	9.2	1.11	0.89	33.84	0.55
07CP13-4	11.7	0.7	15.3	81.3	157.2	34.8	5.3	1.22	0.81	32.53	0.54
07CP13-5	5.6	0.3	19.0	95.5	23.7	41.1	5.0	0.66	0.79	31.19	0.52
07CP13-6	15.8	0.9	19.7	98.4	64.6	42.6	5.0	1.99	0.83	32.17	0.54
07CP14-1	7.2	0.4	10.0	35.5	44.5	18.4	3.5	0.42	1.18	36.21	0.58
07CP14-2	10.9	0.7	3.0	11.9	22.6	5.9	3.9	0.22	1.59	39.72	0.62
07CP14-3	7.4	0.4	10.9	36.1	37.3	19.4	3.3	0.41	0.80	30.95	0.52
07CP14-4*	32.0	1.9	29.0	183.4	76.1	71.6	6.3	7.38	1.24	36.75	0.58
07CP14-5	6.2	0.4	18.2	86.0	96.9	38.4	4.7	0.75	0.98	34.87	0.57
07CP14-6	6.1	0.4	6.3	43.3	69.9	16.6	6.9	0.30	0.75	31.84	0.53
Book Cliffs, Sego Canyon Vertical Transect											
07CP15-1	26.9	1.6	8.8	34.8	128.6	17.4	4.0	1.35	0.70	30.14	0.51
07CP15-2	37.4	2.2	17.5	34.3	69.1	25.8	2.0	3.37	1.87	41.89	0.64
07CP15-3	37.5	2.3	8.3	7.1	35.0	10.1	0.8	1.43	2.41	47.39	0.68
07CP15-4	37.5	2.3	6.1	6.2	46.6	7.8	1.0	1.04	1.93	41.01	0.64
07CP15-5	33.4	2.0	15.9	63.5	221.0	31.6	4.0	3.78	2.14	42.88	0.64
07CP15-6	24.7	1.5	11.2	55.3	18.1	24.0	5.0	1.89	1.25	36.35	0.58
07CP16-1	18.2	1.1	46.1	90.4	66.3	67.3	2.0	3.65	0.79	32.15	0.55
07CP16-2	27.3	1.6	20.7	27.3	212.4	28.1	1.3	2.65	1.37	39.08	0.62
07CP16-3	17.6	1.1	21.3	88.5	156.7	42.4	4.2	2.42	1.21	36.46	0.58
07CP16-4	17.5	1.0	8.5	54.4	92.4	21.4	6.4	0.98	0.50	27.35	0.47
07CP16-5*	162.1	9.7	10.4	27.2	15.3	16.8	2.6	7.76	0.78	30.33	0.52
07CP16-6	20.6	1.2	24.9	228.5	190.4	78.4	9.2	4.86	0.96	32.89	0.54
07CP18-1	19.7	1.2	31.0	64.5	68.0	46.2	2.1	2.61	0.69	30.48	0.52

Table 1 cont.

Sample	Age (Ma)	± 2σ (My)	U (ppm)	Th (ppm)	Sm (ppm)	eU (ppm)	Th/U	He (nmol/g)	Mass (µg)	Equiv. Sphere radius (µm)	Ft
Book Cliffs, Sego Canyon Vertical Transect cont.											
07CP18-2	20.3	1.2	16.6	74.3	14.9	33.8	4.5	2.08	0.99	33.54	0.55
07CP18-3*	51.0	3.1	4.1	30.0	90.4	11.4	7.4	1.88	1.37	35.62	0.57
07CP18-4	19.4	1.2	40.8	68.6	62.9	56.9	1.7	3.30	0.79	32.37	0.55
07CP18-5	19.1	1.1	47.4	129.3	69.2	77.5	2.7	5.10	1.59	41.04	0.63
07CP18-6	13.3	0.8	65.4	26.2	72.7	71.8	0.4	3.42	2.00	42.91	0.66
07CP19-1	11.3	0.7	57.5	60.3	36.2	71.6	1.0	2.37	0.70	30.99	0.54
07CP19-2	19.0	1.1	19.3	45.0	56.2	30.0	2.3	1.72	0.98	32.69	0.55
07CP19-3	33.2	2.0	69.7	70.4	92.4	86.4	1.0	10.47	2.52	45.69	0.67
07CP19-4	37.6	2.3	26.4	60.1	40.1	40.5	2.3	5.24	1.80	41.06	0.63
07CP19-5	17.3	1.0	45.0	62.1	108.7	59.8	1.4	3.52	1.56	39.72	0.62
07CP19-6*	90.3	5.4	34.9	44.3	32.6	45.2	1.3	12.64	0.94	33.62	0.57
07CP20-1	29.3	1.8	82.5	235.5	71.1	137.0	2.9	14.13	2.19	42.99	0.64
07CP20-2	23.1	1.4	9.4	8.5	86.4	11.8	0.9	1.05	2.93	49.22	0.69
07CP20-3	11.0	0.7	14.8	33.2	34.7	22.6	2.2	0.79	1.02	35.39	0.58
07CP20-4	10.5	0.6	15.4	31.8	62.9	23.0	2.1	0.74	1.00	33.00	0.55
07CP20-5	21.5	1.3	12.8	5.5	58.5	14.3	0.4	0.94	0.81	31.57	0.56
07CP20-6*	20.4	1.2	222.9	538.3	101.3	347.3	2.4	21.28	0.93	32.89	0.55
07CP21-1	10.9	0.7	11.1	65.4	108.9	26.7	5.9	0.87	0.85	32.57	0.54
07CP21-2	48.4	2.9	5.6	13.3	25.1	8.8	2.4	1.60	2.56	48.42	0.68
07CP21-3	133.7	8.0	1.7	7.1	24.3	3.4	4.3	1.52	1.18	36.95	0.59
07CP21-4	51.8	3.1	9.4	28.1	46.2	16.1	3.0	2.97	2.05	43.55	0.65
07CP21-5	9.6	0.6	3.4	15.7	59.6	7.3	4.7	0.23	1.15	36.04	0.58
07CP21-6	15.6	0.9	2.2	12.7	34.7	5.3	5.8	0.26	1.02	34.73	0.56
07CP22-1	22.6	1.4	5.8	73.3	124.5	23.3	12.6	1.70	1.21	36.13	0.58
07CP22-2	16.2	1.0	1.5	14.8	64.5	5.2	10.0	0.27	1.13	34.99	0.56
07CP22-3	21.3	1.3	33.0	128.7	145.4	63.3	3.9	4.69	1.86	41.77	0.63
07CP22-4	10.0	0.6	2.3	21.1	66.8	7.5	9.1	0.22	0.70	30.64	0.51
07CP22-5	10.5	0.6	3.2	17.7	61.5	7.6	5.4	0.25	1.01	34.69	0.56
07CP22-6	8.6	0.5	3.3	19.3	78.6	8.2	5.8	0.21	0.81	31.54	0.53
07CP23-1	11.7	0.7	36.9	29.9	78.6	44.2	0.8	1.77	1.42	39.26	0.63
07CP23-2	14.7	0.9	7.1	44.8	40.9	17.6	6.3	0.91	2.08	42.74	0.64
07CP23-3	12.9	0.8	15.4	43.2	77.3	25.7	2.8	1.03	0.88	33.98	0.56
07CP23-4	9.9	0.6	4.2	27.3	66.8	10.8	6.5	0.32	0.80	31.69	0.53
07CP23-5	29.2	1.8	5.8	22.9	17.2	11.1	4.0	1.16	2.18	44.10	0.65
07CP23-6	21.8	1.3	22.2	38.3	101.7	31.6	1.7	2.63	3.32	50.74	0.70
07CP24-1	37.0	2.2	7.1	12.4	121.5	10.6	1.7	1.40	1.62	41.41	0.64
07CP24-2	26.5	1.6	12.3	53.8	163.4	25.5	4.4	2.36	1.59	41.11	0.63
07CP24-3	21.7	1.3	236.4	11.6	3.6	239.1	0.0	17.78	1.59	38.26	0.64
07CP24-4	21.2	1.3	20.7	40.9	80.5	30.6	2.0	2.12	1.36	37.11	0.60
07CP25-1	9.6	0.6	8.8	31.1	54.5	16.2	3.5	0.53	1.40	39.10	0.61
07CP25-2	8.3	0.5	20.9	79.3	81.6	39.5	3.8	1.06	1.18	36.74	0.59
07CP25-3	48.0	2.9	46.0	82.4	43.8	65.2	1.8	11.74	2.77	49.18	0.69
07CP25-4	9.1	0.5	9.4	36.6	45.6	18.0	3.9	0.63	3.23	51.75	0.70

Table 1 cont.

Sample	Age (Ma)	± 2σ (My)	U (ppm)	Th (ppm)	Sm (ppm)	eU (ppm)	Th/U	He (nmol/g)	Mass (µg)	Equiv. Sphere radius (µm)	Ft
Book Cliffs, Sego Canyon Vertical Transect cont.											
07CP25-5	36.1	2.2	7.2	39.9	67.9	16.7	5.6	2.16	1.93	43.97	0.65
07CP25-6	37.3	2.2	8.7	32.6	44.6	16.4	3.7	2.08	1.53	39.80	0.62
07CP35-1	11.3	0.7	11.4	34.1	62.4	19.6	3.0	0.68	0.93	33.24	0.55
07CP35-2	13.9	0.8	12.8	37.6	22.2	21.6	2.9	0.94	1.20	35.37	0.58
07CP35-3	13.5	0.8	24.4	69.7	70.8	40.8	2.9	1.67	1.02	33.07	0.55
07CP35-4	16.7	1.0	32.7	83.8	61.2	52.3	2.6	2.66	0.87	33.42	0.56
07CP35-5	8.5	0.5	2.8	14.5	42.8	6.4	5.2	0.18	1.42	39.23	0.61
07CP35-6	8.1	0.5	3.6	19.2	21.9	8.1	5.4	0.22	1.38	38.84	0.61
Book Cliffs, Blaze Canyon Vertical Transect											
07CP27-1	28.6	1.7	36.9	215.5	75.4	86.9	5.8	10.19	5.82	63.15	0.74
07CP27-2*	15.8	0.9	11.2	38.9	16.8	20.3	3.5	1.19	2.79	48.91	0.68
07CP27-3*	52.4	3.1	47.0	197.8	106.3	93.1	4.2	14.85	0.95	33.52	0.55
07CP27-4	35.7	2.1	27.7	78.4	141.1	46.5	2.8	5.47	1.36	37.52	0.60
07CP27-5*	22.4	1.3	36.6	51.3	26.2	48.6	1.4	3.67	1.47	39.09	0.62
07CP27-6	33.9	2.0	19.0	78.6	53.9	37.4	4.1	4.07	1.25	36.45	0.58
07CP28-1	14.3	0.4	26.4	171.7	0.2	66.0	6.5	3.02	1.19	36.34	0.58
07CP28-2	9.1	0.9	2.0	87.6	0.5	22.2	43.7	0.62	1.04	34.82	0.56
07CP28-3	17.0	0.1	83.2	1278.2	0.2	377.5	15.4	18.80	0.88	32.23	0.53
07CP28-4	9.9	2.5	1.1	27.4	0.2	7.4	25.7	0.23	1.23	35.46	0.57
07CP28-5	9.5	0.5	14.2	149.4	0.1	48.5	10.6	1.43	1.06	34.73	0.56
07CP28-6	18.8	0.3	43.3	661.2	0.2	195.5	15.3	10.68	0.89	31.88	0.53
07CP29-1†	25.5	0.4	24.1	73.1	83.1	41.3	3.0	3.31	6.32	48.49	0.57
07CP29-2†	13.2	0.4	9.3	49.6	67.3	21.1	5.3	0.80	4.09	42.33	0.52
07CP29-3†	14.3	0.3	11.6	64.3	62.8	26.7	5.6	1.04	3.44	39.99	0.50
07CP30-1	10.5	0.3	11.9	343.0	0.6	90.8	28.9	2.77	0.81	31.67	0.52
07CP30-2	11.2	0.2	21.2	201.6	0.2	67.6	9.5	2.54	1.71	40.01	0.61
07CP30-3*	27.5	0.4	20.0	283.0	0.9	85.1	14.2	8.29	2.19	43.83	0.64
07CP30-4	11.5	0.2	23.5	266.4	0.1	84.9	11.3	3.26	1.59	39.32	0.61
07CP30-5	11.3	0.3	22.5	198.9	0.2	68.3	8.9	2.48	1.15	36.91	0.58
07CP30-6	3.4	0.1	3.2	161.4	0.1	40.3	50.6	0.46	1.30	38.31	0.59
07CP31-1	10.0	1.1	4.3	12.6	28.3	7.4	2.9	0.23	1.01	34.76	0.57
07CP31-2	16.5	0.4	25.3	72.6	71.2	42.3	2.9	2.12	0.89	33.20	0.55
07CP31-3	21.8	0.3	85.0	127.6	125.2	115.0	1.5	7.59	0.84	32.68	0.55
07CP31-4	12.1	0.5	12.7	34.3	32.7	20.8	2.7	0.80	1.02	35.79	0.58
07CP31-5	4.2	0.2	9.2	38.1	14.9	18.0	4.1	0.23	0.85	33.32	0.55
07CP31-6	10.5	0.5	11.7	34.8	81.5	20.1	3.0	0.68	1.17	35.56	0.58
07CP32-1	7.8	0.4	12.8	33.6	70.8	20.9	2.6	0.48	0.83	31.60	0.54
07CP32-2	14.9	0.9	6.5	53.3	110.2	19.3	8.2	0.94	1.14	36.61	0.58
07CP32-3	17.0	1.1	11.4	43.4	104.4	21.9	3.8	1.07	0.70	30.51	0.52
07CP32-4	22.5	2.1	6.9	27.2	72.4	13.6	3.9	0.91	0.76	32.02	0.54
07CP32-5	9.9	0.6	8.6	41.2	76.2	18.5	4.8	0.55	0.91	32.77	0.54
07CP32-6	2.1	0.1	41.6	102.2	189.3	66.0	2.5	0.43	0.85	33.12	0.55

Table 1 cont.

Sample	Age (Ma)	± 2σ (My)	U (ppm)	Th (ppm)	Sm (ppm)	eU (ppm)	Th/U	He (nmol/g)	Mass (µg)	Equiv. Sphere radius (µm)	Ft
Book Cliffs, Tusher Canyon											
07CP63-1	5.7	0.3	19.3	60.7	81.6	33.7	3.1	0.55	0.74	30.80	0.52
07CP63-2	13.1	0.8	7.7	22.6	36.8	13.1	2.9	0.48	0.68	29.68	0.51
07CP63-3	3.7	0.2	13.2	42.1	25.2	23.0	3.2	0.24	0.69	30.92	0.52
07CP63-4	18.7	1.1	1.9	10.4	47.5	4.5	5.6	0.24	0.59	29.75	0.50
07CP63-5	4.9	0.3	9.5	50.6	85.5	21.5	5.4	0.31	0.75	31.17	0.52
07CP63-6*	31.6	1.9	0.7	9.2	43.4	3.0	13.4	0.26	0.49	27.52	0.47
07CP65-1*	3.3	0.2	2.0	11.0	13.6	4.6	5.6	0.05	1.51	38.37	0.60
07CP65-2	8.5	0.5	4.2	22.3	33.0	9.5	5.3	0.27	1.49	39.18	0.61
07CP65-3	7.5	0.5	21.2	56.1	61.8	34.4	2.7	0.86	1.37	38.11	0.60
07CP65-4	19.9	1.2	6.6	24.6	33.5	12.4	3.8	0.82	1.33	38.04	0.60
07CP65-5	15.2	0.9	9.8	31.3	41.7	17.2	3.2	0.87	1.62	38.96	0.61
07CP65-6	12.5	0.8	13.0	31.2	59.5	20.5	2.4	0.77	0.78	32.15	0.54
Between Book Cliffs and Canyonlands											
07CP40-1	28.5	1.7	18.1	56.6	42.4	31.33	3.1	2.59	0.79	31.25	0.53
07CP40-2	23.4	1.4	34.1	25.0	216.2	40.98	0.7	3.76	3.40	52.37	0.71
07CP40-3	5.9	0.4	4.5	31.8	66.4	12.15	7.1	0.25	1.59	41.10	0.62
07CP40-4	7.8	0.5	2.3	9.3	46.4	4.67	4.1	0.13	2.04	41.92	0.63
07CP40-5	32.0	1.9	7.7	35.1	32.8	15.94	4.6	1.95	3.25	51.62	0.69
07CP40-6	8.7	0.5	10.4	3.2	17.7	11.21	0.3	0.33	1.30	38.43	0.63
07CP42-1	15.0	0.9	10.9	70.0	81.9	27.45	6.4	1.59	3.34	51.96	0.69
07CP42-2*	90.4	5.4	3.2	61.2	46.9	17.54	19.1	5.81	2.39	46.28	0.66
07CP42-3	9.5	0.6	3.1	44.9	54.7	13.72	14.5	0.48	2.65	45.59	0.65
07CP42-4	4.5	0.3	9.3	96.3	109.2	32.02	10.3	0.52	2.45	44.95	0.65
07CP42-5	6.0	0.4	4.5	77.5	143.6	23.08	17.1	0.46	1.30	37.99	0.59
07CP42-6	5.5	0.3	18.1	141.8	97.1	51.19	7.9	0.84	0.82	32.54	0.54
07CP48-1	21.1	1.3	20.5	65.5	32.2	35.75	3.2	2.26	0.85	32.77	0.55
07CP48-2*	2.9	0.2	0.0	12.5	8.1	2.90	-527.5	0.03	1.05	34.74	0.56
07CP48-3*	122.4	7.3	8.8	20.4	7.7	13.52	2.3	4.64	0.73	29.72	0.51
07CP48-4	18.6	1.1	6.8	13.5	4.5	9.93	2.0	0.51	0.59	29.40	0.51
07CP48-5	14.0	0.8	36.3	45.0	47.5	46.94	1.2	1.86	0.61	29.73	0.52
07CP48-6	25.3	1.5	38.6	16.4	36.8	42.55	0.4	3.17	0.70	30.45	0.54
07CP51-1	12.3	0.7	22.6	60.6	28.8	36.71	2.7	1.33	0.80	32.15	0.54
07CP51-2	8.9	0.5	8.6	56.3	40.7	21.79	6.5	0.55	0.66	30.22	0.51
07CP51-3	19.5	1.2	0.9	12.5	36.3	3.96	14.1	0.28	1.87	42.96	0.63
07CP51-4*	65.7	3.9	-0.2	0.9	-2.5	-0.06	-3.6	-0.01	1.63	41.28	0.60
07CP51-5	6.9	0.4	7.1	36.9	57.3	15.84	5.2	0.37	1.50	39.88	0.61
07CP51-6*	267.8	16.1	0.1	3.0	-2.7	0.74	44.7	0.62	1.05	35.45	0.57
Canyonlands Vertical Transect, Shafer Trail											
07CP53-1	37.8	2.3	8.2	35.5	106.8	16.9	4.4	2.09	1.30	36.73	0.59
07CP53-2	27.3	0.5	26.1	120.0	91.9	54.2	4.6	4.54	1.03	33.81	0.56
07CP53-3	23.2	0.4	27.6	42.5	52.1	37.6	1.5	2.94	1.47	38.99	0.62
07CP53-4	23.7	0.4	57.6	53.9	114.7	70.6	0.9	5.23	1.04	33.87	0.57
07CP53-5	20.3	1.0	8.5	29.3	58.6	15.6	3.4	1.04	1.24	37.13	0.59
07CP53-6	8.6	0.6	7.3	56.7	96.2	20.8	7.8	0.49	0.63	28.87	0.49

Table 1 cont.

Sample	Age (Ma)	± 2σ (My)	U (ppm)	Th (ppm)	Sm (ppm)	eU (ppm)	Th/U	He (nmol/g)	Mass (µg)	Equiv. Sphere radius (µm)	Ft
Canyonlands Vertical Transect, Shafer Trail cont.											
07CP54-1	19.1	1.3	16.2	80.9	278.9	36.2	5.0	2.02	0.68	30.83	0.52
07CP54-2	5.4	0.5	8.7	16.6	52.2	12.7	1.9	0.19	0.58	29.57	0.51
07CP54-3	15.4	0.5	22.3	49.4	68.1	34.1	2.2	1.55	0.72	31.75	0.54
07CP54-4	9.1	2.3	1.6	9.1	25.0	3.8	5.7	0.10	0.71	31.34	0.53
07CP54-5	23.1	0.5	38.7	39.7	50.1	48.1	1.0	3.28	0.85	31.27	0.54
07CP54-6*	4.1	0.2	44.9	87.1	285.8	66.4	1.9	0.83	0.93	32.27	0.55
07CP55a-1	18.2	0.2	110.5	47.7	73.7	121.8	0.4	7.14	1.22	34.76	0.59
07CP55a-2	14.7	0.4	6.0	60.6	41.7	20.2	10.0	0.97	1.45	37.80	0.59
07CP55a-3*	25.9	1.1	12.9	51.6	113.6	25.4	4.0	2.07	1.16	34.87	0.57
07CP55a-4	14.5	0.2	22.4	23.7	16.7	27.9	1.1	1.48	2.36	46.33	0.68
07CP55a-5	14.6	0.4	18.7	39.1	54.7	27.9	2.1	1.26	0.98	33.82	0.56
07CP55a-6	19.2	1.0	6.9	29.7	66.8	14.1	4.3	0.90	1.45	38.14	0.60
07CP56-1†	17.0	1.0	11.9	17.2	41.1	16.1	1.4	0.94	10.46	57.92	0.62
07CP56-2†	32.7	2.0	14.1	25.1	44.4	20.1	1.8	2.48	17.80	69.02	0.69
07CP56-3†	30.0	1.8	28.1	41.8	64.8	38.1	1.5	4.28	16.04	66.69	0.68
07CP57a-1*	28.2	5.9	0.0	15.9	29.4	3.8	466.9	0.32	0.78	31.33	0.52
07CP57a-2	16.3	0.7	12.4	62.9	33.1	27.1	5.1	1.24	0.63	30.13	0.51
07CP57a-3	16.8	0.5	39.7	183.6	246.1	83.1	4.6	3.92	0.63	29.84	0.51
07CP57a-4*	0.2	0.0	7.5	37.7	51.2	16.4	5.0	0.01	0.84	32.14	0.54
07CP57a-5	20.7	0.5	27.3	49.9	51.1	39.1	1.8	2.47	0.88	33.28	0.56
07CP57a-6	20.9	0.2	91.2	66.0	46.9	106.6	0.7	6.98	0.91	33.90	0.58
07CP58-1	12.3	0.7	12.0	46.3	23.8	22.8	3.9	0.77	0.60	29.35	0.50
07CP58-2	20.3	1.2	77.9	80.1	63.9	96.6	1.0	5.07	0.42	26.50	0.48
07CP58-3	23.0	1.4	46.2	125.6	44.0	75.4	2.7	5.09	0.76	31.84	0.54
07CP58-4	8.3	0.5	1.8	13.9	60.9	5.3	7.6	0.12	0.56	28.37	0.48
07CP58-5	9.2	0.6	13.8	47.6	30.9	24.9	3.5	0.55	0.39	25.44	0.44
07CP58-6*	1169.1	70.1	23.1	52.7	44.7	35.5	2.3	111.96	0.47	27.01	0.47
07CP59a-1	15.6	0.9	15.8	21.7	87.0	21.2	1.4	0.98	0.72	31.31	0.54
07CP59a-2	15.0	1.7	2.6	21.0	34.1	7.6	8.2	0.34	0.80	31.89	0.53
07CP59a-3*	27.5	2.7	7.1	7.1	38.8	8.9	1.0	0.76	0.81	32.90	0.56
07CP59a-4	11.6	2.3	2.5	8.2	65.2	4.8	3.2	0.18	0.86	33.54	0.56
07CP59a-5	8.1	0.6	3.9	51.5	91.1	16.2	13.3	0.37	0.59	29.62	0.50
07CP59a-6	12.1	0.7	7.0	29.4	24.8	13.9	4.2	0.50	0.82	32.60	0.54
07CP60a-1	8.8	0.9	3.1	24.4	74.6	9.1	7.9	0.24	0.85	31.89	0.53
07CP60a-2*	3.1	0.7	0.7	11.2	3.1	3.3	15.6	0.03	0.83	32.61	0.54
07CP60a-3	17.4	1.5	4.7	37.1	64.1	13.6	7.9	0.66	0.61	29.75	0.50
07CP60a-4	8.5	0.7	7.4	28.3	37.2	14.1	3.8	0.33	0.64	29.17	0.50
07CP60a-5*	1069.5	151.3	5.4	10.0	10.3	7.7	1.8	24.87	0.65	30.59	0.53
07CP60a-6*	81.0	1.7	31.1	66.0	23.0	46.5	2.1	11.08	0.76	31.71	0.54
07CP61-1	17.2	1.0	16.9	34.6	40.9	25.1	2.0	1.51	2.21	42.34	0.64
07CP61-2	10.8	0.6	5.7	16.9	40.8	9.8	2.9	0.40	3.10	50.00	0.69
07CP61-3	17.1	1.0	23.1	56.5	26.4	36.2	2.4	2.04	1.27	37.86	0.60
07CP61-4	16.3	1.0	49.4	65.2	97.8	64.9	1.3	3.89	2.29	46.71	0.68

Table 1 cont.

Sample	Age (Ma)	± 2σ (My)	U (ppm)	Th (ppm)	Sm (ppm)	eU (ppm)	Th/U	He (nmol/g)	Mass (µg)	Equiv. Sphere radius (µm)	Ft
Canyonlands Vertical Transect, Shafer Trail cont.											
07CP61-5	24.1	1.4	4.4	28.1	188.0	11.8	6.3	1.11	2.72	48.78	0.68
07CP61-6	17.2	1.0	4.7	22.2	29.5	10.0	4.7	0.58	1.70	39.98	0.62
07CP62a-1	13.5	1.8	1.8	15.1	4.1	5.3	8.5	0.22	0.93	33.74	0.55
07CP62a-2*	5.2	1.2	1.1	19.0	12.4	5.6	16.9	0.07	0.49	27.73	0.47
07CP62a-3	22.2	0.8	15.0	31.0	23.4	22.2	2.1	1.54	0.91	34.36	0.57
07CP62a-4	24.3	1.4	14.8	21.5	20.6	19.9	1.4	1.36	0.61	29.52	0.52
07CP62a-5	13.5	2.4	1.7	15.0	15.9	5.2	9.0	0.21	0.72	31.71	0.53
07CP62a-6	14.4	2.3	3.3	14.5	8.3	6.7	4.4	0.28	0.66	30.63	0.52
Canyonlands Vertical Transect, Lathrop Canyon											
08CP69-1*	17.0	0.1	149.0	88.7	74.9	169.8	0.6	9.98	1.93	40.22	0.64
08CP69-2	20.4	0.3	26.1	88.1	48.1	46.7	3.4	3.25	1.57	40.67	0.62
08CP69-3	25.4	0.6	28.9	15.7	62.3	32.8	0.5	2.78	1.22	37.19	0.61
08CP69-4	20.1	0.5	24.3	18.8	52.5	28.9	0.8	2.01	1.56	40.47	0.64
08CP69-5	18.0	0.3	45.5	26.0	65.8	51.8	0.6	3.28	1.74	41.30	0.65
08CP69-6*	58.0	0.9	39.0	37.9	36.9	47.9	1.0	8.89	1.16	35.19	0.59
08CP70-1	14.4	0.2	68.2	265.8	161.6	130.2	3.9	5.32	0.74	30.61	0.52
08CP70-2	17.7	0.5	18.1	98.3	111.6	41.2	5.4	2.12	0.79	31.30	0.53
08CP70-3	4.5	0.4	2.2	45.1	99.3	13.0	20.9	0.17	0.70	30.69	0.51
08CP70-4	21.6	0.4	28.0	116.8	62.2	55.2	4.2	3.47	0.79	31.54	0.53
08CP70-5	15.5	0.7	19.1	56.0	148.0	32.8	2.9	1.55	0.85	32.97	0.55
08CP70-6*	104.1	1.4	83.0	92.7	85.1	104.8	1.1	30.66	0.57	29.22	0.52
08CP71-1	16.7	1.3	10.5	43.9	53.0	20.8	4.2	1.30	3.12	49.16	0.68
08CP71-2	22.2	1.8	56.0	398.3	165.6	148.5	7.1	11.75	2.01	44.44	0.65
08CP71-3	41.5	3.3	10.6	37.3	62.4	19.5	3.5	2.62	1.28	36.44	0.59
08CP71-4	24.5	2.0	150.0	70.8	95.5	166.8	0.5	13.12	1.17	34.93	0.59
08CP71-5*	87.4	7.0	26.3	132.5	164.5	57.6	5.0	15.91	1.05	35.18	0.57
08CP71-6	10.8	0.9	11.1	34.3	69.3	19.4	3.1	0.69	1.21	37.13	0.59
Canyonlands, North of confluence											
08CP66-1	25.0	1.8	4.9	36.5	106.4	13.9	7.4	1.15	1.19	37.37	0.59
08CP66-2	17.6	0.4	13.0	20.9	27.5	17.9	1.6	1.11	2.06	42.88	0.65
08CP66-3	14.3	0.4	12.8	69.2	58.2	29.0	5.4	1.27	0.90	33.86	0.56
08CP66-4*	46.6	1.5	13.5	34.2	30.9	21.5	2.5	3.18	1.12	35.48	0.58
08CP66-5	14.9	0.3	38.7	86.8	65.5	59.0	2.2	2.63	0.82	32.45	0.55
08CP66-6	21.1	0.3	28.6	23.8	22.3	34.2	0.8	2.56	1.74	42.55	0.65
08CP72-1	15.2	1.2	72.7	45.2	35.3	83.3	0.6	3.46	0.49	27.83	0.50
08CP72-2	10.5	0.8	36.1	29.7	74.1	43.3	0.8	1.41	0.89	33.16	0.57
08CP72-3	11.1	0.9	4.6	41.9	13.6	14.3	9.1	0.43	0.60	28.71	0.49
08CP72-4	11.8	0.9	6.0	38.4	19.4	14.9	6.4	0.50	0.76	30.12	0.51
08CP72-5	21.6	1.7	153.4	102.2	75.8	177.3	0.7	11.10	0.74	30.22	0.54
08CP72-6	17.8	1.4	43.4	197.3	66.0	89.2	4.5	4.62	0.71	31.63	0.53
Uinta Basin cores											
FMF-6351-1	1.2	0.0	11.2	80.5	21.5	29.9	7.2	0.13	1.9	43.3	0.64
FMF-6351-2*	1.6	0.2	2.4	23.3	46.5	8.0	9.6	0.04	0.8	31.3	0.52

Table 1 cont.

Sample	Age (Ma)	± 2σ (My)	U (ppm)	Th (ppm)	Sm (ppm)	eU (ppm)	Th/U	He (nmol/g)	Mass (µg)	Equiv. Sphere radius (µm)	Ft
Uinta Basin cores cont.											
FMF-6351-3	3.4	0.0	55.8	219.6	78.4	106.7	3.9	1.14	1.2	35.6	0.58
FMF-6351-4*	0.2	0.0	829.6	2856.7	1036.9	1492.4	3.4	1.23	2.2	43.3	0.64
FMF-6351-5	3.3	0.1	2.3	50.2	30.8	14.0	22.3	0.16	1.5	38.8	0.60
FMF-6351-6	3.6	0.0	60.4	230.6	55.4	113.7	3.8	1.33	1.4	36.9	0.59
FMF-6480-1*	0.2	0.0	1.4	15.4	49.0	5.2	11.2	0.00	1.2	37.7	0.59
FMF-6480-2*	0.7	0.0	14.4	118.1	27.5	41.7	8.2	0.08	1.0	33.3	0.55
FMF-6480-3	1.7	0.0	70.1	265.0	37.7	131.3	3.8	0.67	0.9	33.4	0.55
FMF-6480-4*	1.3	0.1	1.9	30.8	100.6	9.5	16.6	0.04	1.2	36.2	0.57
FMF-6480-5	3.2	0.1	51.0	25.9	80.0	57.3	0.5	0.56	0.9	33.0	0.57
FMF-6480-6*	0.9	0.0	17.9	11.1	57.1	20.7	0.6	0.05	0.8	31.3	0.55
FMF-6686-1	4.2	0.6	2.0	38.7	32.7	11.1	19.6	0.12	0.5	28.0	0.47
FMF-6686-2	3.7	0.3	3.9	28.3	41.7	10.6	7.3	0.12	1.0	34.4	0.56
FMF-6686-3	1.3	0.0	35.0	217.5	54.6	85.4	6.2	0.32	0.9	31.6	0.53
FMF-6686-4	2.5	0.0	35.5	406.5	64.1	129.4	11.4	0.96	1.0	33.2	0.54
FMF-6686-5*	0.2	0.0	1.7	17.5	25.7	5.8	10.6	0.00	1.1	36.2	0.58
FMF-6686-6	1.1	0.0	46.5	69.0	104.8	62.9	1.5	0.22	1.3	36.2	0.59
FMF-7289-1*	0.5	0.0	4.4	33.6	37.0	12.3	7.6	0.02	2.4	44.4	0.65
FMF-7289-2*	0.9	0.0	2.9	24.3	31.9	8.7	8.3	0.03	2.3	45.3	0.65
FMF-7289-3*	0.2	0.0	4.8	35.4	70.1	13.3	7.3	0.01	1.7	40.7	0.62
FMF-7289-4	5.8	0.1	8.7	78.3	39.0	26.9	9.0	0.57	2.4	46.9	0.66
FMF-7289-5	4.0	0.3	4.0	39.3	121.8	13.7	9.8	0.21	2.8	48.9	0.68
FMF-7289-6	0.7	0.1	1.3	7.8	29.0	3.2	6.1	0.01	1.9	41.9	0.63
NB-4412-1†	3.4	0.2	21.7	123.6	37.1	50.3	5.7	0.63	15.5	66.1	0.67
NB-4412-2†	6.9	0.4	23.0	106.2	59.1	47.7	4.6	1.23	19.1	70.5	0.67
NB-4412-3†	4.0	0.2	55.0	100.5	97.6	78.6	1.8	1.14	14.1	63.8	0.66
NB-7468-1	2.0	0.0	75.8	342.3	57.6	154.8	4.5	1.05	1.6	39.6	0.61
NB-7468-2*	0.4	0.0	5.0	44.6	37.5	15.5	8.9	0.02	1.6	41.2	0.62
NB-7468-3*	0.3	0.0	4.3	74.8	44.4	21.7	17.5	0.02	1.0	35.3	0.57
NB-7468-4*	0.3	0.0	5.4	60.1	54.6	19.5	11.1	0.02	1.1	36.1	0.58
NB-7468-5*	0.0	0.0	3.4	43.9	21.2	13.6	12.9	0.00	0.8	33.6	0.55
NB-7468-6	1.0	0.0	11.8	81.1	55.1	30.8	6.8	0.10	1.4	39.0	0.60
NB-8542-1*	0.4	0.0	22.9	75.3	39.7	40.5	3.3	0.06	2.1	44.1	0.65
NB-8542-2	1.8	0.1	17.7	55.0	54.6	30.6	3.1	0.18	1.1	35.3	0.58
NB-8542-3*	0.7	0.0	10.7	68.0	123.5	26.9	6.4	0.07	2.2	44.3	0.65
NB-8542-4*	0.7	0.0	19.5	79.4	71.4	38.1	4.1	0.08	0.8	32.1	0.54
TS-8799-1*	0.6	0.0	1.1	29.3	47.0	8.1	26.2	0.02	1.2	35.3	0.56
TS-8799-2	0.3	0.0	101.0	130.4	201.0	132.0	1.3	0.13	1.5	39.6	0.63
TS-8799-3*	0.1	0.0	6.7	154.4	142.7	43.0	23.0	0.01	1.3	36.6	0.57
TS-8799-4*	0.2	0.0	3.8	166.2	67.6	42.4	44.2	0.03	1.3	37.0	0.58
TS-8799-5*	0.5	0.0	4.4	28.8	107.0	11.6	6.5	0.02	1.4	37.7	0.59
TS-8799-6	1.6	0.1	27.3	71.0	75.2	44.0	2.6	0.24	1.6	40.8	0.63
SO-4695-1	2.8	0.1	4.5	60.7	35.2	18.7	13.4	0.16	1.0	34.8	0.56

Table 1 cont.

Sample	Age (Ma)	± 2σ (My)	U (ppm)	Th (ppm)	Sm (ppm)	eU (ppm)	Th/U	He (nmol/g)	Mass (µg)	Equiv. Sphere radius (µm)	Ft
Uinta Basin cores cont.											
SO-4695-2	1.8	0.0	28.8	138.9	39.1	61.0	4.8	0.35	1.2	35.9	0.58
SO-4695-3	1.2	0.0	14.3	98.8	86.6	37.5	6.9	0.16	2.6	46.6	0.66
Book Cliffs cores											
2BC-67-1	10.9	0.7	4.8	38.1	79.0	13.9	8.0	0.54	1.7	42.3	0.63
2BC-67-2	10.0	0.6	10.3	33.9	53.7	18.4	3.3	0.61	1.3	38.1	0.60
2BC-67-3	8.3	0.5	15.8	99.4	29.0	38.8	6.3	1.16	2.6	45.2	0.65
2BC-67-4	7.0	0.4	2.9	31.7	70.7	10.6	10.8	0.25	1.5	37.7	0.59
2BC-67-5	12.9	0.8	15.0	38.0	143.9	24.5	2.5	1.05	1.2	37.3	0.60
2BC-67-6	3.9	0.2	6.4	45.2	104.5	17.4	7.0	0.20	0.8	31.9	0.53
2BC-181-1	17.4	1.0	37.7	138.9	66.0	70.0	3.7	4.01	1.4	38.1	0.60
2BC-181-2	13.4	0.8	213.0	874.5	267.8	415.7	4.1	18.75	1.6	39.6	0.61
2BC-181-3	22.0	1.3	63.2	297.1	63.7	131.9	4.7	9.16	1.2	35.6	0.57
2BC-181-4	17.4	1.0	90.4	264.9	100.9	151.9	2.9	8.42	1.1	35.9	0.58
2BC-181-5	17.1	1.0	20.8	104.1	14.8	44.8	5.0	2.52	1.3	38.3	0.60
2BC-181-6	19.0	1.1	58.1	181.3	80.2	100.2	3.1	6.14	1.3	36.8	0.59
2BC-248-1	18.2	1.1	29.3	79.3	17.0	47.6	2.7	3.06	2.0	43.6	0.65
2BC-248-2	20.9	1.3	1.6	12.6	72.7	4.9	7.8	0.34	1.2	36.3	0.58
2BC-248-3	12.7	0.8	18.0	65.8	23.8	33.3	3.7	1.33	1.1	35.2	0.57
2BC-248-4	9.1	0.5	4.7	31.2	75.8	12.3	6.6	0.36	1.4	36.2	0.58
2BC-248-5	5.6	0.3	8.2	39.3	53.7	17.5	4.8	0.30	1.0	33.8	0.56
2BC-248-6	16.2	1.0	86.9	279.4	77.1	151.6	3.2	8.72	2.3	44.3	0.65
2BC-305-1	10.1	0.1	38.7	849.5	0.8	234.3	21.9	6.73	0.7	31.0	0.52
2BC-305-2	2.4	0.0	13.4	651.5	0.3	163.4	48.7	1.10	0.7	30.7	0.51
2BC-305-3	2.0	0.1	4.4	301.6	0.3	73.8	68.3	0.42	0.7	30.6	0.51
2BC-305-4	10.8	0.1	61.6	1029.2	0.3	298.5	16.7	8.94	0.6	30.0	0.50
2BC-305-5	2.6	0.1	6.3	328.8	0.4	81.9	52.6	0.61	0.7	31.0	0.51
2BC-305-6	5.7	0.3	12.3	108.9	113.8	37.9	8.9	0.58	0.6	28.8	0.49
2BC-469-1	11.8	0.7	87.8	149.3	26.9	122.3	1.7	4.07	0.7	30.1	0.52
2BC-469-2	15.0	0.9	53.1	41.9	153.9	63.5	0.8	2.66	0.6	28.6	0.51
2BC-469-3	10.8	0.6	56.7	114.3	77.2	83.4	2.0	2.48	0.6	29.0	0.50
2BC-469-4	9.1	0.5	7.9	22.3	44.4	13.2	2.8	0.41	1.6	40.5	0.62
2BC-469-5*	25.9	1.6	6.4	34.6	53.5	14.6	5.4	1.15	1.0	33.2	0.55
2BC-469-6	7.3	0.4	5.7	48.2	123.0	17.4	8.5	0.39	0.9	33.0	0.54
2BC-591-1†	10.5	0.6	34.4	174.9	108.6	75.2	5.1	2.65	10.0	56.5	0.61
2BC-591-2†	8.3	0.5	20.5	120.1	78.4	48.6	5.9	1.45	13.0	62.3	0.65
2BC-591-3†	6.9	0.4	31.0	161.1	106.8	68.6	5.2	1.51	6.9	50.5	0.58
2BC-675-1	10.2	0.6	6.8	40.1	99.0	16.5	5.9	0.50	0.7	31.7	0.53
2BC-675-2*	14.5	0.9	8.0	41.4	85.6	18.0	5.2	0.80	1.0	33.3	0.55
2BC-675-3	8.9	0.5	10.7	70.0	175.7	27.7	6.6	0.73	0.8	31.5	0.53
2BC-675-4	6.2	0.4	6.1	23.1	64.3	11.8	3.8	0.22	0.8	32.4	0.54
2BC-675-5	7.9	0.5	2.8	27.8	64.3	9.6	9.8	0.22	0.6	30.4	0.51
2BC-675-6	7.7	0.5	40.2	112.9	53.3	66.5	2.8	1.55	1.2	32.8	0.55

Table 1 cont.

Sample	Age (Ma)	± 2σ (My)	U (ppm)	Th (ppm)	Sm (ppm)	eU (ppm)	Th/U	He (nmol/g)	Mass (µg)	Equiv. Sphere radius (µm)	Ft
Book Cliffs cores cont.											
3BC-120-1	9.3	0.7	8.1	36.6	94.9	17.0	4.5	0.50	1.0	34.9	0.57
3BC-120-2	13.4	3.4	2.4	5.5	53.2	4.0	2.3	0.17	0.9	32.5	0.55
3BC-120-3	25.0	2.0	8.8	29.3	66.2	15.9	3.3	1.15	0.7	31.0	0.53
3BC-120-4	19.1	2.5	5.4	19.2	83.4	10.2	3.6	0.58	0.7	31.3	0.53
3BC-120-5	30.2	4.0	8.7	2.5	10.7	9.3	0.3	0.86	0.8	31.3	0.56
3BC-120-6	15.5	1.3	7.0	25.6	88.4	13.4	3.7	0.67	1.1	35.5	0.58
4BC-187-1	12.1	0.3	10.2	71.9	17.0	26.8	7.0	1.06	1.4	37.5	0.59
4BC-187-2	12.2	0.4	14.4	42.1	69.1	24.4	2.9	1.07	2.1	44.7	0.65
4BC-187-3	12.5	0.4	11.8	60.8	83.3	26.2	5.1	1.18	2.3	44.8	0.65
4BC-187-4	1.2	0.0	39.4	151.3	39.3	74.4	3.8	0.31	1.9	41.6	0.63
4BC-187-5	17.2	0.3	32.3	57.1	86.0	45.9	1.8	2.86	2.3	44.9	0.66
4BC-187-6*	26.0	0.4	31.9	99.4	85.5	55.2	3.1	5.38	3.1	49.1	0.68
4BC-340-1	7.6	0.4	6.6	93.0	85.9	28.4	14.1	0.58	0.6	28.6	0.48
4BC-340-2	5.2	0.2	15.0	91.8	55.9	36.4	6.1	0.49	0.5	27.6	0.47
4BC-340-3	5.5	0.4	3.6	97.0	77.2	26.3	27.2	0.37	0.5	27.0	0.46
4BC-340-4	10.4	0.9	5.0	54.1	81.0	17.8	10.9	0.50	0.6	29.0	0.49
4BC-340-6	16.8	0.2	126.2	197.5	81.0	172.1	1.6	8.01	0.6	29.1	0.51
4BC-477-1	8.8	0.2	42.9	112.9	79.2	69.2	2.6	1.79	0.8	31.6	0.54
4BC-477-3	9.4	0.1	30.7	115.4	49.6	57.5	3.8	1.67	1.1	34.6	0.57
4BC-477-4	7.9	0.2	11.4	73.9	32.9	28.5	6.5	0.77	1.7	40.6	0.62
4BC-477-5	6.5	0.2	4.7	62.4	26.0	19.2	13.2	0.41	1.3	37.4	0.59
4BC-477-6	8.7	0.3	10.4	50.0	31.7	22.0	4.8	0.64	1.3	38.2	0.60
5BC-306-1*	20.4	0.5	18.9	72.9	96.7	36.2	3.8	2.86	3.7	53.0	0.70
5BC-306-2	7.3	0.1	13.8	115.2	81.0	40.8	8.3	1.03	1.8	41.6	0.63
5BC-306-3	10.2	0.3	14.9	94.4	123.7	37.3	6.3	1.46	3.3	51.5	0.69
5BC-306-4	14.0	0.2	54.7	125.8	105.7	84.1	2.3	4.02	1.6	40.4	0.62
5BC-306-5	5.5	0.2	5.9	69.3	57.2	22.1	11.7	0.41	1.7	40.1	0.61
5BC-306-6	16.3	0.2	9.8	90.0	17.5	30.6	9.2	1.84	2.7	47.8	0.67
5BC-474-1	7.0	0.3	9.1	36.6	63.3	17.8	4.0	0.43	1.8	59.0	0.63
5BC-474-2*	20.0	0.3	18.6	53.7	30.8	31.2	2.9	2.27	2.4	64.2	0.67
5BC-474-3	12.3	0.1	36.8	101.1	21.6	60.2	2.8	2.50	1.7	57.8	0.62
5BC-474-4	8.5	0.2	18.2	73.0	66.6	35.3	4.0	1.07	2.1	61.6	0.65
5BC-474-5	9.0	0.5	4.9	31.3	84.4	12.5	6.4	0.43	2.8	68.0	0.68
5BC-474-6	8.9	0.5	2.2	26.0	50.7	8.4	11.8	0.30	4.0	76.6	0.71
GC1-54-1	35.9	3.4	2.1	9.7	20.3	4.5	4.5	0.59	2.2	44.9	0.65
GC1-54-2	12.7	1.1	2.2	11.7	25.6	5.0	5.4	0.23	2.4	46.2	0.66
GC1-54-3	9.7	1.3	2.0	11.4	51.1	4.9	5.8	0.16	1.6	40.1	0.62
GC1-54-4	15.7	0.2	43.6	140.9	79.2	76.4	3.2	4.03	1.4	39.2	0.61
GC1-54-5	27.3	0.4	41.9	55.8	48.8	55.0	1.3	4.99	1.3	38.1	0.61
GC1-54-6	13.5	0.5	11.3	47.5	30.8	22.4	4.2	0.96	1.2	35.8	0.58
GC1-153-1	35.9	5.1	2.2	5.0	27.9	3.5	2.3	0.44	2.0	41.1	0.63
GC1-153-2	40.6	8.7	1.0	9.2	27.0	3.3	8.8	0.44	1.3	37.0	0.58
GC1-153-3	38.9	4.0	1.3	9.8	18.4	3.6	7.6	0.52	2.5	46.4	0.66

Table 1 cont.

Sample	Age (Ma)	± 2σ (My)	U (ppm)	Th (ppm)	Sm (ppm)	eU (ppm)	Th/U	He (nmol/g)	Mass (µg)	Equiv. Sphere radius (µm)	Ft
Book Cliffs cores cont.											
GC1-153-4	21.5	0.2	16.3	129.8	22.9	46.3	8.0	3.49	1.9	42.9	0.64
GC1-153-5	55.8	5.2	2.1	24.3	76.5	8.1	11.5	1.62	1.8	42.6	0.63
GC1-153-6	29.1	5.8	1.6	10.9	25.0	4.2	6.8	0.39	1.1	35.6	0.57
GC1-288-1	15.8	2.3	2.6	13.4	22.1	5.9	5.1	0.29	1.0	34.5	0.56
GC1-288-2	11.6	1.7	2.4	6.8	17.9	4.1	2.8	0.16	1.4	39.3	0.61
GC1-288-3	16.0	1.8	1.8	16.2	28.4	5.7	9.1	0.30	1.5	37.4	0.59
GC1-288-4*	29.9	6.8	2.0	17.0	24.5	6.0	8.5	0.49	0.6	29.0	0.49
GC1-288-5	13.4	0.8	5.3	31.3	39.3	12.7	5.9	0.56	1.2	36.9	0.59
GC1-288-6	15.6	0.9	13.0	46.2	9.8	23.7	3.5	1.02	0.6	29.4	0.50
GC1-445-1	19.4	1.2	7.4	42.5	22.6	17.3	5.8	1.07	1.1	36.2	0.58
GC1-445-2	18.1	1.1	43.1	141.5	64.4	76.0	3.3	4.88	1.9	43.6	0.65
GC1-445-3	26.2	1.6	32.9	196.8	119.3	78.8	6.0	6.95	1.5	39.6	0.61
GC1-445-4	14.4	0.9	40.2	63.7	107.9	55.4	1.6	2.45	1.0	33.1	0.56
GC1-445-5	12.3	0.7	12.3	75.7	14.7	29.8	6.2	1.25	1.9	41.0	0.62
GC1-445-6*	69.9	4.2	1.0	8.5	71.8	3.3	8.3	0.75	1.0	33.3	0.55
GC1-609-1	8.5	0.5	1.1	20.8	58.7	6.2	18.6	0.16	0.9	32.7	0.54
GC1-609-2	14.0	0.8	9.1	50.5	29.3	20.9	5.5	0.83	0.7	30.5	0.52
GC1-609-3	13.8	0.8	3.9	25.4	27.2	9.9	6.5	0.39	0.7	30.5	0.51
GC1-609-4	9.4	0.6	8.1	52.5	103.0	20.7	6.5	0.60	1.0	33.9	0.55
GC1-609-5	16.9	1.0	10.5	54.1	33.7	23.1	5.2	1.20	1.0	34.1	0.56
GC1-609-6	12.9	0.8	20.2	43.2	113.9	30.7	2.1	1.27	1.1	35.7	0.58
GC1-749-1	16.5	1.0	2.3	30.3	25.3	9.4	13.3	0.49	1.2	35.4	0.57
GC1-749-2	17.9	1.1	46.4	178.0	54.3	87.6	3.8	4.81	1.0	34.0	0.56
GC1-749-3	9.1	0.5	2.7	22.0	83.8	8.2	8.2	0.23	1.0	33.9	0.55
GC1-749-4	11.9	0.7	1.4	19.2	71.3	6.2	13.2	0.22	0.7	30.4	0.51
GC1-749-5	17.5	1.1	1.5	16.2	64.5	5.5	10.9	0.26	0.5	27.9	0.47
GC1-749-6	11.2	0.7	18.3	92.0	68.5	39.8	5.0	1.38	0.9	34.5	0.56
GC1-1006-1	8.9	0.5	3.5	17.3	46.5	7.7	5.0	0.23	1.3	38.3	0.60
GC1-1006-2	18.8	1.1	15.4	18.1	24.9	19.7	1.2	1.17	1.0	34.6	0.58
GC1-1006-3	8.2	0.5	8.7	39.9	111.2	18.4	4.6	0.45	0.9	32.3	0.54
GC1-1006-4	10.9	0.7	6.4	24.8	66.0	12.5	3.9	0.39	0.7	29.8	0.51
GC1-1006-5	21.3	1.3	3.4	19.3	56.6	8.2	5.6	0.50	0.7	30.5	0.51
GC1-1006-6	17.4	1.0	2.5	10.4	47.3	5.1	4.1	0.27	0.9	32.6	0.54
3FED335-1*	15.3	0.9	8.3	6.5	18.4	9.9	0.8	0.45	0.8	30.6	0.54
3FED335-2	6.0	0.4	69.0	114.7	247.5	96.7	1.7	1.89	1.1	37.1	0.60
3FED335-3	4.9	0.3	5.3	51.9	83.5	17.6	9.8	0.28	1.2	36.7	0.58
1AFED258-1†	4.7	0.3	16.2	44.2	64.8	26.7	2.7	0.48	20.7	72.4	0.69
1AFED258-2†	5.0	0.3	15.0	45.7	76.2	25.9	3.0	0.52	29.3	81.0	0.73
1AFED258-3*†	18.7	1.1	8.6	43.3	124.6	19.2	5.0	1.27	11.3	59.2	0.63
PH-4669-1	4.4	0.3	5.5	55.4	132.9	18.9	10.2	0.26	1.0	34.4	0.56
PH-4669-2	2.4	0.2	5.2	33.3	72.4	13.2	6.4	0.09	0.8	31.4	0.53
PH-4669-3*	28.8	5.2	2.2	25.0	194.0	8.9	11.5	0.81	0.8	32.9	0.54

Table 1 cont.

Sample	Age (Ma)	± 2σ (My)	U (ppm)	Th (ppm)	Sm (ppm)	eU (ppm)	Th/U	He (nmol/g)	Mass (µg)	Equiv. Sphere radius (µm)	Ft
Book Cliffs cores cont.											
PH-4669-4	2.7	0.1	14.4	55.3	154.0	27.9	3.8	0.23	0.8	33.1	0.55
PH-4669-5	7.4	0.2	17.3	88.4	111.6	38.2	5.1	0.81	0.7	30.9	0.52
RGU1-1751-1	6.4	0.1	29.9	278.2	100.1	94.4	9.3	1.69	0.7	30.0	0.51
RGU1-1751-2	3.2	0.1	4.5	125.7	91.4	33.8	28.2	0.30	0.6	29.6	0.50
RGU1-1751-3	4.9	0.1	7.8	153.5	60.8	43.4	19.8	0.57	0.6	28.7	0.48
RGU1-1751-4	3.7	0.1	4.4	164.6	39.1	42.4	37.8	0.47	0.8	32.1	0.53
RGU1-1751-5*	18.8	0.3	29.6	125.9	57.1	58.9	4.2	3.27	0.8	32.2	0.54
RGU1-1751-6	10.1	0.6	4.7	89.0	119.8	25.8	18.8	0.72	0.6	29.4	0.49
Ppt-2499-1	9.0	0.1	40.2	320.2	72.6	114.3	8.0	3.12	0.9	33.6	0.55
Ppt-2499-2	11.1	0.3	29.8	37.7	78.5	38.9	1.3	1.37	1.1	35.0	0.58
Ppt-2499-3	6.4	0.2	9.5	62.6	11.8	23.9	6.6	0.49	1.2	35.9	0.58
Ppt-2499-4*	34.6	0.5	49.7	60.5	91.9	64.0	1.2	7.41	1.4	38.3	0.61
Ppt-2499-5	10.8	0.2	39.1	70.7	77.0	55.8	1.8	1.86	0.9	33.8	0.57
Ppt-2499-6	6.8	0.1	26.9	80.6	61.4	45.8	3.0	0.97	1.0	34.6	0.57
Canyonlands cores											
LLE-2656-1	6.5	0.1	34.0	159.6	88.0	71.2	4.7	1.36	0.9	32.2	0.54
LLE-2656-2	11.0	0.2	66.5	120.9	35.8	94.5	1.8	2.88	0.6	29.1	0.51
LLE-2656-3	6.0	0.2	12.0	102.8	41.5	35.9	8.6	0.62	0.9	31.1	0.52
LLE-2656-4	7.5	1.1	4.4	21.7	32.3	9.6	4.9	0.20	0.6	30.6	0.52
LLE-2797-1†	14.8	0.2	24.4	66.5	68.2	40.1	2.7	1.95	6.7	53.1	0.60
LLE-2797-3†	13.3	0.2	28.9	51.4	54.0	41.0	1.8	2.00	15.4	65.7	0.68
SM-3032-1	8.3	1.1	1.6	16.1	29.9	5.5	10.1	0.15	1.2	37.2	0.59
SM-3032-2	11.0	0.2	74.7	67.3	25.6	90.3	0.9	2.85	0.7	30.1	0.53
SM-3032-3	9.4	1.2	22.1	45.6	542.5	35.3	2.1	0.95	0.6	28.6	0.50
SM-3032-4	4.4	0.3	8.3	47.1	37.3	19.4	5.6	0.23	0.6	29.1	0.50
SM-3032-5	9.9	0.3	26.2	167.5	114.8	65.3	6.4	1.78	0.6	29.5	0.50
SM-3032-6*	19.5	4.6	2.6	25.6	82.2	8.9	9.9	0.43	0.4	25.3	0.43
Monument Uplift cores											
DC-212-1	8.7	0.5	25.6	33.3	77.3	33.6	1.3	0.96	1.2	36.5	0.60
DC-212-2	12.6	0.8	5.7	51.2	254.6	18.7	9.0	0.72	0.9	32.4	0.54
DC-212-3	6.4	0.4	15.0	58.3	152.9	29.2	3.9	0.65	1.7	40.8	0.62
DC-212-4	10.9	0.7	4.6	35.9	289.4	14.3	7.8	0.52	1.0	35.3	0.57
DC-282-1	8.4	0.2	44.5	63.3	119.0	59.6	1.4	1.63	1.3	36.1	0.59
DC-282-2	6.2	0.7	5.2	42.4	207.5	16.0	8.2	0.30	0.8	31.6	0.53
DC-282-3	5.1	0.5	4.1	33.5	150.4	12.5	8.2	0.20	0.9	32.7	0.54
DC-282-4	5.0	0.2	9.9	44.0	105.5	20.5	4.5	0.35	1.5	39.4	0.61
DC-282-5	4.3	0.2	7.1	49.7	86.2	19.0	7.0	0.29	1.9	42.9	0.64
DC-282-6	7.4	0.7	3.3	26.3	113.7	9.9	8.0	0.26	1.8	40.5	0.62
DC-430-1	4.3	0.3	5.3	6.2	24.1	6.9	1.2	0.12	5.3	58.4	0.74
DC-430-2*	18.0	1.1	3.5	7.4	38.5	5.4	2.1	0.37	3.1	50.2	0.69
DC-430-3	7.5	0.5	40.9	33.2	111.7	49.1	0.8	1.44	4.2	52.8	0.71
DC-430-4	7.3	0.4	9.5	9.9	16.1	11.9	1.0	0.32	3.2	46.3	0.68

Table 1 cont.

Sample	Age (Ma)	± 2σ (My)	U (ppm)	Th (ppm)	Sm (ppm)	eU (ppm)	Th/U	He (nmol/g)	Mass (µg)	Equiv. Sphere radius (µm)	Ft
Monument Uplift cores cont.											
DC-655-1	6.1	0.8	4.8	10.3	125.4	7.8	2.1	0.19	3.0	49.0	0.68
DC-655-2	9.1	0.1	41.1	7.1	76.7	43.2	0.2	1.52	3.1	49.4	0.71
DC-655-3	3.5	1.1	1.9	8.5	201.1	4.9	4.4	0.06	1.0	33.1	0.55
DC-655-4	5.0	0.3	3.4	5.5	25.6	4.8	1.6	0.09	2.7	48.7	0.69
DC-655-5	5.4	0.3	13.3	14.6	78.1	17.0	1.1	0.30	1.0	34.6	0.58
DC-655-6	5.4	0.3	5.2	30.9	62.6	12.7	5.9	0.21	1.2	34.4	0.56
DC-1896-1	3.2	0.1	15.6	92.6	209.5	38.0	5.9	0.49	4.0	55.1	0.71
DC-1896-2	5.2	0.2	21.6	135.0	228.3	53.8	6.3	0.88	1.3	35.1	0.57
DC-1896-3	5.4	0.1	38.9	173.1	177.3	79.6	4.5	1.23	0.6	30.4	0.52
DC-2006-1	5.7	0.4	1.9	6.3	19.8	3.4	3.4	0.07	2.6	47.6	0.67
DC-2006-2*	92.4	35.8	1.7	5.3	219.4	4.0	3.2	1.57	2.30	46.8	0.67
DC-2006-3	8.6	0.7	9.8	37.3	187.4	19.4	3.8	0.58	1.68	40.1	0.62
DC-2006-4	8.2	0.5	7.3	7.1	73.2	9.3	1.0	0.31	4.95	55.7	0.73
DC-2006-5	6.2	0.2	40.1	39.2	222.2	50.2	1.0	1.02	1.14	35.8	0.59
DC-2006-6	7.0	0.4	2.6	6.5	17.7	4.2	2.5	0.11	3.02	50.3	0.69

* Excluded aliquot

† Multigrain aliquots with inclusions

Table 2. Core sample general information

Sample Name	Elevation (m)	Depth (m)	Latitude (deg)	Longitude (deg)	Well Name	Well Operator
Uinta Basin cores						
FMF-6351	-338	1936	39.9604	-109.3724	2-7 Flat Mesa Federal	Enserch Exploration
FMF-6480	-378	1976	39.9604	-109.3724	2-7 Flat Mesa Federal	Enserch Exploration
FMF-6686	-440	2038	39.9604	-109.3724	2-7 Flat Mesa Federal	Enserch Exploration
FMF-7289	-624	2222	39.9604	-109.3724	2-7 Flat Mesa Federal	Enserch Exploration
NB-4412	228	1345	39.9456	-109.4289	21 15-10-22 Natural Buttes	Coastal Oil & Gas
NB-7468	-704	2277	39.9456	-109.4289	21 15-10-22 Natural Buttes	Coastal Oil & Gas
NB-8542	-1031	2604	39.9456	-109.4289	21 15-10-22 Natural Buttes	Coastal Oil & Gas
TS-8799	-443	2683	39.5701	-109.2908	13-25-14-23 Trap Spring	Coseka Resources
SO-4695	41	1431	40.0267	-109.6437	So Ouray Unit 1	Sun Oil Co
Book Cliffs cores						
2BC-67	1947	20	39.4161	-109.1355	2 Book Cliffs	USGS-CG
2BC-181	1912	55	39.4161	-109.1355	2 Book Cliffs	USGS-CG
2BC-248	1891	76	39.4161	-109.1355	2 Book Cliffs	USGS-CG
2BC-305	1874	93	39.4161	-109.1355	2 Book Cliffs	USGS-CG
2BC-469	1824	143	39.4161	-109.1355	2 Book Cliffs	USGS-CG
2BC-591	1787	180	39.4161	-109.1355	2 Book Cliffs	USGS-CG
2BC-675	1761	206	39.4161	-109.1355	2 Book Cliffs	USGS-CG
3BC-120	1978	37	39.3579	-109.2478	3 Book Cliffs	USGS-CG
4BC-187	1783	57	39.2851	-109.3039	4 Book Cliffs	USGS-CG
4BC-340	1736	104	39.2851	-109.3039	4 Book Cliffs	USGS-CG
4BC-477	1695	145	39.2851	-109.3039	4 Book Cliffs	USGS-CG
5BC-306	1780	93	39.1832	-109.4350	5 Book Cliffs	USGS-CG
5BC-474	1728	145	39.1832	-109.4350	5 Book Cliffs	USGS-CG
GC1-54	1995	16	39.3288	-109.2665	GC-1	C K Geo Energy
GC1-153	1964	47	39.3288	-109.2665	GC-1	C K Geo Energy
GC1-288	1923	88	39.3288	-109.2665	GC-1	C K Geo Energy
GC1-445	1875	136	39.3288	-109.2665	GC-1	C K Geo Energy

Table 2 cont.

Sample Name	Elevation (m)	Depth (m)	Latitude (deg)	Longitude (deg)	Well Name	Well Operator
Book Cliffs cores cont.						
GC1-609	1825	186	39.3288	-109.2665	GC-1	C K Geo Energy
GC1-749	1783	228	39.3288	-109.2665	GC-1	C K Geo Energy
GC1-1006	1704	307	39.3288	-109.2665	GC-1	C K Geo Energy
3FED335	650	915	39.1395	-109.4163	3 Federal 335	Anschutz Corp.
1AFED258	458	1188	39.2705	-109.2852	1-A Federal 258	Anschutz Corp.
PH-4669	148	1423	38.9812	-109.8492	Blaze C 1	Phillips Petroleum Co
RGU1-1751	1234	534	39.5694	-110.8598	State of Utah RGU-1	River Gas of Utah Inc
Ppt-2499	1078	762	39.7196	-110.0484	Peters Point 1	Reserve Oil & Gas Co
Canyonlands cores						
LLE-2656	519	810	38.6951	-109.6760	24-20-26-2	Long Island L&E
LLE-2797	476	853	38.6951	-109.6760	24-20-26-2	Long Island L&E
SM-3032	463	924	38.6806	-109.6760	24-20-35-2-Seven-Mile	Unknown
Monument Uplift cores						
DC-212	1442	65	37.2377	-109.9006	DC-411811-1/Dolores	Kerr McGee Corp.
DC-282	1421	86	37.2377	-109.9006	DC-411811-1/Dolores	Kerr McGee Corp.
DC-430	1376	131	37.2377	-109.9006	DC-411811-1/Dolores	Kerr McGee Corp.
DC-655	1250	200	37.2088	-109.8825	DC-411824-2/Dolores	Dolores Bench Ltd
DC-1896	980	578	37.1943	-109.9367	DC-411828-1/Dolores	Kerr McGee Corp.
DC-2006	947	611	37.1943	-109.9367	DC-411828-1/Dolores	Kerr McGee Corp.

Table 3. Surface sample general information

Sample	Elevation (m)	Formation	Latitude (deg)	Longitude (deg)
Book Cliffs, Hay Canyon Vertical Transect				
07CP02	2392	Green River Fm.	39.4187	-109.3996
07CP03	2332	Green River Fm.	39.4095	-109.3969
07CP04	2212	Wasatch Fm.	39.4005	-109.3957
07CP05	2135	Wasatch Fm.	39.3944	-109.3906
07CP06	2043	Wasatch Fm.	39.3844	-109.3898
07CP07	1930	Wasatch Fm.	39.3645	-109.4006
07CP08	1852	Wasatch Fm.	39.3395	-109.3990
07CP09	1757	Tuscher Fm.	39.3175	-109.3710
07CP10	1669	Ferrer SS	39.2922	-109.3441
07CP11	1611	Neslen Fm.	39.2808	-109.3090
07CP13	1582	Sego SS	39.2681	-109.2829
07CP14	1499	Mancos B	39.2541	-109.2381
Book Cliffs, Sego Canyon Vertical Transect				
07CP15	2589	Wasatch Fm.	39.1469	-109.7209
07CP16	2470	Wasatch Fm.	39.1348	-109.7148
07CP18	2242	Wasatch Fm.	39.1143	-109.7048
07CP19	2126	Wasatch Fm.	39.1018	-109.7038
07CP20	2045	Wasatch Fm.	39.0925	-109.6984
07CP21	1944	Tuscher Fm.	39.0780	-109.7032
07CP22	1896	Ferrer SS	39.0626	-109.7026
07CP23	1803	Ferrer SS	39.0483	-109.7054
07CP24	1741	Neslen Fm.	39.0340	-109.7024
07CP25	1693	Sego SS	39.0232	-109.7105
07CP35	1669	Castlegate SS	39.0196	-109.7112
Book Cliffs, Blaze Canyon Vertical Transect				
07CP27	2013	Ferrer SS	38.9983	-109.7721
07CP28	1963	Neslen Fm.	38.9959	-109.7745
07CP29	1920	Neslen Fm.	38.9934	-109.7716
07CP30	1863	Sego SS	38.9936	-109.7702
07CP31	1650	Castlegate SS	38.9988	-109.8084
07CP32	1594	Blackhawk Fm.	38.9982	-109.8101
Book Cliffs, Tusher Canyon				
07CP63	1340	Blackhawk Fm.	39.0885	-110.0589
07CP65	1402	Castlegate SS	39.0972	-110.0224
Between Book Cliffs and Canyonlands				
07CP40	1373	Cedar Mountain Fm.	38.8135	-109.9052
07CP42	1548	Morrison Fm.	38.7425	-109.8783
07CP48	1546	Navajo SS	38.6378	-109.7523
07CP51	1850	Navajo SS	38.5669	-109.7918

Table 3 cont.

Sample	Elevation (m)	Formation	Latitude (deg)	Longitude (deg)
Canyonlands Vertical Transect, Shafer Trail				
07CP53	1396	Moenkopi Fm.	38.4615	-109.7869
07CP54	1390	Moenkopi Fm.	38.4468	-109.7773
07CP55a	1317	Cutler Fm.	38.4631	-109.7713
07CP56	1326	Cutler Fm.	38.4621	-109.7923
07CP57a	1397	Moenkopi Fm.	38.4560	-109.8110
07CP58	1512	Chinle Fm.	38.4533	-109.8152
07CP59a	1579	Wingate SS	38.4490	-109.8188
07CP60a	1646	Wingate SS	38.4486	-109.8184
07CP61	1720	Kayenta Fm.	38.4473	-109.8193
07CP62a	1792	Navajo SS	38.4452	-109.8214
Canyonlands Vertical Transect, Lathrop Canyon				
08CP69	1200	Cutler Fm.	38.3710	-109.7742
08CP70	1263	Cutler Fm.	38.3920	-109.7865
08CP71	1341	White Rim SS	38.4005	-109.7937
Canyonlands, North of confluence				
08CP66	1900	Kayenta Fm.	38.3034	-109.8675
08CP72	1572	Moenkopi Fm.	38.2644	-109.8667

Figure 1. Figure inset shows the Colorado Plateau geographic province in the western United States with location the study area in eastern Utah (red box) and locations of previous thermochronometric studies on the Colorado Plateau. Digital elevation model (DEM) of eastern Utah shows the four main focus areas: the Monument Uplift, Canyonlands, Book Cliffs, and Uinta Basin. Red boxes show locations of Figures 2, 3, and 4. Core sample locations are shown in red and surface sample locations are shown in white. Core samples used in this study have a black center, and cores samples collected but not utilized have a white center, commonly due low apatite yields. Surface samples analyzed by Stockli et al. (2002) are shown in yellow. Regional cross-section lines A-A'and B-B' are shown in Figures 5 and 17.

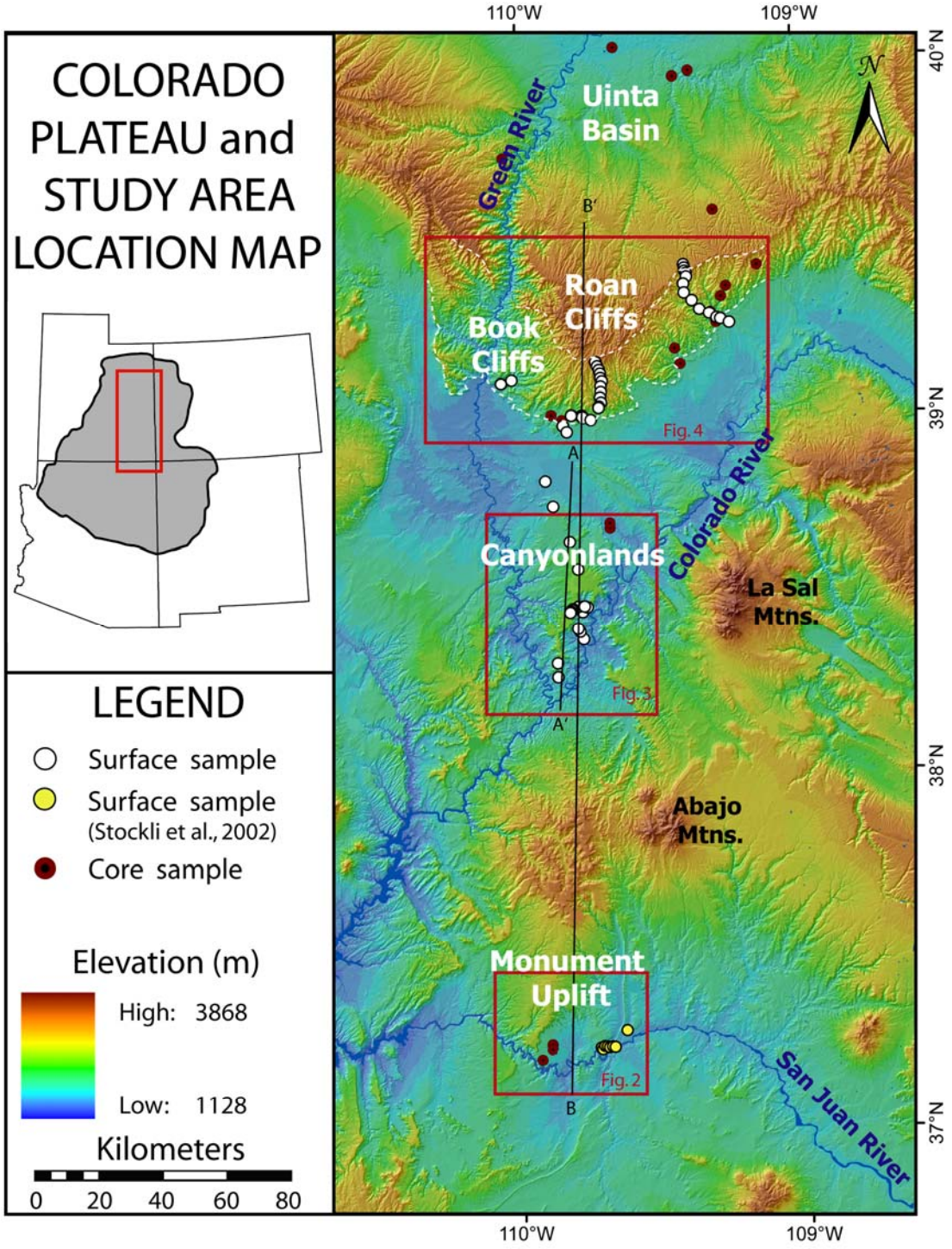
COLORADO PLATEAU and STUDY AREA LOCATION MAP
LEGEND
Surface sample
Surface sample (Stockli et al., 2002)
Core sample
Elevation (m)
High: 3868
Low: 1128
Kilometers
0 20 40 60 80
110°W
109°W
40°N
39°N
38°N
37°N
N
Uinta Basin
Green River
Roan Cliffs
Book Cliffs
Fig. 4
Colorado River
Canyonlands
Fig. 3
La Sal Mtns.
Abajo Mtns.
Monument Uplift
Fig. 2
San Juan River
A
A′
B
B′

Figure 2. DEM of the Monument Uplift region, whose location is shown in Fig. 1, with cross-section A-A'. Schematic cross-section of Monument Uplift (10x vertical exaggeration) showing Pennsylvanian (PP) through Jurassic strata (Jgc and Jsr) exposed across Comb Ridge Monocline. Locations of surface samples collected by Stockli et al., (2002) shown (MU-). Drill wells located near the cross-section area (triangles) are solid where core was sampled for thermochronometric analyses (this study).

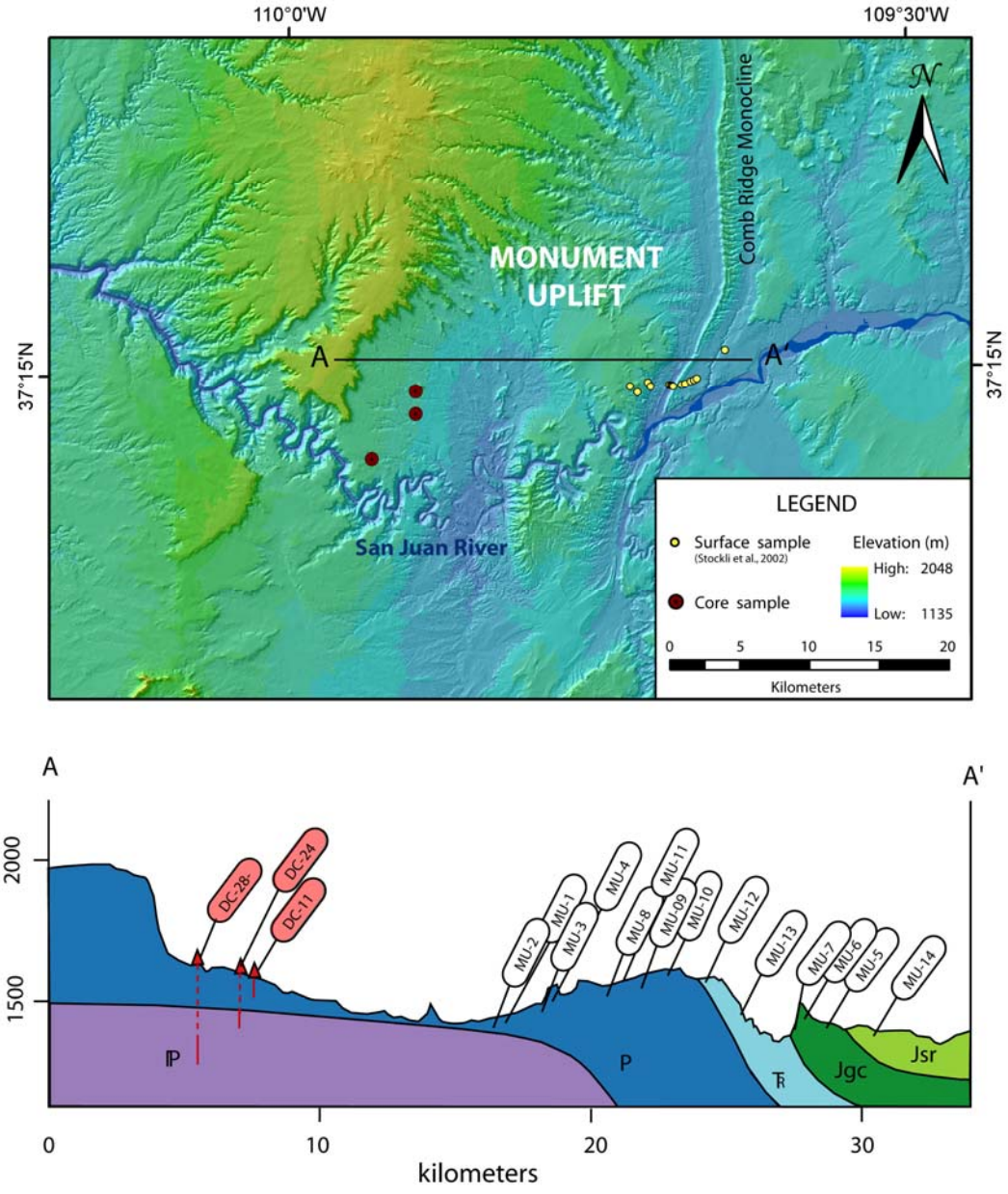
110°0'W
109°30'W
37°15'N
37°15'N
MONUMENT
UPLIFT
Comb Ridge Monocline
N
A
A'
San Juan River
LEGEND
Surface sample
(Stockli et al., 2002)
Core sample
Elevation (m)
High: 2048
Low: 1135
0 5 10 15 20
Kilometers
A
A'
meters
2000
1500
DC-28
DC-24
DC-11
MU-1
MU-2
MU-3
MU-4
MU-8
MU-09
MU-10
MU-11
MU-12
MU-13
MU-7
MU-6
MU-5
MU-14
P
P
Jsr
Jgc
0
10
20
30
kilometers

Figure 3. DEM of Canyonlands region, with location of cross-section A-A'. Schematic cross section (5x vertical exaggeration) of Canyonlands vertical transect with surface sample locations. Stratigraphic symbols are as follows: PPh- Hermosa Group., Pc- Cutler Group, Pw- White Rim Sandstone, T_Rm- Moenkopi Fm., T_Rc- Chinle Fm., Jw- Wingate Sandstone., Jk- Kayenta Fm., Jn- Navajo Sandstone.

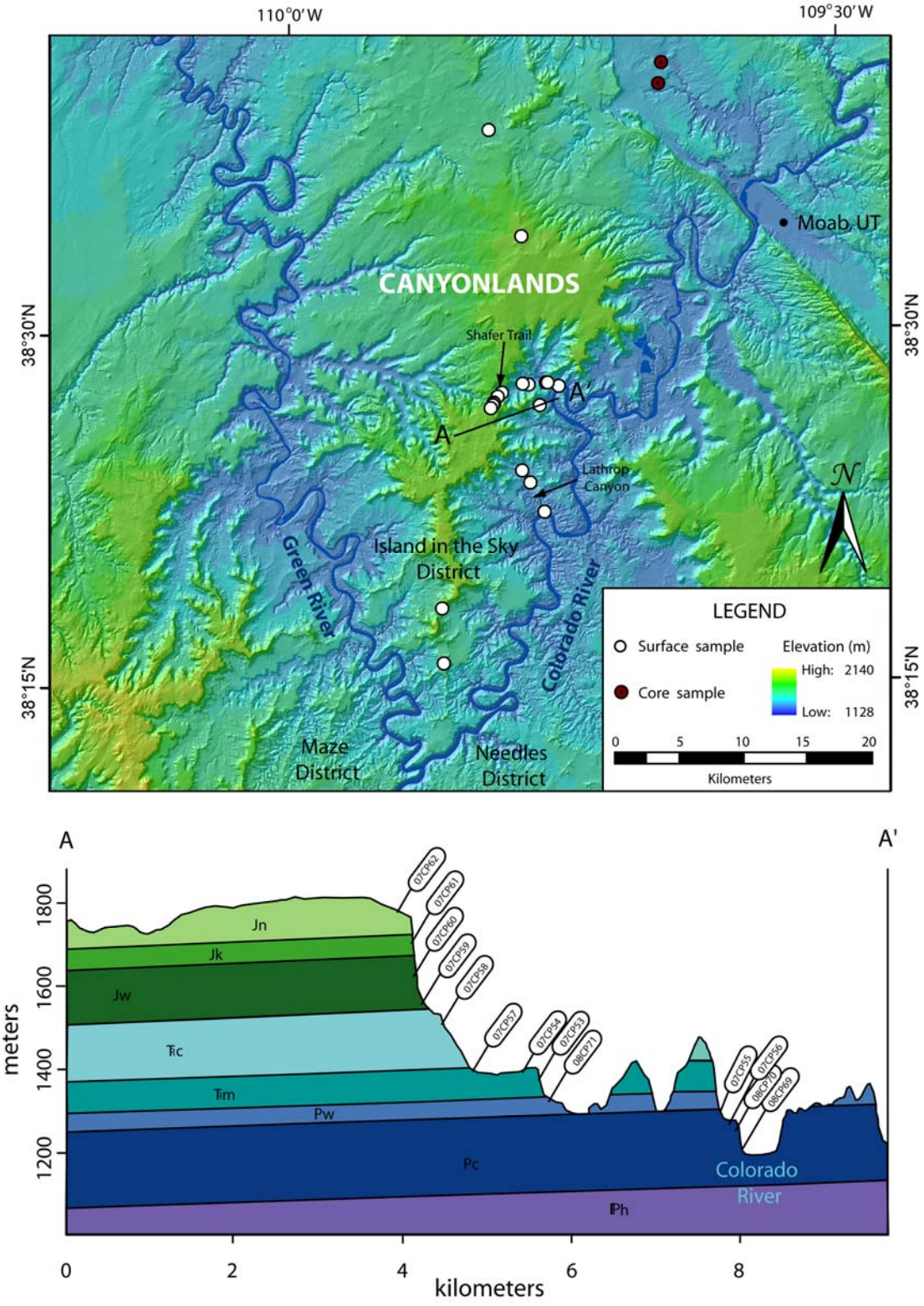
110°0′W
109°30′W
38°30′N
38°15′N
CANYONLANDS
Moab, UT
Shafer Trail
A
A′
Lathrop Canyon
Island in the Sky District
Green River
Colorado River
Maze District
Needles District
N
LEGEND
Surface sample
Core sample
Elevation (m)
High: 2140
Low: 1128
0 5 10 15 20
Kilometers
A
A'
meters
1800
1600
1400
1200
Jn
Jk
Jw
Trc
Trm
Pw
Pc
Ph
07CP62
07CP61
07CP60
07CP59
07CP58
07CP57
07CP54
07CP53
08CP71
07CP55
07CP56
08CP70
08CP69
Colorado River
0 2 4 6 8
kilometers

Figure 4. DEM of central Book Cliffs region showing locations of cross-sections A-A' and B-B'. Schematic cross-sections (10x vertical exaggeration) of Hay Canyon transect A-A', and Sego Canyon transect B-B', shown with surface sample locations. Nearby core locations, designated as red triangles and red sample names, are projected onto the cross-section lines. Core lines are solid where core was sampled. Stratigraphic symbols are as follows: Jm- Morrison Fm., Km- Mancos Shale, Kc- Castlegate Sandstone, Kbt- Buck Tongue of Mancos Shale, Ks- Sego Sandstone, Kn- Neslen Fm., Kf- Farrer Fm., Kt- Tusher Fm., Tw- Wasatch Fm., and Tgr- Green River Fm. Stratigraphy is the same for the Blaze Canyon, slightly west of Sego Canyon.

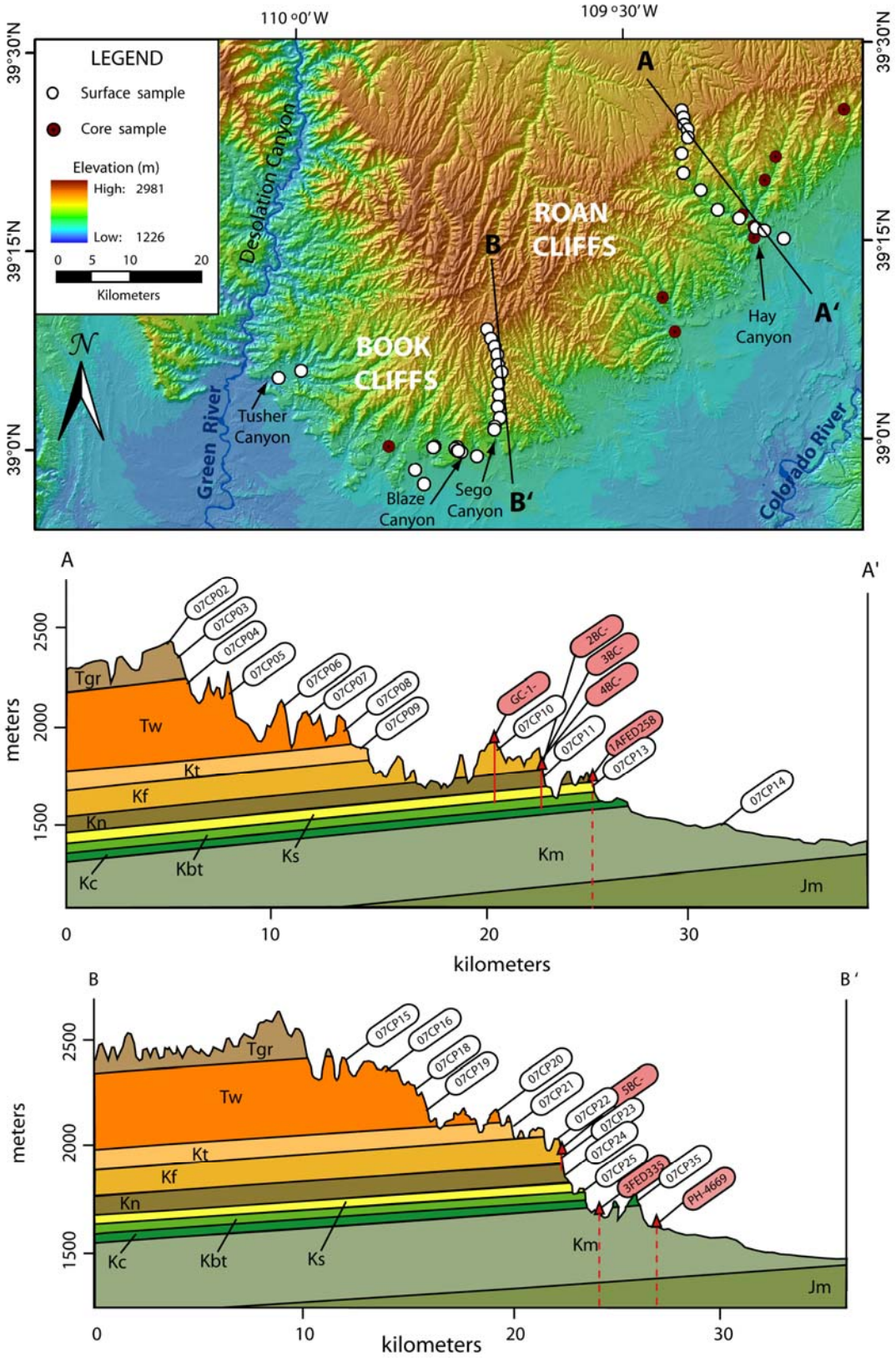
110°0'W
109°30'W
39°30'N
39°15'N
39°0'N
LEGEND
Surface sample
Core sample
Elevation (m)
High: 2981
Low: 1226
0 5 10 20
Kilometers
Desolation Canyon
Green River
Colorado River
ROAN CLIFFS
BOOK CLIFFS
Tusher Canyon
Blaze Canyon
Sego Canyon
Hay Canyon
A
A'
B
B'
A
A'
meters
2500
2000
1500
Tgr
Tw
Kt
Kf
Kn
Kc
Kbt
Ks
Km
Jm
07CP02
07CP03
07CP04
07CP05
07CP06
07CP07
07CP08
07CP09
GC-1-
07CP10
07CP11
2BC-
3BC-
4BC-
1AFED258
07CP13
07CP14
0
10
20
30
kilometers
B
B'
meters
2500
2000
1500
Tgr
Tw
Kt
Kf
Kn
Kc
Kbt
Ks
Km
Jm
07CP15
07CP16
07CP18
07CP19
07CP20
07CP21
07CP22
5BC-
07CP23
07CP24
07CP25
3FED332
07CP35
PH-4669
0
10
20
30
kilometers

Figure 5. Schematic cross-section (10x vertical exaggeration) showing sample locations collected for regional thermochronometric studies, between the Book Cliffs and Canyonlands. Location of cross-section line A-A' shown in Figure 1. Nearby core locations, designated as red triangles, are projected onto the cross section lines. The two cores shown are part of the Canyonlands vertical transect. Core lines are solid where core was sampled.

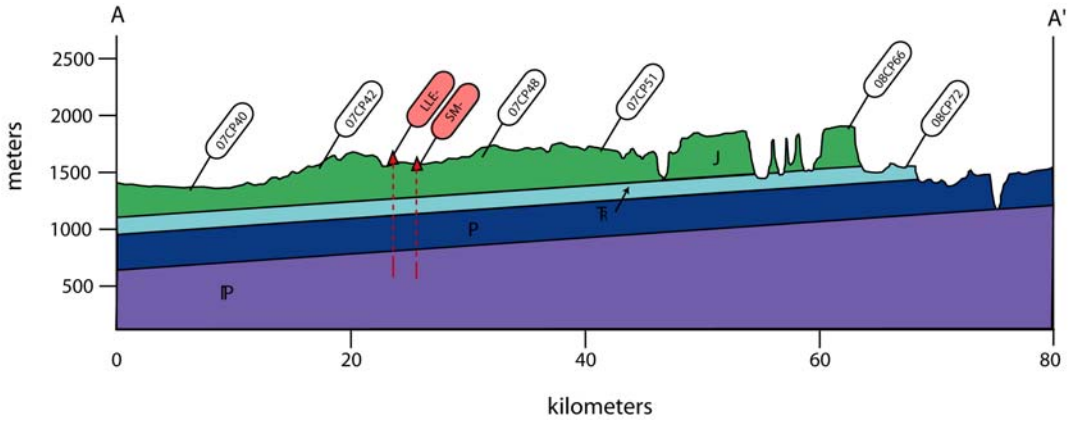
A
A'
2500
2000
1500
1000
500
meters
07CP40
07CP42
LLE
SM
07CP48
07CP51
08CP66
08CP72
J
P
P
0
20
40
60
80
kilometers

Figure 6. A.) AHe age-elevation plot for cores and surface samples in the Monument Uplift region (error is 2σ). Approximate cooling history shown in green envelope. B.) The thermal modeling results from aliquots (gray dots) that define the two edges of the cooling envelope in A). Modeled ages that match observed AHe ages within 2σ are shown in gray and 1σ shown in black. The inset histogram shows the distribution of geothermal gradients which fit the data, with 30°C/km being the best-fit gradient. C.) Random thermal histories for Monument Uplift that match observed AHe ages (2σ fits in gray, 1σ fits in black). Red boxes show user-defined constraints to the thermal histories, based on depositional age of uppermost sample and thermochronometric constraints. D.) An enlarged plot of C), showing more detail since 15 Ma. Most thermal histories have a maximum reheating temperature ~55−70°C. Timing of rapid cooling for the two sides of the cooling envelope (A) is between ~4−10 Ma, due to erosion in late Miocene to early Pliocene.

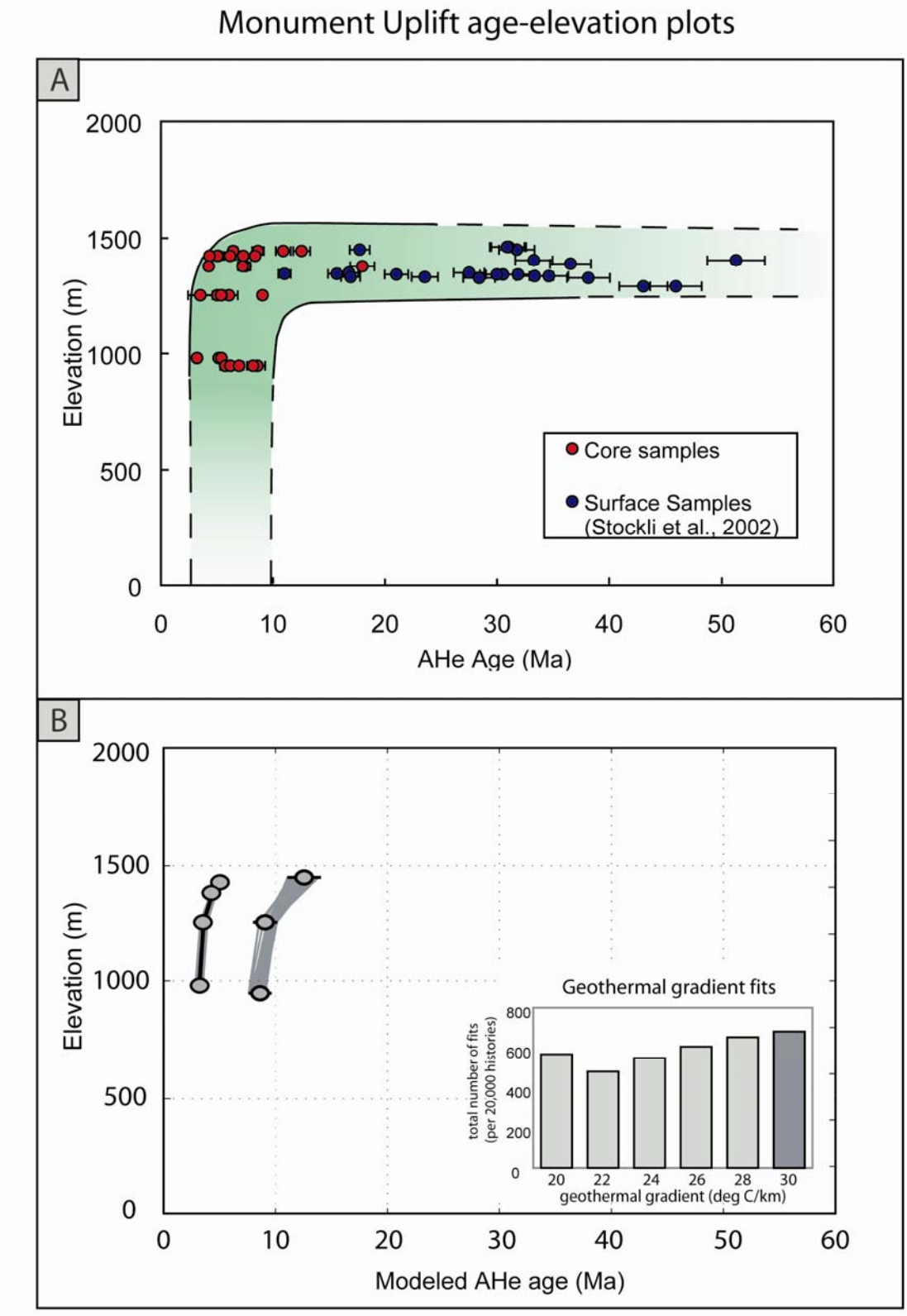
Monument Uplift age-elevation plots
A
Elevation (m)
AHe Age (Ma)
Core samples
Surface Samples
(Stockli et al., 2002)
B
Elevation (m)
Modeled AHe age (Ma)
Geothermal gradient fits
total number of fits
(per 20,000 histories)
geothermal gradient (deg C/km)

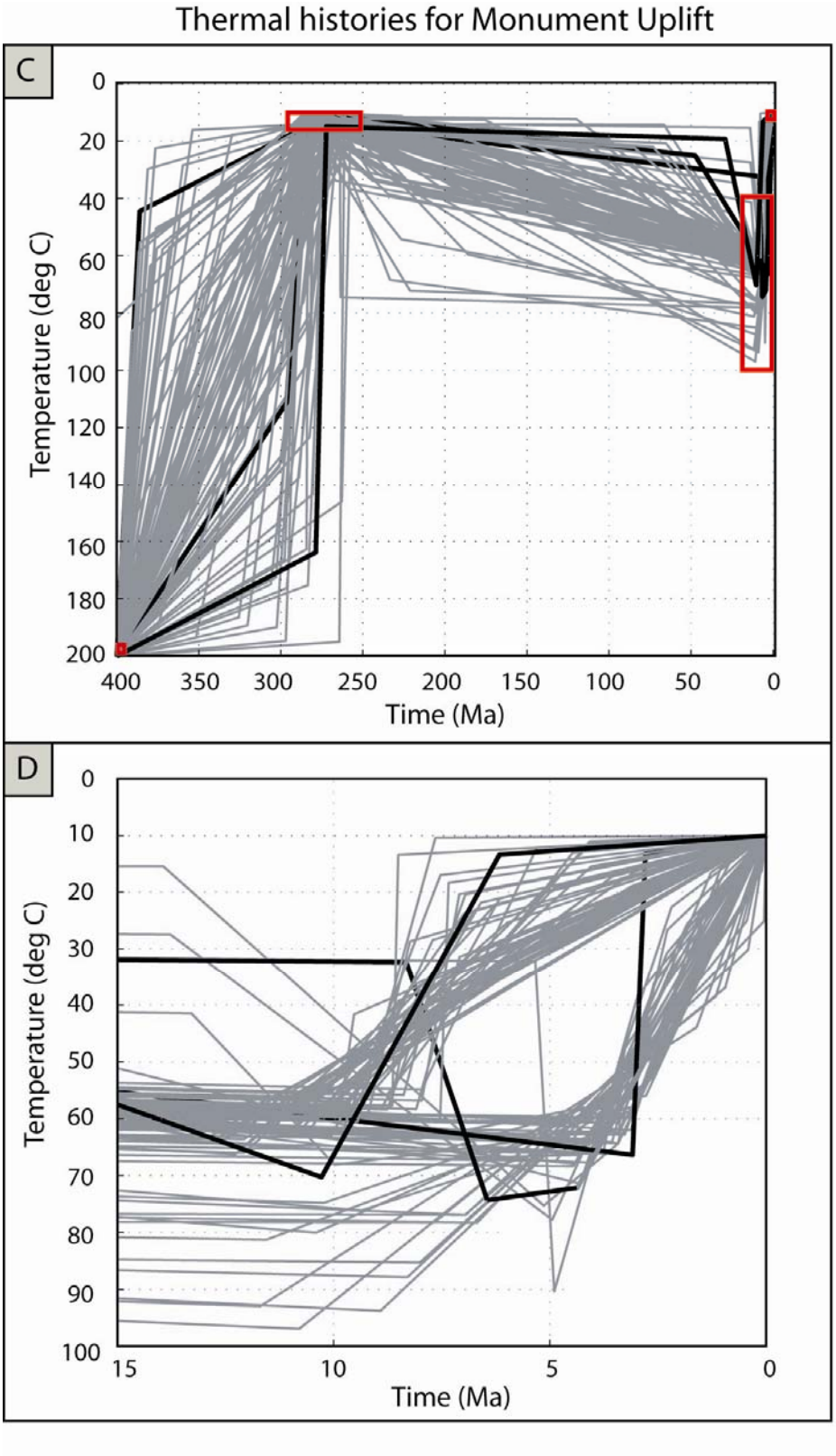
Thermal histories for Monument Uplift
C
Temperature (deg C)
0
20
40
60
80
100
120
140
160
180
200
400
350
300
250
200
150
100
50
0
Time (Ma)
D
Temperature (deg C)
0
10
20
30
40
50
60
70
80
90
100
15
10
5
0
Time (Ma)

Figure 7. A.) Age-elevation plot of regional thermochronometric samples. B.) Ages of regional samples plotted against Latitude to determine any south to north erosional trends. AHe ages decrease with increasing distance north, suggesting a northward progressing erosional cooling trend. However since samples were collected from different elevations, it is difficult to isolate lateral cooling from vertical cooling. More data may be needed to assess the south to north spatial trends of erosion.

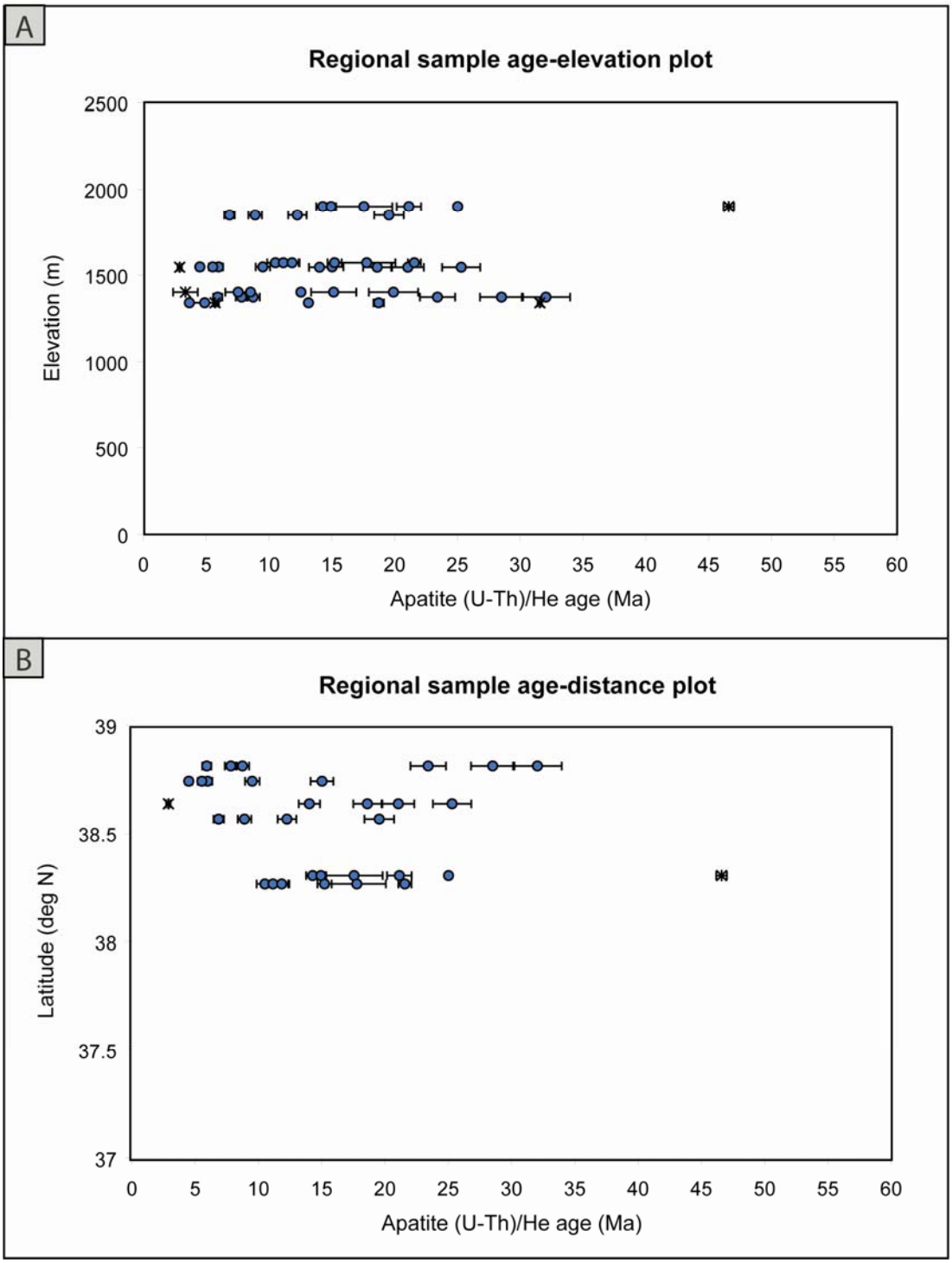
A
Regional sample age-elevation plot
Elevation (m)
2500
2000
1500
1000
500
0
0 5 10 15 20 25 30 35 40 45 50 55 60
Apatite (U-Th)/He age (Ma)
B
Regional sample age-distance plot
Latitude (deg N)
39
38.5
38
37.5
37
0 5 10 15 20 25 30 35 40 45 50 55 60
Apatite (U-Th)/He age (Ma)

Figure 8. A.) Age-elevation plot of cores and surface samples from Canyonlands region (error is 2σ). Approximate cooling history shown in yellow path. A few outliers, shown as stars, were identified for either having no helium or the possible presence of an inclusion. B.) Modeled AHe ages that match aliquots at the boundaries of the cooling envelope (gray lines 2σ fits, black lines 1σ fits). One modeled age from each edge of the envelope that did not match the observed age was excluded, therefore some of the gray lines may not fall within the error bars. The best fitting geothermal gradient in the Canyonlands region is 20^{o}C/km. C.) Random thermal histories for Canyonlands that match observed AHe ages (2σ fits in gray, 1σ fits in black). Red boxes show user-defined constraints to the thermal histories. D.) An enlarged plot of C), showing more detail since 15 Ma. Maximum reheating temperatures are varied, but most 1σ fits show maximum temperatures ~50−70^{o}C and timing of rapid cooling is mainly ~4−7 Ma.

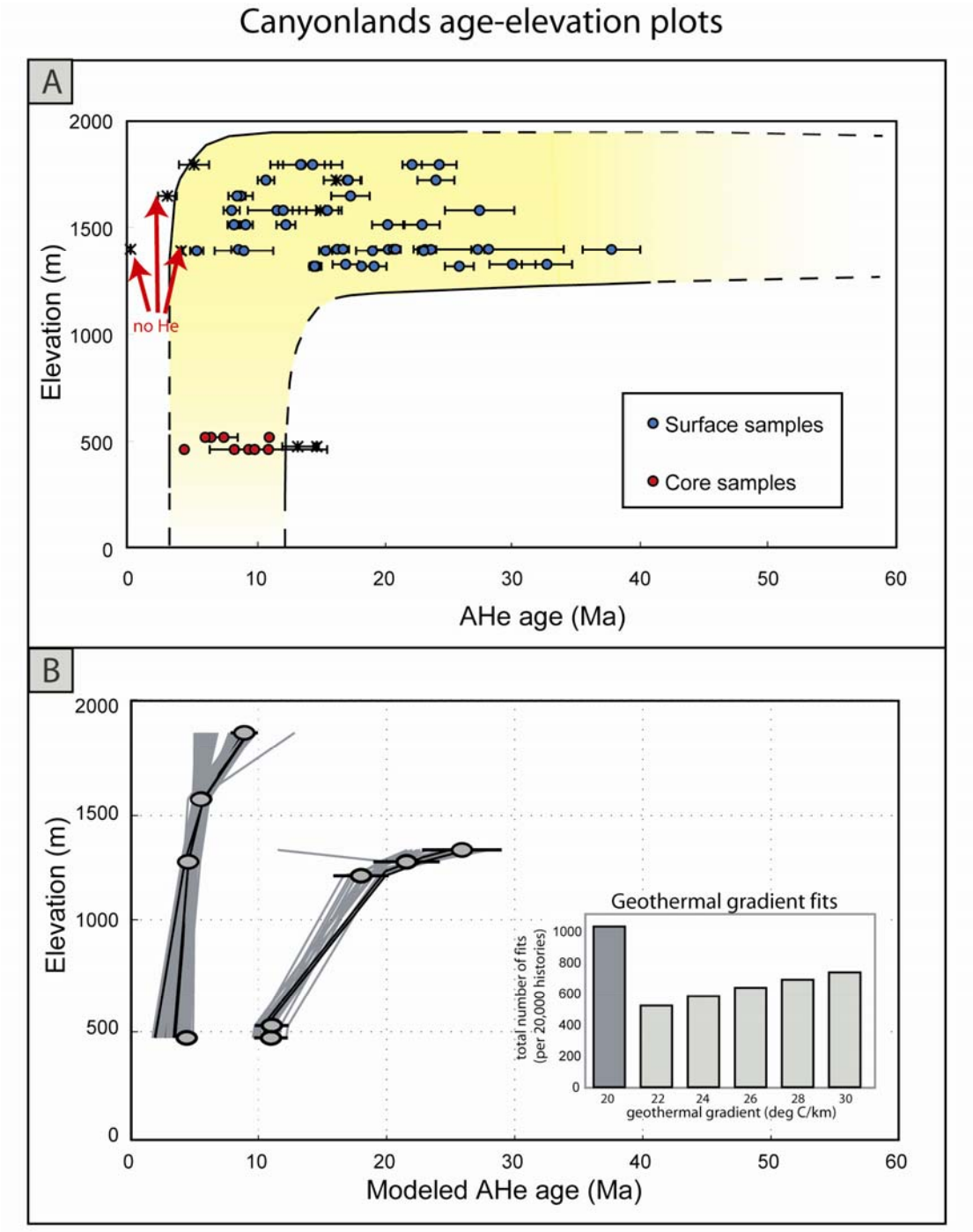
Canyonlands age-elevation plots
A
Elevation (m)
AHe age (Ma)
no He
Surface samples
Core samples
B
Modeled AHe age (Ma)
Geothermal gradient fits
total number of fits
(per 20,000 histories)
geothermal gradient (deg C/km)

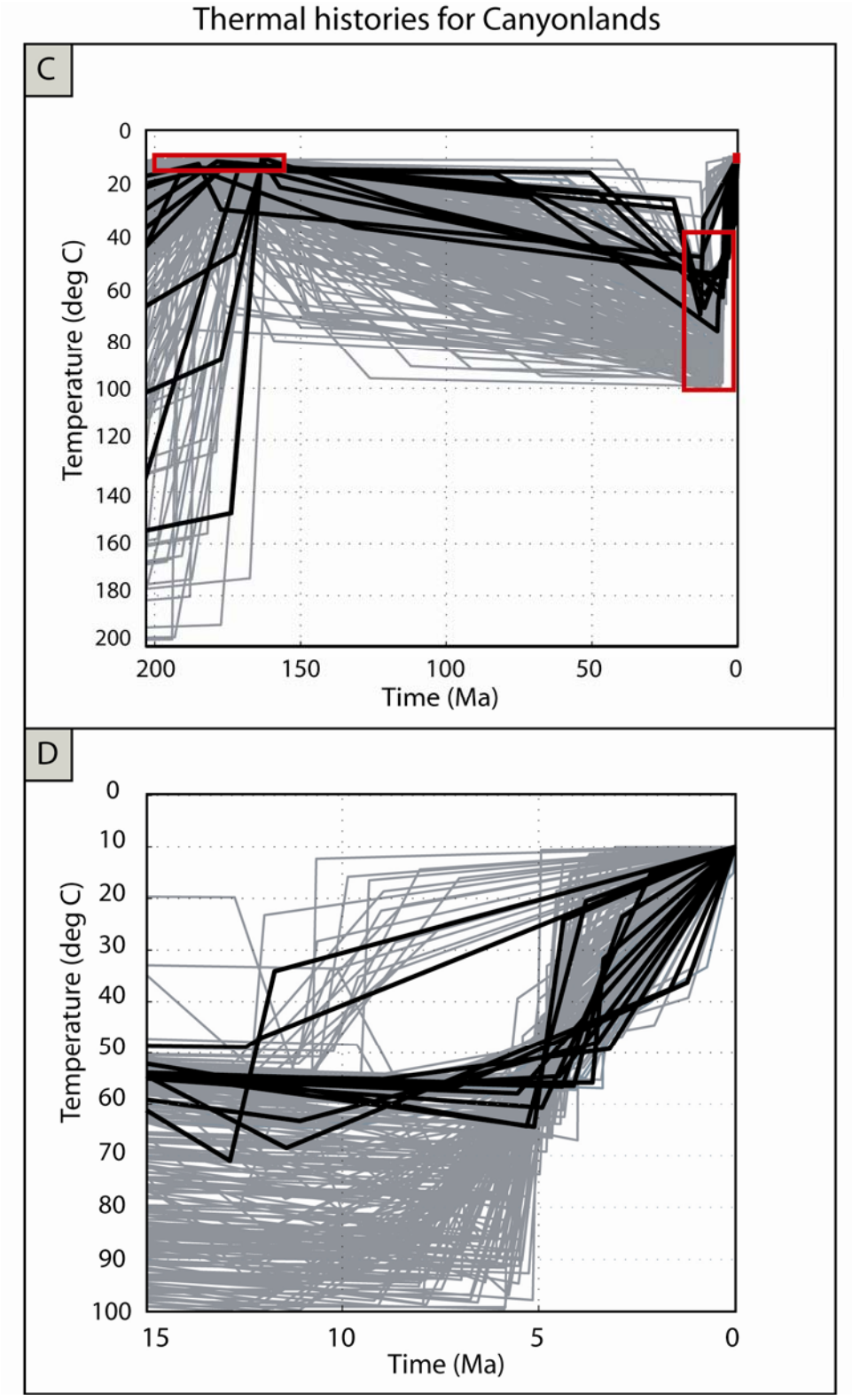
Thermal histories for Canyonlands
C
Temperature (deg C)
0
20
40
60
80
100
120
140
160
180
200
200
150
100
50
0
Time (Ma)
D
Temperature (deg C)
0
10
20
30
40
50
60
70
80
90
100
15
10
5
0
Time (Ma)

Figure 9. A.) Age-elevation plots for Hay Canyon traverse (error is 2σ). Approximate cooling path shown in blue. Excluded ages, shown as stars, are attributed to inclusions. B.) Modeled AHe ages for aliquots defining the cooling envelope (11A) in Hay Canyon (gray lines 2σ fits, black lines 1σ fits). One modeled age from each side of the cooling envelope could be excluded, therefore some of the gray lines may fall outside the 2σ error. The best fit geothermal gradient was 20°C/km. C.) Random thermal histories for Hay Canyon that match AHe ages (2σ fits in gray, 1σ fits in black). Red boxes show user-defined constraints to the thermal histories. D.) An enlarged plot of C.), showing more detail since 15 Ma. Maximum reheating temperatures are ~40−60°C and timing of rapid cooling is mainly ~5−10 Ma.

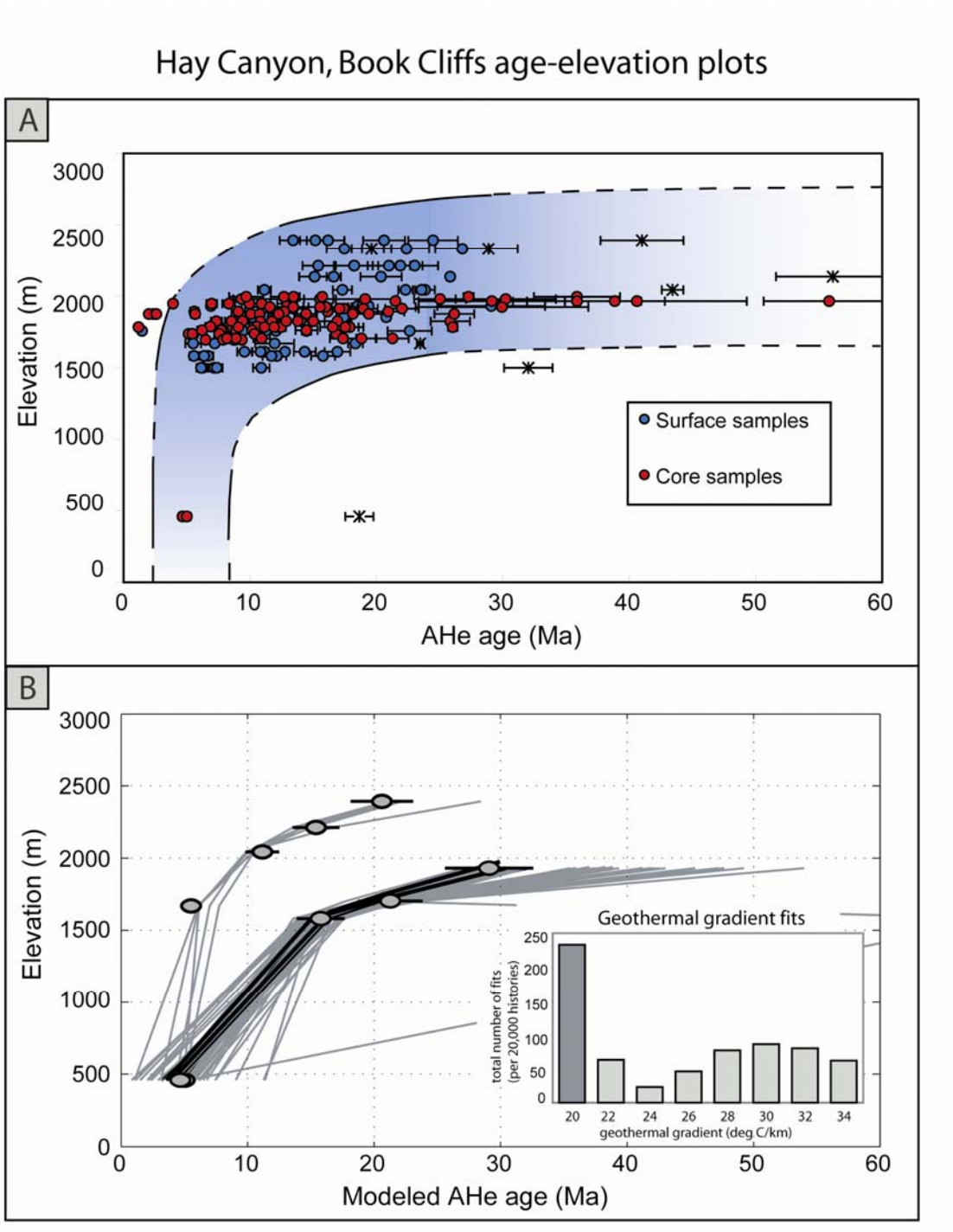
Hay Canyon, Book Cliffs age-elevation plots
A
Elevation (m)
AHe age (Ma)
Surface samples
Core samples
B
Elevation (m)
Modeled AHe age (Ma)
Geothermal gradient fits
total number of fits
(per 20,000 histories)
geothermal gradient (deg.C/km)

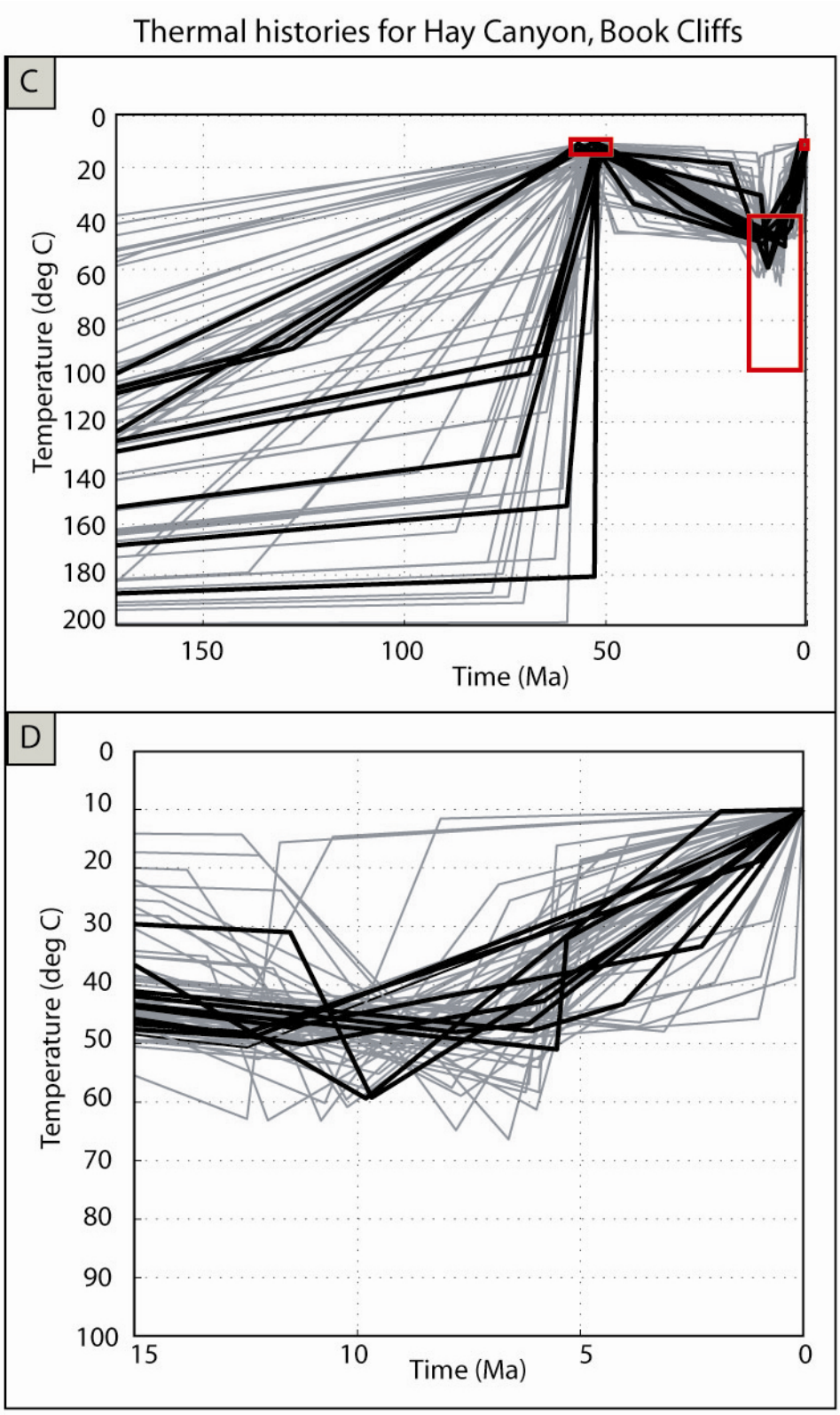
Thermal histories for Hay Canyon, Book Cliffs
C
Temperature (deg C)
0
20
40
60
80
100
120
140
160
180
200
150
100
50
0
Time (Ma)
D
Temperature (deg C)
0
10
20
30
40
50
60
70
80
90
100
15
10
5
0
Time (Ma)

Figure 10. A.) Age-elevation plot of AHe ages from the Sego Canyon transect. The approximate cooling path is shown in the blue envelope. Outliers, shown by stars, are likely due to inclusions. B.) Modeled AHe ages matching the observed ages within either 1σ (black) or 2σ (gray). One modeled age per envelope boundary was permitted to be excluded, so all paths may not fit within the 2σ error of observed data. The geothermal gradient fit distribution is shown in the histogram inset with gradients of 30°C/km fitting the observed ages the best. C.) Random thermal histories for Sego Canyon that match observed AHe ages (2σ fits in gray, 1σ fits in black). Red boxes show user-defined constraints to the thermal histories. D.) An enlarged plot of C), showing more detail since 15 Ma. Maximum reheating temperatures are ~45−65°C and timing of rapid cooling is mainly ~6−10 Ma.

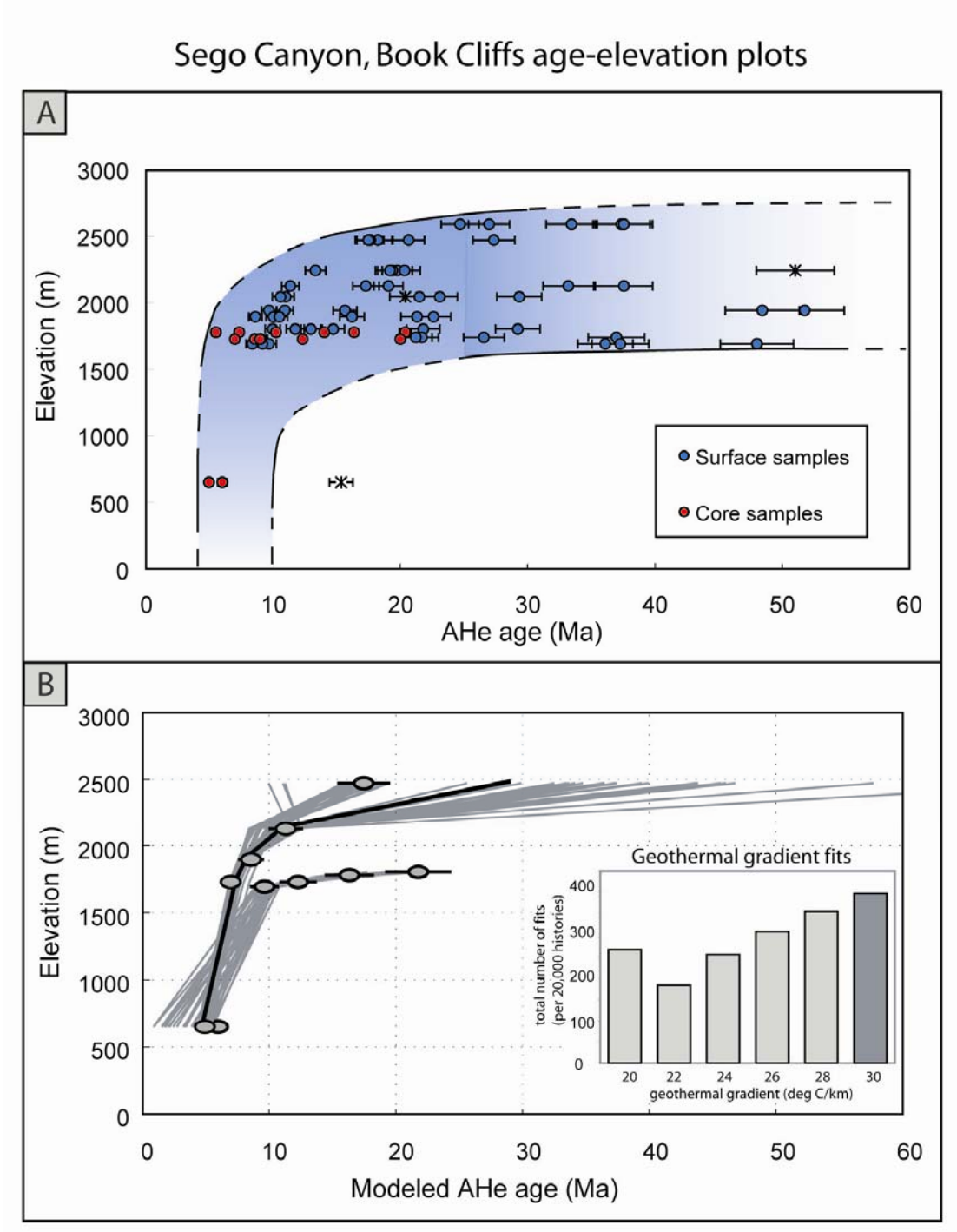
Sego Canyon, Book Cliffs age-elevation plots
A
Elevation (m)
AHe age (Ma)
Surface samples
Core samples
B
Elevation (m)
Modeled AHe age (Ma)
Geothermal gradient fits
total number of fits (per 20,000 histories)
geothermal gradient (deg C/km)

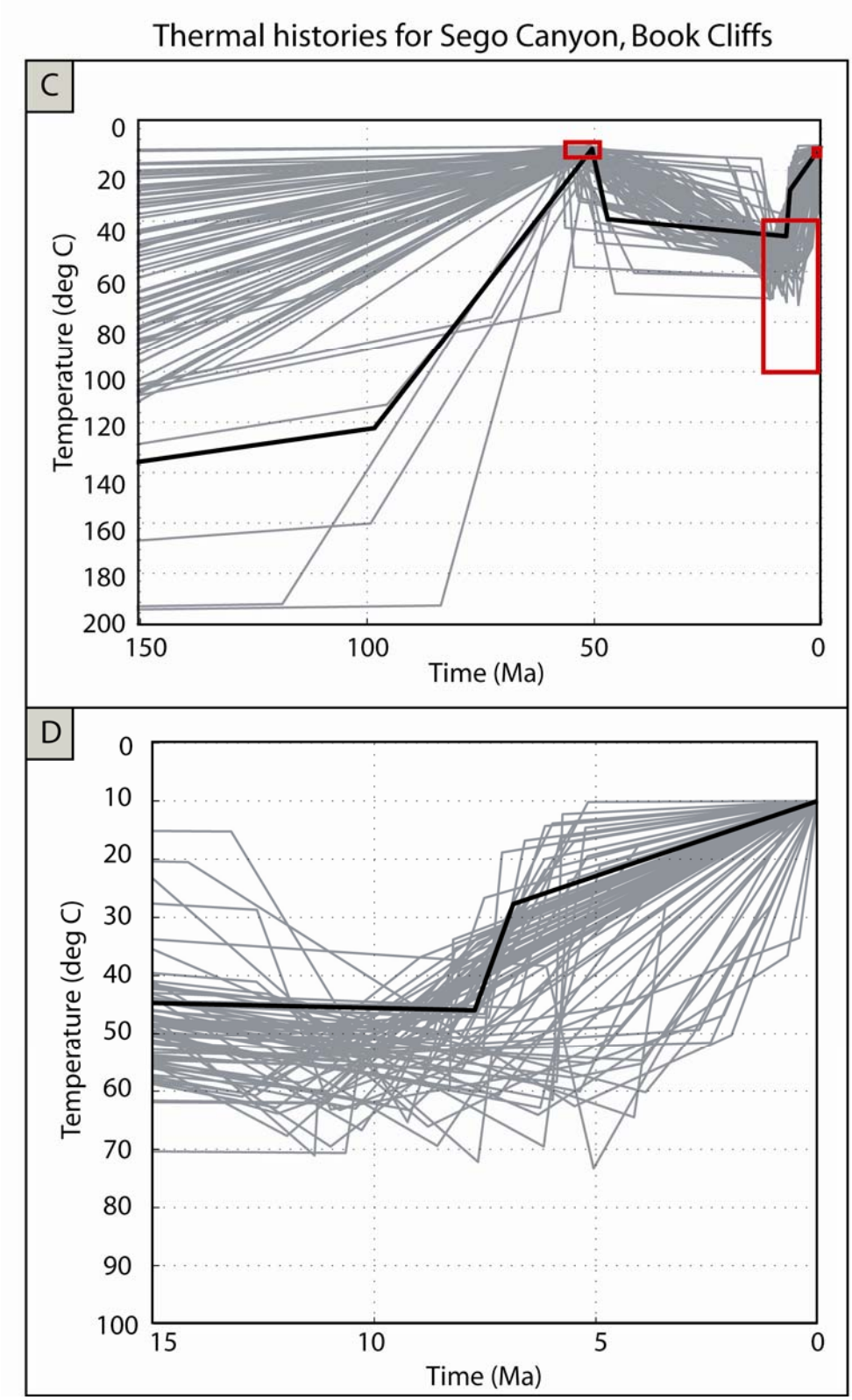
Thermal histories for Sego Canyon, Book Cliffs
C
Temperature (deg C)
0
20
40
60
80
100
120
140
160
180
200
150
100
50
0
Time (Ma)
D
Temperature (deg C)
0
10
20
30
40
50
60
70
80
90
100
15
10
5
0
Time (Ma)

Figure 11. A.) Age-elevation plots for Blaze Canyon traverse (error is 2σ). Approximate cooling path shown in blue. Excluded ages, shown as stars, are attributed to inclusions. B.) Modeled AHe ages for aliquots defining the cooling envelope (13A) in Blaze Canyon (gray lines 2σ fits, black lines 1σ fits). The best fit geothermal gradient, shown in the histogram, was 34^{o}C/km. C.) Modeled thermal histories for Blaze Canyon, Book Cliffs that match observed AHe ages (2σ fits in gray, 1σ fits in black). Red boxes show user-defined constraints to the thermal histories. D.) An enlarged plot of C.), showing more detail since 15 Ma. Maximum burial temperatures are mainly 50−70^{o}C. Timing of rapid erosion ranges from ~4−7 Ma.

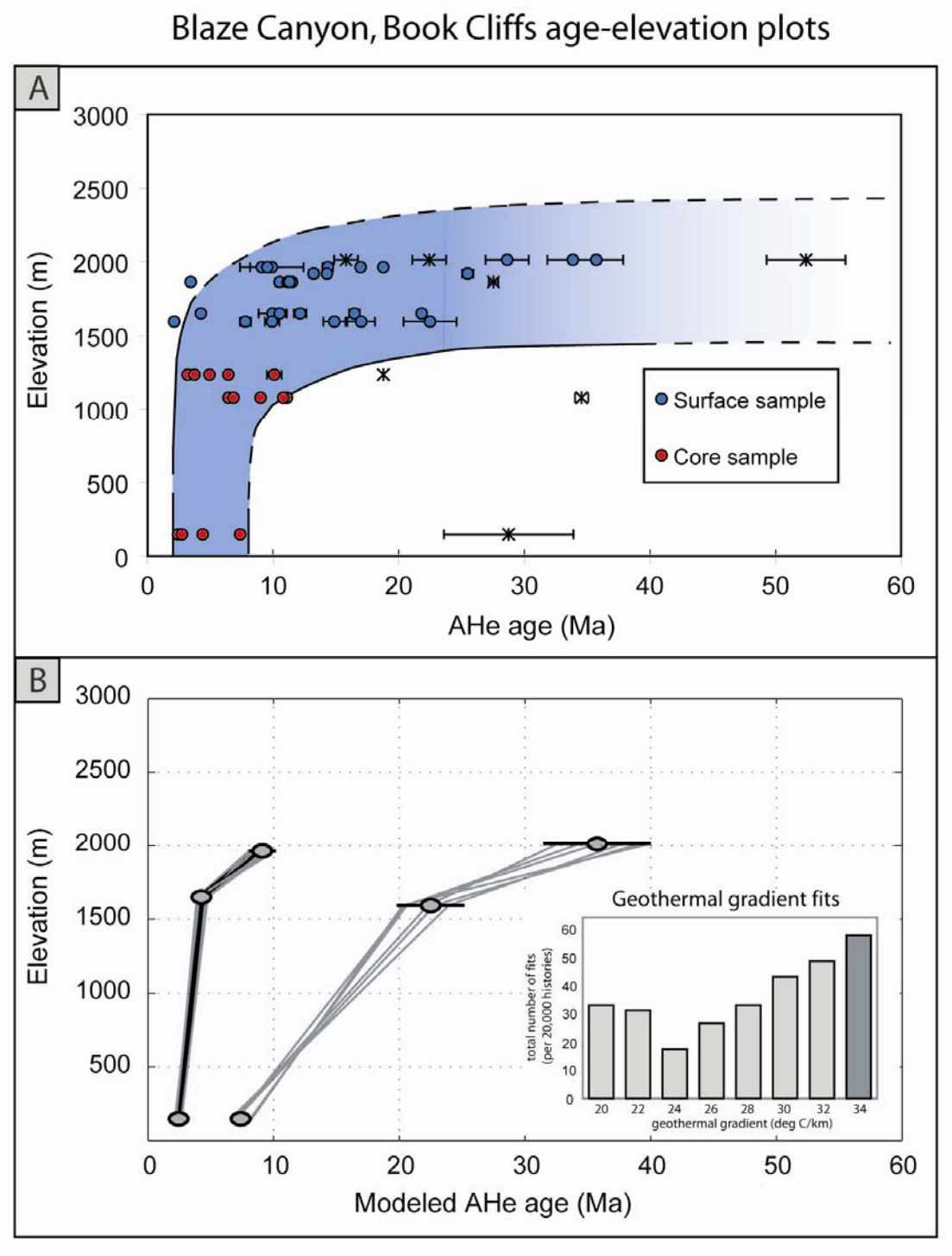
Blaze Canyon, Book Cliffs age-elevation plots
A
Elevation (m)
AHe age (Ma)
Surface sample
Core sample
B
Elevation (m)
Modeled AHe age (Ma)
Geothermal gradient fits
total number of fits (per 20,000 histories)
geothermal gradient (deg C/km)

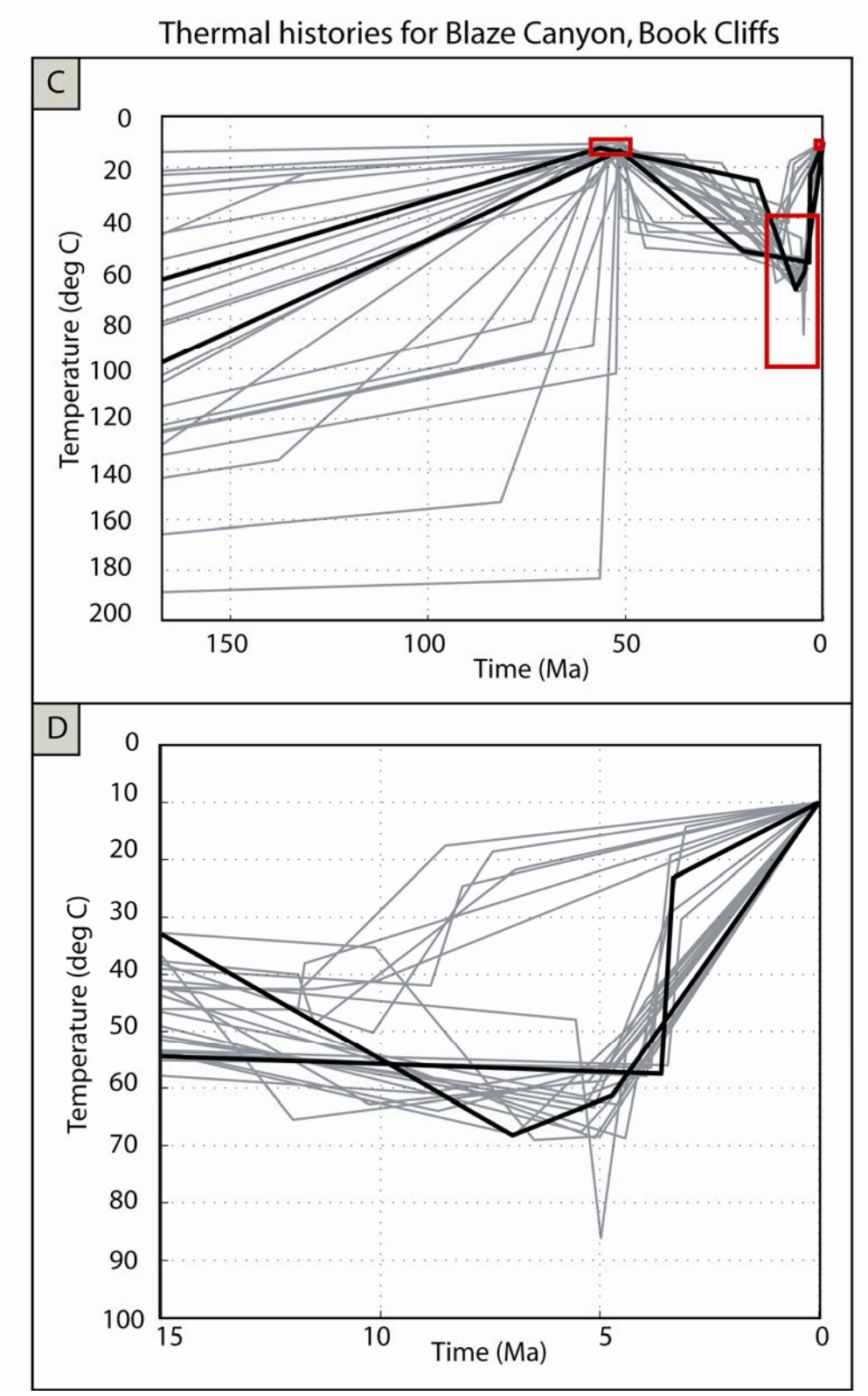
Thermal histories for Blaze Canyon, Book Cliffs
C
Temperature (deg C)
0
20
40
60
80
100
120
140
160
180
200
150
100
50
0
Time (Ma)
D
Temperature (deg C)
0
10
20
30
40
50
60
70
80
90
100
15
10
5
0
Time (Ma)

Figure 12. A.) Age-elevation plot for AHe results in the Uinta Basin (error is 2σ but error bars are very small). Some of AHe ages from the shallowest cores represent cooling in the late Miocene and early Pliocene (e.g., sample at ~250 m elevation), however most were from very deep cores (> 2000 m depth) and have been reset due to thermal reheating during burial in the basin B.) Thermal modeling results of Uinta Basin, with no outliers allowed. The best-fit geothermal gradient was 34^{o}C/km. C). Modeled thermal histories for Uinta Basin that match observed AHe ages (2σ fits in gray, 1σ fits in black). Red boxes show user-defined constraints to the thermal histories. D.) Close up of plot of C.), showing more detail since 15 Ma. Maximum burial temperatures of the upper core sample range from 60−90^{o}C. 1σ fits show thermal histories that have an onset of erosional exhumation ~5−9 Ma.

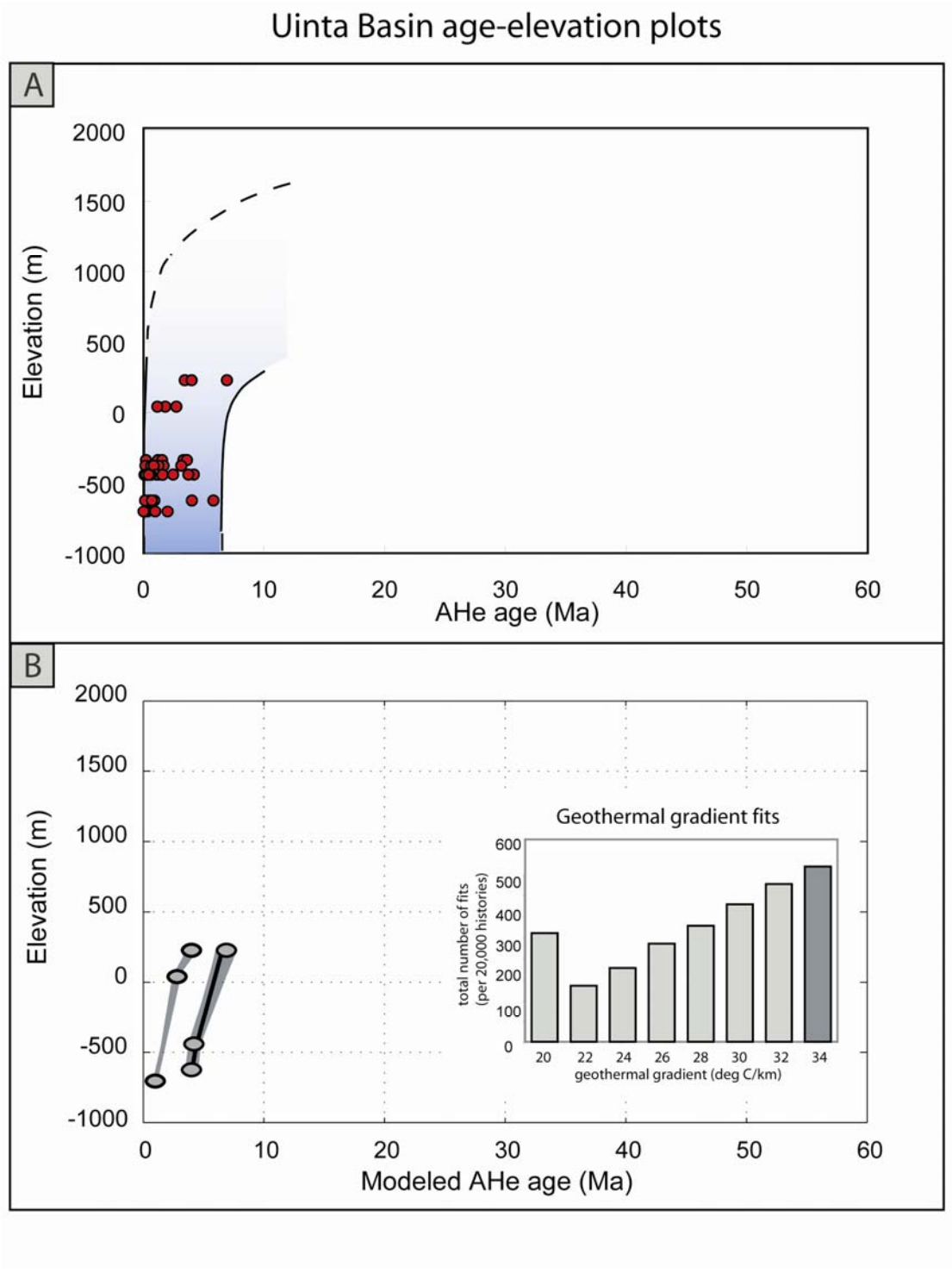
Uinta Basin age-elevation plots
A
Elevation (m)
2000
1500
1000
500
0
-500
-1000
0
10
20
30
40
50
60
AHe age (Ma)
B
Elevation (m)
2000
1500
1000
500
0
-500
-1000
0
10
20
30
40
50
60
Modeled AHe age (Ma)
Geothermal gradient fits
total number of fits
(per 20,000 histories)
600
500
400
300
200
100
0
20
22
24
26
28
30
32
34
geothermal gradient (deg C/km)

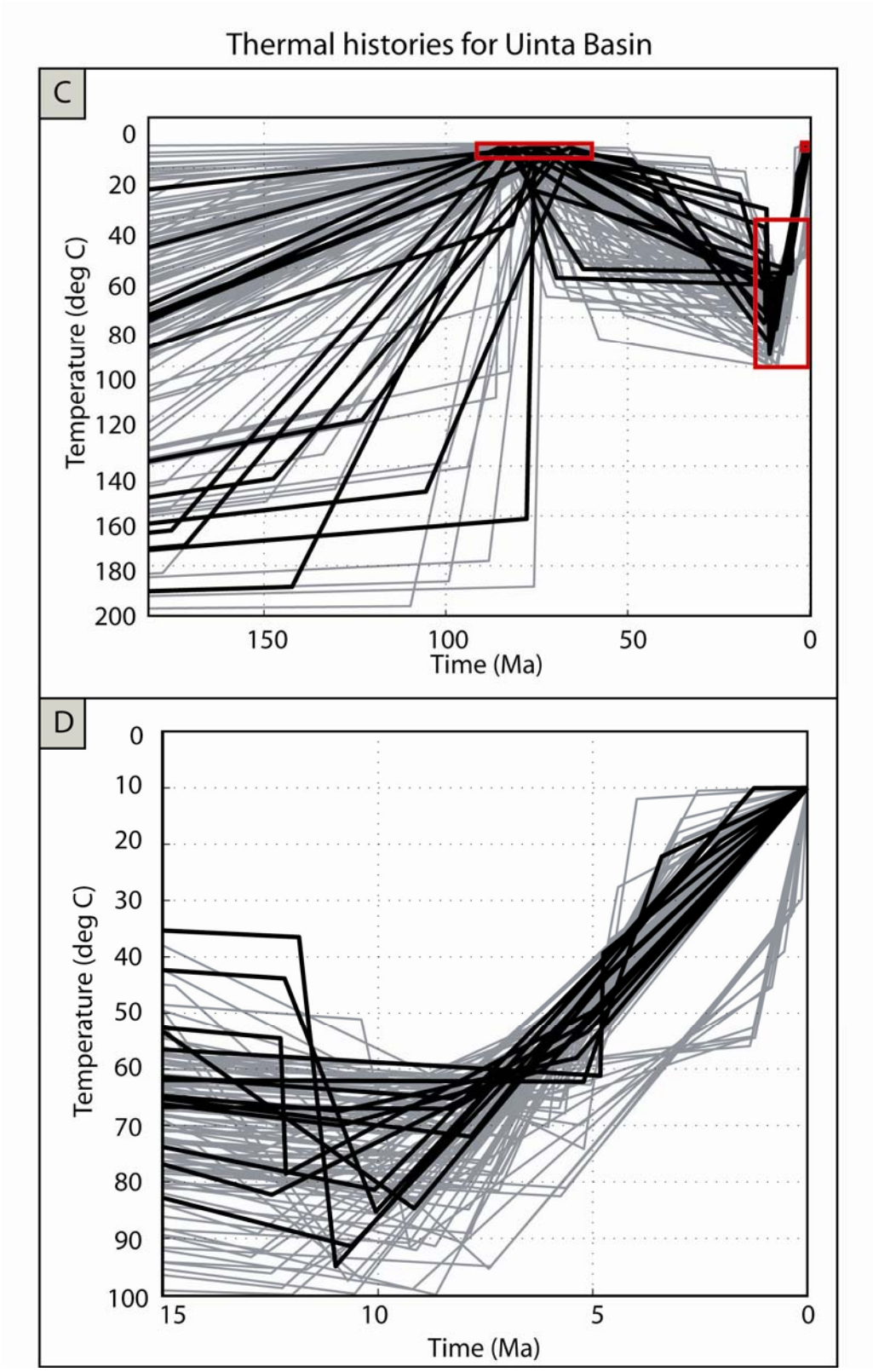
Thermal histories for Uinta Basin
C
Temperature (deg C)
0
20
40
60
80
100
120
140
160
180
200
150
100
50
0
Time (Ma)
D
Temperature (deg C)
0
10
20
30
40
50
60
70
80
90
100
15
10
5
0
Time (Ma)

Figure 13. Single grain radii (spherical radius equivalent) of all sample aliquots plotted against AHe ages to determine if a positive relationship between the two factors exists. There is not a correlation between larger grains and larger ages, so grain size is not the controlling factor in the scatter in observed AHe ages.

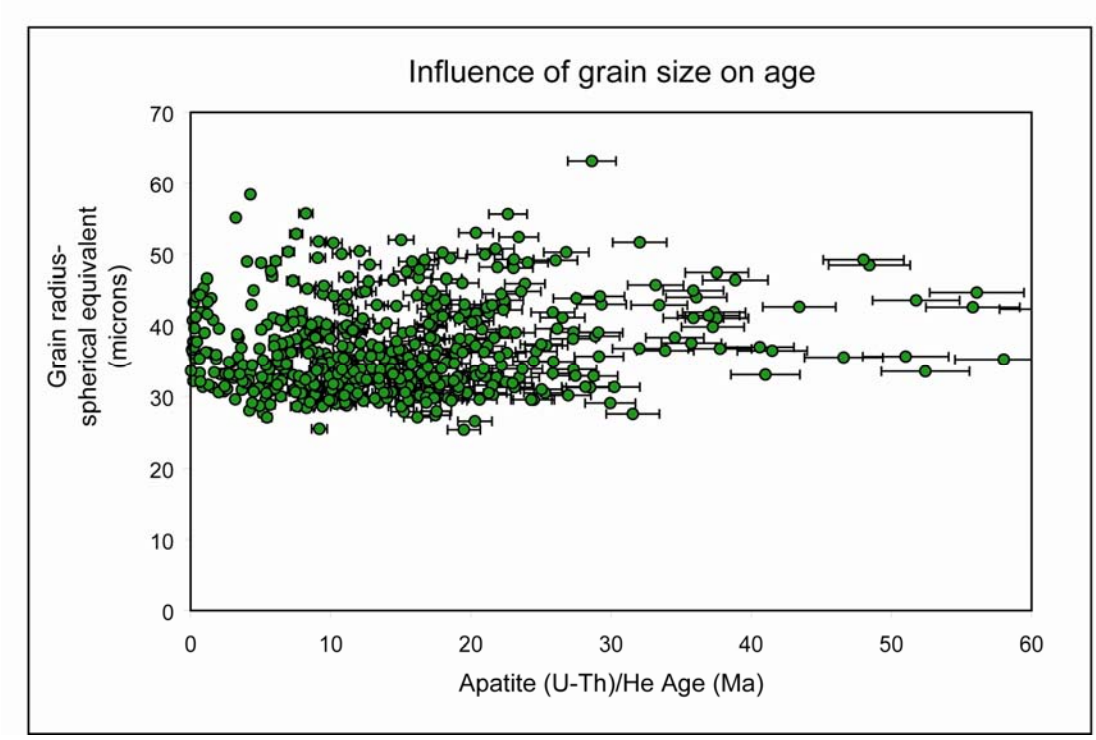
Influence of grain size on age
Grain radius-spherical equivalent (microns)
0
10
20
30
40
50
60
70
0
10
20
30
40
50
60
Apatite (U-Th)/He Age (Ma)

Figure 14. [eU] vs. AHe age plots for all regions of study. All samples with low [eU] (<20 ppm), shown below the horizontal line, will not have ages that correlate with [eU] since low concentrations will cause little radiation damage. Samples that have cooled quickly, ages less than 11 Ma, will not show a correlation with [eU] since radiation damage does not have time to accumulate. Samples having higher [eU] that cooled slowly in the HePRZ show the effects of increased He retentivity due to increased radiation damage and have ages with a positive relationship with [eU].

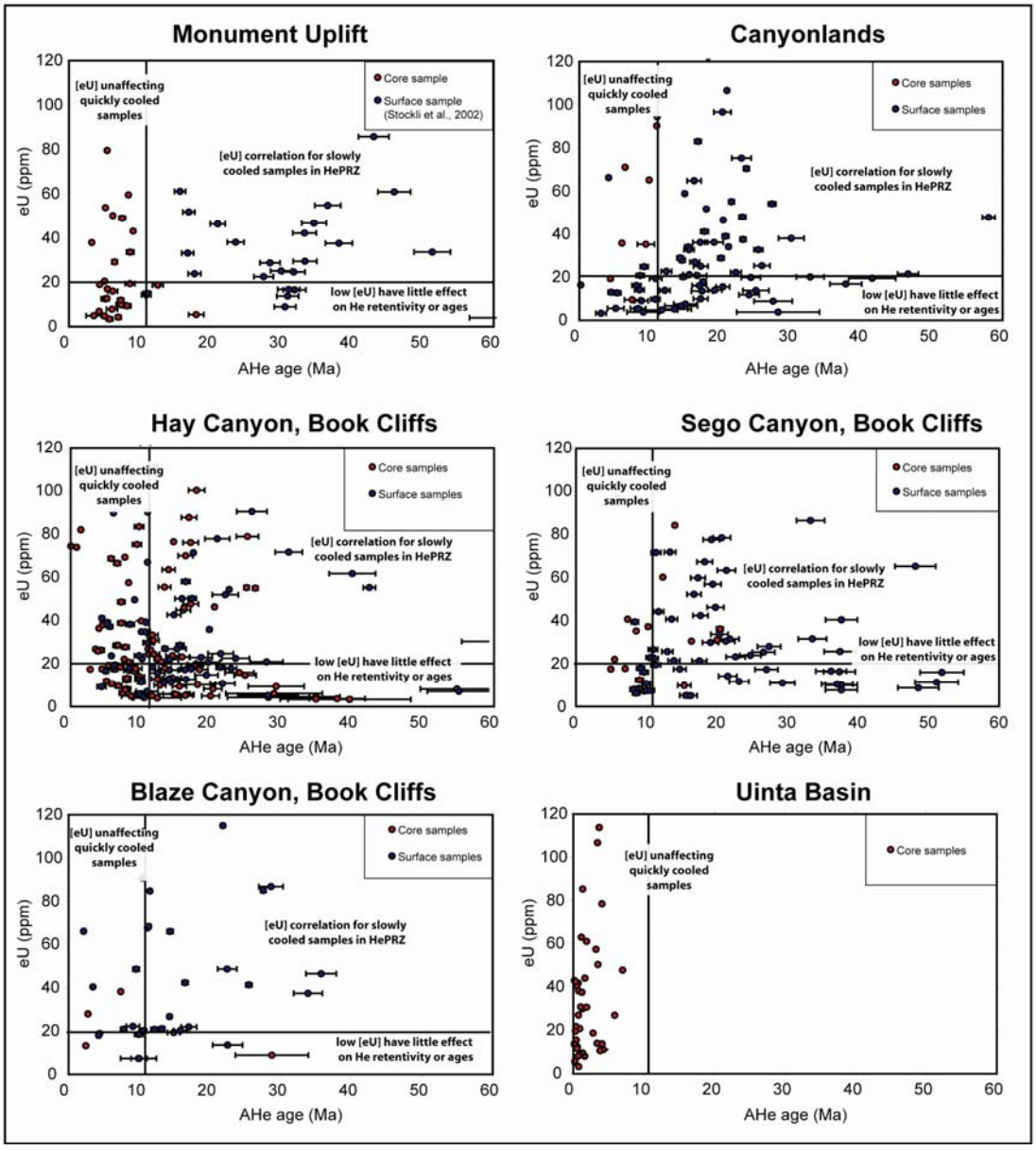
Monument Uplift
Core sample
Surface sample (Stockli et al., 2002)
[eU] unaffecting quickly cooled samples
[eU] correlation for slowly cooled samples in HePRZ
low [eU] have little effect on He retentivity or ages
eU (ppm)
AHe age (Ma)
Canyonlands
Core samples
Surface samples
[eU] unaffecting quickly cooled samples
[eU] correlation for slowly cooled samples in HePRZ
low [eU] have little effect on He retentivity or ages
eU (ppm)
AHe age (Ma)
Hay Canyon, Book Cliffs
Core samples
Surface samples
[eU] unaffecting quickly cooled samples
[eU] correlation for slowly cooled samples in HePRZ
low [eU] have little effect on He retentivity or ages
eU (ppm)
AHe age (Ma)
Sego Canyon, Book Cliffs
Core samples
Surface samples
[eU] unaffecting quickly cooled samples
[eU] correlation for slowly cooled samples in HePRZ
low [eU] have little effect on He retentivity or ages
eU (ppm)
AHe age (Ma)
Blaze Canyon, Book Cliffs
Core samples
Surface samples
[eU] unaffecting quickly cooled samples
[eU] correlation for slowly cooled samples in HePRZ
low [eU] have little effect on He retentivity or ages
eU (ppm)
AHe age (Ma)
Uinta Basin
Core samples
[eU] unaffecting quickly cooled samples
eU (ppm)
AHe age (Ma)

Figure 15. Age-elevation exhumation summary plot of cores from the Monument Uplift, Canyonlands, and Book Cliffs recording late Miocene to early Pliocene cooling (error is 2σ). Cooling envelopes and the timing of exhumation for all regions overlap well and the inflection point marks a change from relatively slow erosional exhumation to faster cooling and erosion ~3−11 Ma. Book Cliffs approximate cooling history shown in blue, Canyonlands in yellow, and Monument Uplift in green.

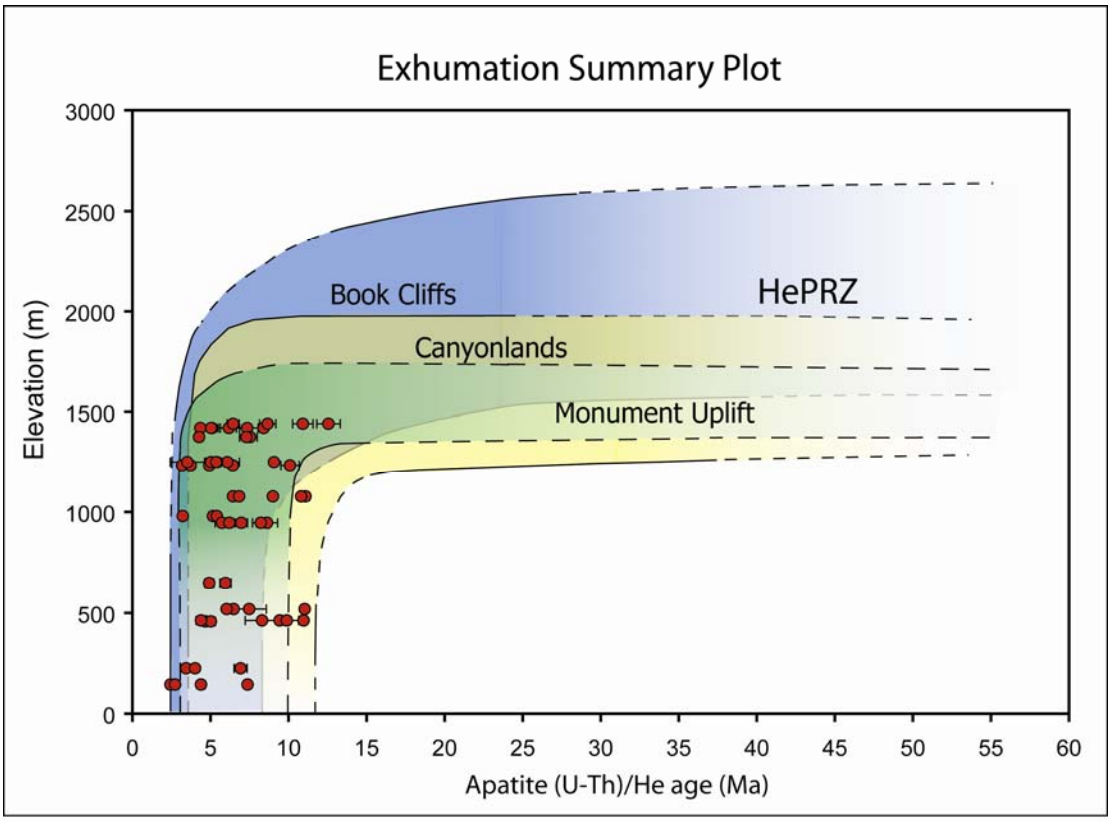
Exhumation Summary Plot
Elevation (m)
3000
2500
2000
1500
1000
500
0
Book Cliffs
HePRZ
Canyonlands
Monument Uplift
0
5
10
15
20
25
30
35
40
45
50
55
60
Apatite (U-Th)/He age (Ma)

Figure 16. Probability density plot (Ludwig, 2003) of AHe ages shown in Figure 13, interpreted to represent exhumation ages in late Miocene-early Pliocene. Reset Uinta Basin cores are excluded. In general, the greatest number of ages fall ~4.3-7.7 Ma, with a mean of 6.6 ± 0.3 Ma (reported error for mean is SDOM). The AHe ages with the highest probability are ~6.3 and ~5 Ma.

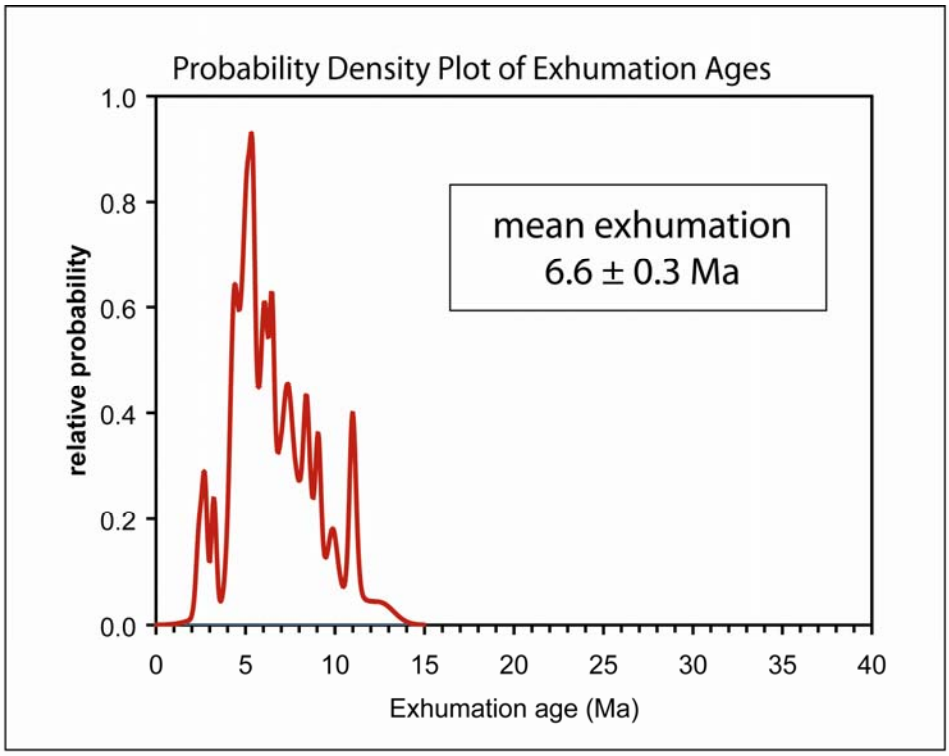
Probability Density Plot of Exhumation Ages
relative probability
1.0
0.8
0.6
0.4
0.2
0.0
0
5
10
15
20
25
30
35
40
Exhumation age (Ma)
mean exhumation
6.6 ± 0.3 Ma

Figure 17. Topographic profile, B-B' illustrated in Figure 1, from Monument Uplift to Uinta Basin with erosion estimations for the central Colorado Plateau (10x vertical exaggeration). Results from this study are shown in red, with 1.5−2 km of erosion in the Monument Uplift area, 2−3 km in the Canyonlands region, 0.9−2.2 km in the Book Cliffs, and 0.2−1.2 km in Uinta Basin. Nuccio and Condon (1996), shown in blue dashed line, estimate 2 km erosion from Monument Uplift to the confluence in Canyonlands and erosion up to 3.5−4 km in the Moab region of Canyonlands. Pederson et al. (2002b), shown in black, estimates 1−2 km in Monument Uplift, 1.5−3 km in Canyonlands, 1−1.5 km in the Book Cliffs, and 0.5−1 km in the Uinta Basin.

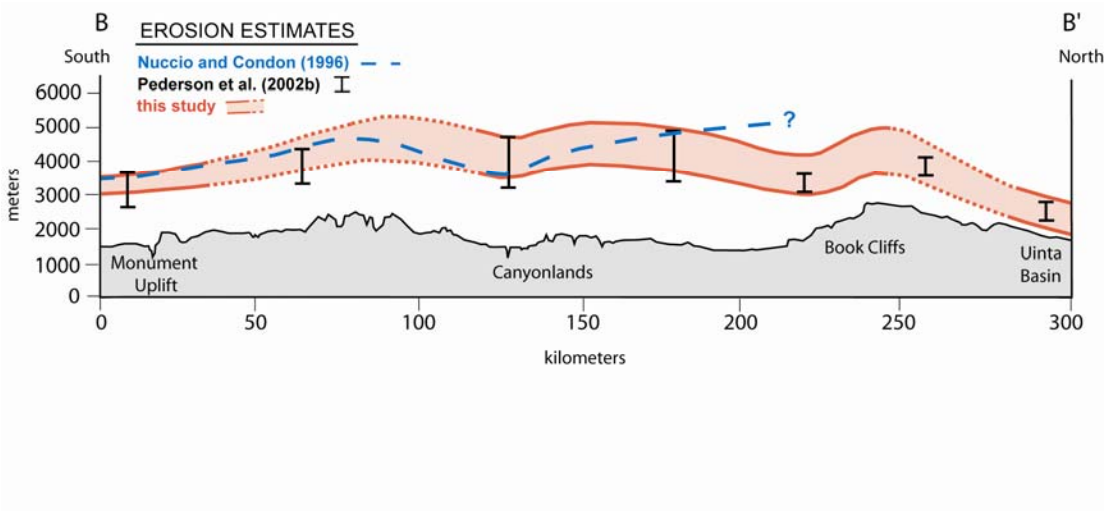
B
EROSION ESTIMATES
B'
South
North
Nuccio and Condon (1996)
Pederson et al. (2002b)
this study
?
6000
5000
4000
3000
2000
1000
0
meters
Monument Uplift
Canyonlands
Book Cliffs
Uinta Basin
0
50
100
150
200
250
300
kilometers

Figure 18. A.) Map of Colorado Plateau showing the locations of other thermochronologic studies. B.) Magnitude of erosional exhumation on the central Colorado Plateau since 10 Ma. The spatial distribution of erosion from our study, combined with other erosion estimates, shows a bull's eye pattern as predicted by other studies (e.g., Pederson et al., 2007). Erosional exhumation is greatest in the Canyonlands region, followed by the surrounding Monument Uplift and Book Cliffs, and decreasing towards the edges of the plateau.

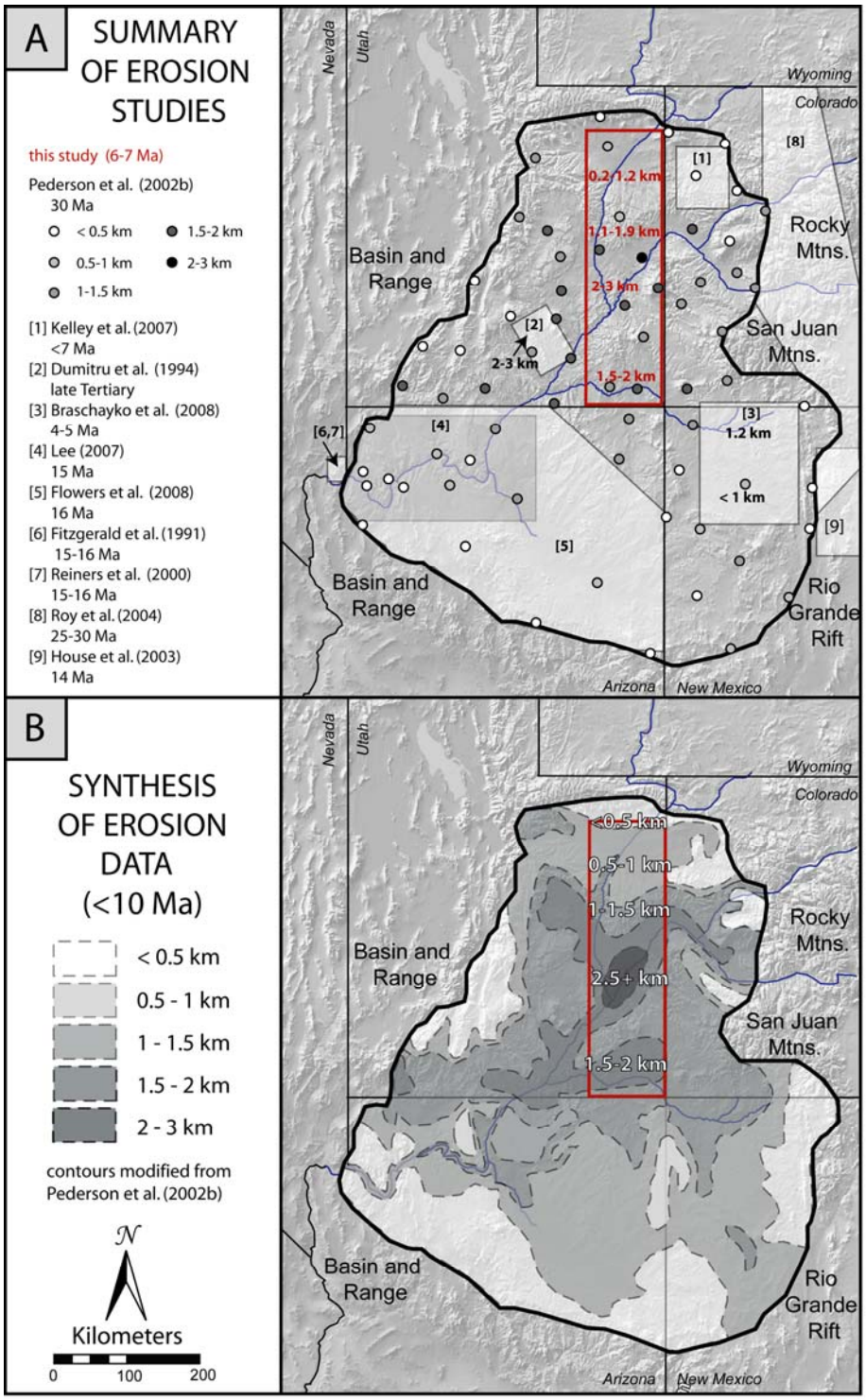
A
SUMMARY OF EROSION STUDIES
this study (6-7 Ma)
Pederson et al. (2002b)
30 Ma
< 0.5 km
0.5-1 km
1-1.5 km
1.5-2 km
2-3 km
[1] Kelley et al. (2007)
<7 Ma
[2] Dumitru et al. (1994)
late Tertiary
[3] Braschayko et al. (2008)
4-5 Ma
[4] Lee (2007)
15 Ma
[5] Flowers et al. (2008)
16 Ma
[6] Fitzgerald et al. (1991)
15-16 Ma
[7] Reiners et al. (2000)
15-16 Ma
[8] Roy et al. (2004)
25-30 Ma
[9] House et al. (2003)
14 Ma
Nevada
Utah
Wyoming
Colorado
Arizona
New Mexico
Basin and Range
Rocky Mtns.
San Juan Mtns.
Rio Grande Rift
0.2-1.2 km
1.1-1.9 km
2-3 km
1.5-2 km
2-3 km
1.2 km
< 1 km
[1]
[2]
[3]
[4]
[5]
[6,7]
[8]
[9]
B
SYNTHESIS OF EROSION DATA (<10 Ma)
< 0.5 km
0.5 - 1 km
1 - 1.5 km
1.5 - 2 km
2 - 3 km
contours modified from Pederson et al. (2002b)
N
Kilometers
0
100
200
<0.5 km
0.5-1 km
1-1.5 km
2.5+ km
1.5-2 km

APPENDICES

	Page
Appendix A: (U-Th)/He Analytical Procedure	123
Appendix B: Collection methods and sample description	126
Appendix C: Grain dimensions table	128
Appendix D: Photographs of core samples	145

Appendix A: (U-Th)/He Analytical procedure

Mineral Separation

Apatite for thermochronometric analyses is isolated by using standard heavy mineral separation techniques. Rock samples were crushed and rinsed over a water table to density sort the grains. A series of heavy liquids (e.g., bromoform and methylene iodide) and Franz magnetic separator sort the minerals based on differences in mineral densities and magnetic properties, respectively.

Grain selection

Individual apatite grains are examined closely under a binocular microscope with crossed polars for possible mineral inclusions, such as zircon or monazite, whose high U and Th concentrations may produce erroneously high He ages. Ideally, apatite grains should be greater than 70 μm in diameter and euhedral, the typical morphology to properly apply the F_T α ejection correction, (Farley et al., 1996). However, detrital apatite grains from this region were commonly broken, mildly abraided, or rounded to an oblong shape. These apatite grains were usually smaller than the 70 μm standard, and it was common to select grains 55−70 μm wide. Under higher magnifications, each grain was scrutinized on each side for fluid or birefringent zircon or monazite inclusions. The lengths and widths of six single grains were photographed, measured, and grains were packed into individual platinum foil packets, or aliquots.

In order to yield an age from a sample with poor quality apatite or very few grains, apatite with inclusions can be analyzed following methods from Vermeesch et al. (2007). For these analyses, 18 grains of apatite were chosen per sample (six

grains/aliquot). The inclusions in the grains should be as small as possible, on the order of a few microns. This method attempts to randomize the number and location of inclusions for the Ft correction (Vermeesch et al., 2007).

Isotopic measurements

The ^{4}He concentration of apatite is determined by indirectly heating grains using the Nd-YAG laser method as described by House et al. (2000). A focused Nd-YAG laser beam heats the packet for five minutes at ~1080^{o}C to extract the He. The released ^{4}He is spiked with ^{3}He, cryogenically purified, and measured on a quadrupole mass spectrometer. To ensure complete He extraction, samples are heated a second time and this reextract is compared to ^{4}He blank levels. Samples with reextracts higher than background ^{4}He levels may indicate the presence of inclusions and such ages are discarded. For apatite samples with known inclusions (e.g., Vermeesch et al., 2007), multiple reextracts may be necessary to ensure total He extraction.

After degassing, Pt packets are transferred to vials, spiked with a HNO_3-based solution containing a ^{235}U- ^{230}Th-^{149}Sm tracer, and heated to 90^{o}C for 90 minutes to ensure complete dissolution (e.g., House et al., 2000; Blackburn et al., 2007). U, Th, and Sm content of the sample are subsequently measured by isotope dilution on an inductively coupled plasma mass spectrometer (ICP-MS).

For samples with known inclusions, pressure digestion vessels, a more rigorous dissolution method usually reserved for zircon grains (Reiners, 2005), is required to ensure all inclusions are dissolved (Vermeesch et al., 2007). Grains are

removed from their packets to prevent PtAr interference on the ICP-MS and placed in Teflon microcapsules with a combination of concentrated HF and HNO_3 acids (House et al., 2000). Microcapsules are inserted in the pressure digestion vessels and are placed in an oven at 220^{o}C for 3 days. HF is subsequently dried to completion, and 6 N HCl acid is added and heated in an oven at 180^{o}C for 12 hours to dissolve any fluoride salts. After HCl dry down, a 70% HNO_3 solution is introduced and placed in the oven at 90^{o}C for 45 minutes. Samples are then diluted with 500 μL of Milli-Q water in preparation for analysis on the ICP-MS.

Appendix B: Collection methods and sample description

Surface samples were collected in the Canyonlands and Book Cliffs along transects using the method described by Stockli et al. (2000). Vertical transects record cooling with changes in elevation or depth and lateral transects, or traverses, record cooling along both vertical and horizontal distances. In both transects, samples are collected approximately every 100 m of elevation change. In addition to these transects, some individual surface samples were collected for regional thermochronometric studies to address any north to south spatial trends in erosion. Surface samples collected were primarily arkosic sandstones with a wide variation in grain size from very-fine to coarse-grained. Occasionally, a quartz arenite or siltstone sample was also collected.

Core samples were collected at the USGS Denver Core Research Center and the Utah Core Research Center. For each core, samples were collected at ~50 m depth increments wherever an apatite-bearing sandstone could be found. Cores were usually ~4 or ~10 cm wide, and sample sizes were ~2–3 kg. In addition, only cores were sampled; no cuttings were collected to reduce the risk of sample contamination from various depths in the well and also to avoid thermal resetting when cuttings are oven-dried after collection. However, working with cores does have some drawbacks. We can only sample cores available to the public, and sample quantities are limited. Also we are constrained by the lithology of the core; in this region of Utah, many cores have been taken of the Paradox Fm., predominately halite, other evaporates, and limestone which are unsuitable for thermochronology because they

do not contain apatite. In addition, information important to thermochronometric studies is not always available, such as well bottom-hole temperatures. Nevertheless, core sampling is key to our study of the erosion in the central Colorado Plateau; we sampled as many cores that were available in the region and bottom-hole temperatures can be estimated from recent geothermal gradient data.

Appendix C. Grain dimensions

Sample	Length (µm)	Width (µm)	Equivalent sphere radius (µm)	Mass (µg)	Ft correction
Book Cliffs, Hay Canyon Vertical Transect					
07CP02-1	68.01	56.70	27.06	0.45	0.47
07CP02-2	83.82	58.36	29.13	0.59	0.49
07CP02-3	121.01	62.21	33.05	0.97	0.56
07CP02-4	96.54	61.44	31.28	0.76	0.53
07CP02-5	76.46	61.27	29.54	0.59	0.51
07CP02-6	106.97	55.70	29.52	0.69	0.51
07CP03-1	172.21	80.67	43.56	2.32	0.65
07CP03-2	124.98	81.44	41.26	1.72	0.63
07CP03-3	145.99	79.89	41.95	1.93	0.63
07CP03-4	121.23	75.18	38.49	1.42	0.61
07CP03-5	140.60	81.50	42.31	1.94	0.65
07CP03-6	189.80	93.92	50.24	3.47	0.69
07CP04-1	179.44	86.63	46.54	2.79	0.67
07CP04-2	157.93	93.02	48.14	2.83	0.67
07CP04-3	170.15	95.54	49.92	3.22	0.69
07CP04-4	153.07	92.25	47.52	2.70	0.67
07CP04-5	171.62	90.90	48.03	2.94	0.67
07CP04-6	129.28	94.17	46.50	2.38	0.67
07CP05-1	106.57	71.02	35.80	1.11	0.57
07CP05-2	117.54	84.12	41.71	1.72	0.63
07CP05-3	106.46	72.73	36.46	1.17	0.58
07CP05-4	169.31	83.40	44.65	2.44	0.65
07CP05-5	142.37	80.20	41.88	1.90	0.63
07CP05-6	170.85	91.96	48.44	2.99	0.68
07CP06-1	148.14	89.03	45.89	2.43	0.67
07CP06-2	125.39	84.86	42.63	1.87	0.64
07CP06-3	170.45	83.63	44.80	2.47	0.66
07CP06-4	119.62	84.98	42.21	1.79	0.64
07CP06-5	114.08	69.75	35.82	1.15	0.60
07CP06-6	119.12	90.88	44.37	2.04	0.65
07CP07-1	140.11	75.99	39.97	1.68	0.62
07CP07-2	142.29	73.51	39.02	1.59	0.61
07CP07-3	139.98	99.44	49.39	2.87	0.68
07CP07-4	104.09	72.16	36.05	1.12	0.58
07CP07-5	153.44	88.48	45.99	2.49	0.66
07CP07-6	117.25	70.08	36.16	1.19	0.60

Appendix C cont.

Sample	Length (µm)	Width (µm)	Equivalent sphere radius (µm)	Mass (µg)	Ft correction
Book Cliffs, Hay Canyon Vertical Transect cont.					
07CP08-1	114.94	85.79	42.11	1.75	0.63
07CP08-2	133.47	74.71	39.06	1.54	0.61
07CP08-3	102.92	83.51	40.14	1.49	0.61
07CP08-4	164.20	82.79	44.14	2.33	0.65
07CP08-5	105.40	94.98	44.38	1.97	0.65
07CP08-6	151.99	73.51	39.48	1.70	0.62
07CP09-1	139.87	91.83	46.44	2.44	0.66
07CP09-2	178.42	95.62	50.41	3.38	0.69
07CP09-3	178.14	80.72	43.83	2.40	0.65
07CP09-4	157.67	84.33	44.47	2.32	0.65
07CP09-5	176.10	108.43	55.60	4.29	0.71
07CP09-6	143.89	91.99	46.80	2.52	0.67
07CP10-1	106.49	56.26	29.74	0.70	0.51
07CP10-2	108.57	72.10	36.37	1.17	0.59
07CP10-3	97.27	59.69	30.63	0.72	0.51
07CP10-4	84.49	61.07	30.21	0.65	0.51
07CP10-5	104.00	60.31	31.31	0.78	0.52
07CP10-6	98.50	64.59	32.67	0.85	0.55
07CP11-1	127.71	99.92	48.48	2.64	0.67
07CP11-2	106.86	78.90	38.83	1.38	0.61
07CP11-3	122.16	86.41	42.97	1.89	0.64
07CP11-4	111.47	80.32	39.76	1.49	0.62
07CP11-5	95.38	70.69	34.76	0.99	0.57
07CP11-6	143.97	84.81	43.89	2.15	0.65
07CP13-1	100.59	67.22	33.86	0.94	0.56
07CP13-2	108.16	67.13	34.37	1.01	0.56
07CP13-3	86.84	70.39	33.84	0.89	0.55
07CP13-4	89.66	66.05	32.53	0.81	0.54
07CP13-5	108.71	59.37	31.19	0.79	0.52
07CP13-6	102.64	62.60	32.17	0.83	0.54
07CP14-1	113.75	70.77	36.21	1.18	0.58
07CP14-2	129.83	76.82	39.72	1.59	0.62
07CP14-3	114.00	58.17	30.95	0.80	0.52
07CP14-4	117.30	71.52	36.75	1.24	0.58
07CP14-5	91.11	72.08	34.87	0.98	0.57
07CP14-6	84.06	65.58	31.84	0.75	0.53

Appendix C cont.

Sample	Length (µm)	Width (µm)	Equivalent sphere radius (µm)	Mass (µg)	Ft correction
Book Cliffs, Sego Canyon Vertical Transect					
07CP15-1	99.78	58.10	30.14	0.70	0.51
07CP15-2	137.98	80.86	41.89	1.87	0.64
07CP15-3	114.50	100.77	47.39	2.41	0.68
07CP15-4	161.14	76.03	41.01	1.93	0.64
07CP15-5	160.28	80.35	42.88	2.14	0.64
07CP15-6	126.03	69.28	36.35	1.25	0.58
07CP16-1	92.18	64.50	32.15	0.79	0.55
07CP16-2	100.15	81.31	39.08	1.37	0.62
07CP16-3	115.74	71.05	36.46	1.21	0.58
07CP16-4	83.77	53.82	27.35	0.50	0.47
07CP16-5	119.52	56.20	30.33	0.78	0.52
07CP16-6	121.26	61.82	32.89	0.96	0.54
07CP18-1	91.79	60.27	30.48	0.69	0.52
07CP18-2	118.07	63.70	33.54	0.99	0.55
07CP18-3	159.40	64.44	35.62	1.37	0.57
07CP18-4	87.91	66.06	32.37	0.79	0.55
07CP18-5	104.38	85.62	41.04	1.59	0.63
07CP18-6	140.16	83.01	42.91	2.00	0.66
07CP19-1	86.44	62.70	30.99	0.70	0.54
07CP19-2	129.02	60.56	32.69	0.98	0.55
07CP19-3	162.11	86.62	45.69	2.52	0.67
07CP19-4	140.80	78.48	41.06	1.80	0.63
07CP19-5	124.23	77.73	39.72	1.56	0.62
07CP19-6	103.28	66.12	33.62	0.94	0.57
07CP20-1	165.15	80.08	42.99	2.19	0.64
07CP20-2	151.09	96.81	49.22	2.93	0.69
07CP20-3	91.50	73.42	35.39	1.02	0.58
07CP20-4	128.92	61.26	33.00	1.00	0.55
07CP20-5	106.35	60.60	31.57	0.81	0.56
07CP20-6	114.01	62.69	32.89	0.93	0.55
07CP21-1	99.34	64.16	32.57	0.85	0.54
07CP21-2	114.40	103.85	48.42	2.56	0.68
07CP21-3	99.55	75.60	36.95	1.18	0.59
07CP21-4	136.00	85.24	43.55	2.05	0.65
07CP21-5	110.89	70.83	36.04	1.15	0.58
07CP21-6	103.77	68.83	34.73	1.02	0.56

Appendix C cont.

Sample	Length (µm)	Width (µm)	Equivalent sphere radius (µm)	Mass (µg)	Ft correction
Book Cliffs, Sego Canyon Vertical Transect cont.					
07CP22-1	122.10	69.30	36.13	1.21	0.58
07CP22-2	123.18	66.46	34.99	1.13	0.56
07CP22-3	138.57	80.48	41.77	1.86	0.63
07CP22-4	93.25	60.40	30.64	0.70	0.51
07CP22-5	103.19	68.83	34.69	1.01	0.56
07CP22-6	106.53	60.50	31.54	0.81	0.53
07CP23-1	107.49	79.91	39.26	1.42	0.63
07CP23-2	154.52	80.69	42.74	2.08	0.64
07CP23-3	79.30	73.25	33.98	0.88	0.56
07CP23-4	102.05	61.52	31.69	0.80	0.53
07CP23-5	145.17	85.15	44.10	2.18	0.65
07CP23-6	166.64	98.01	50.74	3.32	0.70
07CP24-1	102.12	87.38	41.41	1.62	0.64
07CP24-2	103.57	86.07	41.11	1.59	0.63
07CP24-3	153.94	70.60	38.26	1.59	0.64
07CP24-4	133.35	70.16	37.11	1.36	0.60
07CP25-1	106.50	79.72	39.10	1.40	0.61
07CP25-2	103.94	74.00	36.74	1.18	0.59
07CP25-3	131.49	100.86	49.18	2.77	0.69
07CP25-4	138.98	105.99	51.75	3.23	0.70
07CP25-5	108.51	92.76	43.97	1.93	0.65
07CP25-6	119.16	78.84	39.80	1.53	0.62
07CP35-1	107.74	64.44	33.24	0.93	0.55
07CP35-2	130.98	66.41	35.37	1.20	0.58
07CP35-3	132.39	61.08	33.07	1.02	0.55
07CP35-4	89.52	68.51	33.42	0.87	0.56
07CP35-5	108.54	79.57	39.23	1.42	0.61
07CP35-6	107.16	78.86	38.84	1.38	0.61
Book Cliffs, Blaze Canyon Vertical Transect					
07CP27-1	164.89	130.55	63.15	5.82	0.74
07CP27-2	139.06	98.37	48.91	2.79	0.68
07CP27-3	109.51	64.84	33.52	0.95	0.55
07CP27-4	127.40	71.87	37.52	1.36	0.60
07CP27-5	120.33	76.82	39.09	1.47	0.62
07CP27-6	123.63	69.85	36.45	1.25	0.58
07CP28-1	114.51	70.96	36.34	1.19	0.58
07CP28-2	107.91	68.29	34.82	1.04	0.56

Appendix C cont.

Sample	Length (µm)	Width (µm)	Equivalent sphere radius (µm)	Mass (µg)	Ft correction
Book Cliffs, Blaze Canyon Vertical Transect cont.					
07CP28-3	112.90	61.28	32.23	0.88	0.53
07CP28-4	134.98	66.19	35.46	1.23	0.57
07CP28-5	112.49	67.32	34.73	1.06	0.56
07CP28-6	121.05	59.53	31.88	0.89	0.53
07CP29-1†	127.26	70.23	52.66	1.30	0.57
	107.49	87.07	57.45	1.69	
	90.19	77.50	50.14	1.12	
	96.93	62.55	44.52	0.79	
	79.87	66.11	43.31	0.72	
	100.41	58.00	42.84	0.70	
07CP29-2†	83.12	63.81	42.86	0.70	0.52
	90.82	57.43	41.16	0.62	
	76.72	62.77	41.28	0.63	
	69.72	60.57	39.04	0.53	
	72.60	68.94	43.14	0.71	
	102.49	64.86	46.47	0.89	
07CP29-3†	80.38	61.97	41.57	0.64	0.50
	85.84	62.87	42.90	0.70	
	68.49	62.33	39.56	0.55	
	95.00	55.42	40.80	0.60	
	74.33	56.76	38.20	0.50	
	64.37	57.93	36.91	0.45	
07CP30-1	104.41	61.12	31.67	0.81	0.52
07CP30-2	144.44	75.56	40.01	1.71	0.61
07CP30-3	151.16	83.64	43.83	2.19	0.64
07CP30-4	136.62	74.90	39.32	1.59	0.61
07CP30-5	91.71	77.66	36.91	1.15	0.58
07CP30-6	99.46	79.35	38.31	1.30	0.59
07CP31-1	99.98	69.67	34.76	1.01	0.57
07CP31-2	98.09	66.02	33.20	0.89	0.55
07CP31-3	94.84	65.31	32.68	0.84	0.55
07CP31-4	80.86	78.17	35.79	1.02	0.58
07CP31-5	83.87	69.79	33.32	0.85	0.55
07CP31-6	122.99	67.81	35.56	1.17	0.58
07CP32-1	110.92	60.06	31.60	0.83	0.54
07CP32-2	96.14	75.55	36.61	1.14	0.58
07CP32-3	95.41	59.69	30.51	0.70	0.52
07CP32-4	83.25	66.30	32.02	0.76	0.54

Appendix C cont.

Sample	Length (µm)	Width (µm)	Equivalent sphere radius (µm)	Mass (µg)	Ft correction
Book Cliffs, Blaze Canyon Vertical Transect cont.					
07CP32-5	110.56	62.88	32.77	0.91	0.54
07CP32-6	89.53	67.69	33.12	0.85	0.55
Book Cliffs, Tusher Canyon					
07CP63-1	101.81	59.39	30.80	0.74	0.52
07CP63-2	101.16	56.80	29.68	0.68	0.51
07CP63-3	82.81	63.39	30.92	0.69	0.52
07CP63-4	70.27	63.82	29.75	0.59	0.50
07CP63-5	98.39	60.85	31.17	0.75	0.52
07CP63-6	73.48	56.48	27.52	0.49	0.47
07CP65-1	139.09	72.38	38.37	1.51	0.60
07CP65-2	121.90	76.78	39.18	1.49	0.61
07CP65-3	117.82	74.80	38.11	1.37	0.60
07CP65-4	111.91	75.72	38.04	1.33	0.60
07CP65-5	147.86	72.77	38.96	1.62	0.61
07CP65-6	87.68	65.51	32.15	0.78	0.54
Between Book Cliffs and Canyonlands					
07CP40-1	107.78	59.64	31.25	0.79	0.53
07CP40-2	146.78	105.79	52.37	3.40	0.71
07CP40-3	104.52	85.75	41.10	1.59	0.62
07CP40-4	162.36	77.96	41.92	2.04	0.63
07CP40-5	143.85	104.46	51.62	3.25	0.69
07CP40-6	96.35	80.60	38.43	1.30	0.63
07CP42-1	147.00	104.67	51.96	3.34	0.69
07CP42-2	135.78	92.21	46.28	2.39	0.66
07CP42-3	178.39	84.61	45.59	2.65	0.65
07CP42-4	165.60	84.49	44.95	2.45	0.65
07CP42-5	105.78	76.91	37.99	1.30	0.59
07CP42-6	92.07	65.54	32.54	0.82	0.54
07CP48-1	97.01	65.12	32.77	0.85	0.55
07CP48-2	111.59	67.50	34.74	1.05	0.56
07CP48-3	114.65	55.32	29.72	0.73	0.51
07CP48-4	76.01	60.98	29.40	0.59	0.51
07CP48-5	80.37	60.76	29.73	0.61	0.52
07CP48-6	95.60	59.53	30.45	0.70	0.54
07CP51-1	93.21	64.27	32.15	0.80	0.54
07CP51-2	86.90	60.58	30.22	0.66	0.51
07CP51-3	118.44	87.23	42.96	1.87	0.63

Appendix C cont.

Sample	Length (µm)	Width (µm)	Equivalent sphere radius (µm)	Mass (µg)	Ft correction
Between Book Cliffs and Canyonlands					
07CP51-4	108.93	85.04	41.28	1.63	0.60
07CP51-5	111.78	80.56	39.88	1.50	0.61
07CP51-6	97.53	72.03	35.45	1.05	0.57
Canyonlands Vertical Transect, Shafer Trail					
07CP53-1	129.33	69.75	36.73	1.30	0.59
07CP53-2	121.56	63.90	33.81	1.03	0.56
07CP53-3	121.48	76.37	38.99	1.47	0.62
07CP53-4	122.41	63.94	33.87	1.04	0.57
07CP53-5	109.19	73.92	37.13	1.24	0.59
07CP53-6	100.04	55.03	28.87	0.63	0.49
07CP54-1	80.98	63.60	30.83	0.68	0.52
07CP54-2	69.21	63.65	29.57	0.58	0.51
07CP54-3	72.35	69.11	31.75	0.72	0.54
07CP54-4	81.24	64.95	31.34	0.71	0.53
07CP54-5	122.27	58.04	31.27	0.85	0.54
07CP54-6	125.02	60.01	32.27	0.93	0.55
07CP55a-1	144.52	63.74	34.76	1.22	0.59
07CP55a-2	138.60	71.12	37.80	1.45	0.59
07CP55a-3	132.14	65.15	34.87	1.16	0.57
07CP55a-4	129.90	93.58	46.33	2.36	0.68
07CP55a-5	110.44	65.43	33.82	0.98	0.56
07CP55a-6	132.78	72.63	38.14	1.45	0.60
07CP56-1†	152.52	72.59	57.19	1.67	0.62
	159.19	74.68	59.12	1.84	
	150.57	83.63	62.58	2.18	
	141.92	67.10	52.98	1.32	
	160.06	70.34	56.91	1.64	
	150.09	76.23	58.77	1.81	
07CP56-2†	141.45	83.86	61.40	2.06	0.69
	126.46	96.30	64.86	2.43	
	153.77	109.77	75.55	3.84	
	167.62	99.03	72.59	3.41	
	156.64	97.24	70.11	3.07	
	162.00	94.52	69.58	3.00	
07CP56-3†	127.46	101.53	67.37	2.72	0.68
	126.35	89.12	61.58	2.08	
	164.35	95.89	70.58	3.13	
	128.82	100.80	67.28	2.71	

Appendix C cont.

Sample	Length (µm)	Width (µm)	Equivalent sphere radius (µm)	Mass (µg)	Ft correction
Canyonlands Vertical Transect, Shafer Trail cont.					
07CP56-3†	121.22	89.12	60.74	1.99	
	129.35	112.65	72.56	3.40	
07CP57a-1	102.84	60.54	31.33	0.78	0.52
07CP57a-2	76.90	62.80	30.13	0.63	0.51
07CP57a-3	83.36	60.35	29.84	0.63	0.51
07CP57a-4	104.91	62.19	32.14	0.84	0.54
07CP57a-5	95.88	66.66	33.28	0.88	0.56
07CP57a-6	90.27	69.62	33.90	0.91	0.58
07CP58-1	82.80	59.18	29.35	0.60	0.50
07CP58-2	60.43	57.67	26.50	0.42	0.48
07CP58-3	87.30	64.77	31.84	0.76	0.54
07CP58-4	85.09	56.17	28.37	0.56	0.48
07CP58-5	70.21	51.64	25.44	0.39	0.44
07CP58-6	75.76	54.54	27.01	0.47	0.47
07CP59a-1	85.44	63.80	31.31	0.72	0.54
07CP59a-2	99.39	62.47	31.89	0.80	0.53
07CP59a-3	80.32	69.67	32.90	0.81	0.56
07CP59a-4	83.28	70.58	33.54	0.86	0.56
07CP59a-5	74.25	62.12	29.62	0.59	0.50
07CP59a-6	90.54	66.05	32.60	0.82	0.54
07CP60a-1	112.08	60.58	31.89	0.85	0.53
07CP60a-2	92.93	65.53	32.61	0.83	0.54
07CP60a-3	76.33	61.87	29.75	0.61	0.50
07CP60a-4	99.05	55.89	29.17	0.64	0.50
07CP60a-5	74.00	65.00	30.59	0.65	0.53
07CP60a-6	91.54	63.48	31.71	0.76	0.54
07CP61-1	177.27	77.53	42.34	2.21	0.64
07CP61-2	156.39	97.83	50.00	3.10	0.69
07CP61-3	102.51	77.32	37.86	1.27	0.60
07CP61-4	108.34	100.92	46.71	2.29	0.68
07CP61-5	132.10	99.62	48.78	2.72	0.68
07CP61-6	143.41	75.61	39.98	1.70	0.62
07CP62a-1	100.01	67.03	33.74	0.93	0.55
07CP62a-2	72.43	57.33	27.73	0.49	0.47
07CP62a-3	77.31	75.19	34.36	0.91	0.57
07CP62a-4	82.08	59.78	29.52	0.61	0.52

Appendix C cont.

Sample	Length (µm)	Width (µm)	Equivalent sphere radius (µm)	Mass (µg)	Ft correction
Canyonlands Vertical Transect, Shafer Trail cont.					
07CP62a-5	73.74	68.43	31.71	0.72	0.53
07CP62a-6	79.44	63.46	30.63	0.66	0.52
Canyonlands Vertical Transect, Lathrop Canyon					
08CP69-1	174.00	73.21	40.22	1.93	0.64
08CP69-2	109.04	83.33	40.67	1.57	0.62
08CP69-3	105.64	74.81	37.19	1.22	0.61
08CP69-4	112.09	82.07	40.47	1.56	0.64
08CP69-5	127.94	81.02	41.30	1.74	0.65
08CP69-6	126.71	66.50	35.19	1.16	0.59
08CP70-1	103.30	58.72	30.61	0.74	0.52
08CP70-2	105.05	60.13	31.30	0.79	0.53
08CP70-3	91.22	60.90	30.69	0.70	0.51
08CP70-4	101.04	61.31	31.54	0.79	0.53
08CP70-5	91.79	66.74	32.97	0.85	0.55
08CP70-6	74.11	61.02	29.22	0.57	0.52
08CP71-1	172.32	93.47	49.16	3.12	0.68
08CP71-2	112.90	92.76	44.44	2.01	0.65
08CP71-3	130.23	68.98	36.44	1.28	0.59
08CP71-4	133.11	65.19	34.93	1.17	0.59
08CP71-5	102.13	70.30	35.18	1.05	0.57
08CP71-6	104.04	75.02	37.13	1.21	0.59
Canyonlands, North of confluence					
08CP66-1	93.51	78.43	37.37	1.19	0.59
08CP66-2	148.49	81.75	42.88	2.06	0.65
08CP66-3	89.84	69.63	33.86	0.90	0.56
08CP66-4	112.59	69.15	35.48	1.12	0.58
08CP66-5	93.81	64.94	32.45	0.82	0.55
08CP66-6	101.90	90.77	42.55	1.74	0.65
08CP72-1	70.61	58.11	27.83	0.49	0.50
08CP72-2	99.93	65.55	33.16	0.89	0.57
08CP72-3	95.59	55.26	28.71	0.60	0.49
08CP72-4	118.21	55.86	30.12	0.76	0.51
08CP72-5	109.11	57.06	30.22	0.74	0.54
08CP72-6	74.52	67.93	31.63	0.71	0.53

Appendix C cont.

Sample	Length (µm)	Width (µm)	Equivalent sphere radius (µm)	Mass (µg)	Ft correction
Uinta Basin cores					
FMF-6351-1	116.0	88.9	43.3	1.9	0.64
FMF-6351-2	119.5	58.3	31.3	0.8	0.52
FMF-6351-3	128.0	67.2	35.6	1.2	0.58
FMF-6351-4	156.8	81.7	43.3	2.2	0.64
FMF-6351-5	136.5	73.6	38.8	1.5	0.60
FMF-6351-6	144.8	68.3	36.9	1.4	0.59
FMF-6480-1	99.7	77.7	37.7	1.2	0.59
FMF-6480-2	118.2	63.1	33.3	1.0	0.55
FMF-6480-3	93.1	67.6	33.4	0.9	0.55
FMF-6480-4	123.4	69.2	36.2	1.2	0.57
FMF-6480-5	97.0	65.6	33.0	0.9	0.57
FMF-6480-6	102.9	60.5	31.3	0.8	0.55
FMF-6686-1	78.5	56.6	28.0	0.5	0.47
FMF-6686-2	115.6	66.1	34.4	1.0	0.56
FMF-6686-3	131.0	58.0	31.6	0.9	0.53
FMF-6686-4	126.6	61.9	33.2	1.0	0.54
FMF-6686-5	98.3	73.8	36.2	1.1	0.58
FMF-6686-6	139.1	67.5	36.2	1.3	0.59
FMF-7289-1	165.5	83.3	44.4	2.4	0.65
FMF-7289-2	135.4	89.7	45.3	2.3	0.65
FMF-7289-3	128.4	79.5	40.7	1.7	0.62
FMF-7289-4	125.4	96.3	46.9	2.4	0.66
FMF-7289-5	139.3	98.3	48.9	2.8	0.68
FMF-7289-6	142.0	80.3	41.9	1.9	0.63
NB-4412-1†	155.5	94.2	68.5	2.9	0.67
	145.8	85.0	62.6	2.2	
	154.7	89.0	65.8	2.5	
	120.1	95.8	63.5	2.3	
	171.1	92.8	70.0	3.1	
	141.7	93.9	66.3	2.6	
NB-4412-2†	189.7	101.8	77.1	4.1	0.67
	184.5	82.6	66.4	2.6	
	208.2	99.2	78.1	4.2	
	189.7	80.1	65.6	2.5	
	153.4	85.7	64.0	2.3	
	215.1	85.9	71.8	3.3	
NB-4412-3†	143.5	91.3	65.3	2.5	0.66
	163.9	93.2	69.2	2.9	
	141.3	85.3	62.1	2.1	

Appendix C cont.

Sample	Length (µm)	Width (µm)	Equivalent sphere radius (µm)	Mass (µg)	Ft correction
Uinta Basin cores cont.					
NB-4412-3†	150.8	82.6	62.1	2.1	
	166.5	90.2	68.1	2.8	
	136.3	74.3	55.9	1.6	
NB-7468-1	131.5	76.2	39.6	1.6	0.61
NB-7468-2	107.4	85.3	41.2	1.6	0.62
NB-7468-3	97.9	71.6	35.3	1.0	0.57
NB-7468-4	104.1	72.2	36.1	1.1	0.58
NB-7468-5	77.0	72.9	33.6	0.8	0.55
NB-7468-6	112.3	78.1	39.0	1.4	0.60
NB-8542-1	127.9	88.1	44.1	2.1	0.65
NB-8542-2	116.2	68.1	35.3	1.1	0.58
NB-8542-3	142.2	86.1	44.3	2.2	0.65
NB-8542-4	95.3	63.7	32.1	0.8	0.54
TS-8799-1	123.6	67.1	35.3	1.2	0.56
TS-8799-2	122.9	77.7	39.6	1.5	0.63
TS-8799-3	124.7	70.1	36.6	1.3	0.57
TS-8799-4	128.5	70.4	37.0	1.3	0.58
TS-8799-5	123.0	73.0	37.7	1.4	0.59
TS-8799-6	104.7	84.8	40.8	1.6	0.63
SO-4695-1	105.1	68.8	34.8	1.0	0.56
SO-4695-2	115.9	69.6	35.9	1.2	0.58
SO-4695-3	154.0	89.8	46.6	2.6	0.66
Book Cliffs cores					
2BC-67-1	107.8	88.3	42.3	1.7	0.63
2BC-67-2	114.0	75.6	38.1	1.3	0.60
2BC-67-3	181.8	83.4	45.2	2.6	0.65
2BC-67-4	140.6	70.7	37.7	1.5	0.59
2BC-67-5	108.1	74.6	37.3	1.2	0.60
2BC-67-6	85.9	65.2	31.9	0.8	0.53
2BC-181-1	124.8	73.6	38.1	1.4	0.60
2BC-181-2	133.7	75.9	39.6	1.6	0.61
2BC-181-3	123.3	67.9	35.6	1.2	0.57
2BC-181-4	91.6	74.7	35.9	1.1	0.58
2BC-181-5	110.6	76.7	38.3	1.3	0.60
2BC-181-6	135.2	69.1	36.8	1.3	0.59

Appendix C cont.

Sample	Length (µm)	Width (µm)	Equivalent sphere radius (µm)	Mass (µg)	Ft correction
Book Cliffs cores cont.					
2BC-248-1	134.9	85.6	43.6	2.0	0.65
2BC-248-2	111.2	71.3	36.3	1.2	0.58
2BC-248-3	122.0	67.2	35.2	1.1	0.57
2BC-248-4	156.9	65.8	36.2	1.4	0.58
2BC-248-5	106.8	66.1	33.8	1.0	0.56
2BC-248-6	160.1	83.6	44.3	2.3	0.65
2BC-305-1	92.3	61.4	31.0	0.7	0.52
2BC-305-2	96.3	60.0	30.7	0.7	0.51
2BC-305-3	91.0	60.7	30.6	0.7	0.51
2BC-305-4	81.6	61.2	30.0	0.6	0.50
2BC-305-5	81.1	64.1	31.0	0.7	0.51
2BC-305-6	78.8	58.7	28.8	0.6	0.49
2BC-469-1	97.4	58.3	30.1	0.7	0.52
2BC-469-2	79.9	57.7	28.6	0.6	0.51
2BC-469-3	76.6	59.6	29.0	0.6	0.50
2BC-469-4	120.8	80.4	40.5	1.6	0.62
2BC-469-5	131.0	61.6	33.2	1.0	0.55
2BC-469-6	102.1	64.7	33.0	0.9	0.54
2BC-591-1†	140.0	74.8	56.7	1.6	0.61
	168.4	80.0	63.1	2.2	
	184.3	82.3	66.2	2.6	
	132.6	68.9	52.7	1.3	
	109.7	62.4	46.3	0.9	
	121.5	74.2	53.8	1.4	
2BC-591-2†	140.0	80.5	59.5	1.9	0.65
	117.8	90.6	60.8	2.0	
	141.0	100.3	69.1	2.9	
	125.2	85.1	59.5	1.9	
	143.5	88.5	64.0	2.3	
	125.9	87.3	60.7	2.0	
2BC-591-3†	107.9	67.6	48.6	1.0	0.58
	99.3	73.4	49.9	1.1	
	105.8	70.2	49.5	1.1	
	114.9	78.7	54.9	1.5	
	106.5	65.9	47.6	1.0	
	123.4	71.5	52.8	1.3	
2BC-675-1	71.9	69.2	31.7	0.7	0.53
2BC-675-2	123.7	62.4	33.3	1.0	0.55
2BC-675-3	94.8	62.4	31.5	0.8	0.53

Appendix C cont.

Sample	Length (µm)	Width (µm)	Equivalent sphere radius (µm)	Mass (µg)	Ft correction
Book Cliffs cores cont.					
2BC-675-4	85.2	66.9	32.4	0.8	0.54
2BC-675-5	79.0	63.0	30.4	0.6	0.51
2BC-675-6	165.6	58.3	32.8	1.2	0.55
3BC-120-1	87.2	73.4	34.9	1.0	0.57
3BC-120-2	108.8	62.5	32.5	0.9	0.55
3BC-120-3	79.8	64.3	31.0	0.7	0.53
3BC-120-4	83.8	64.2	31.3	0.7	0.53
3BC-120-5	96.9	61.4	31.3	0.8	0.56
3BC-120-6	102.8	71.0	35.5	1.1	0.58
4BC-187-1	126.4	72.1	37.5	1.4	0.59
4BC-187-2	124.8	90.4	44.7	2.1	0.65
4BC-187-3	155.0	85.5	44.8	2.3	0.65
4BC-187-4	142.0	79.6	41.6	1.9	0.63
4BC-187-5	152.2	86.0	44.9	2.3	0.66
4BC-187-6	174.3	93.1	49.1	3.1	0.68
4BC-340-1	97.4	54.7	28.6	0.6	0.48
4BC-340-2	73.2	56.8	27.6	0.5	0.47
4BC-340-3	70.8	55.8	27.0	0.5	0.46
4BC-340-4	90.6	56.7	29.0	0.6	0.49
4BC-340-6	80.9	59.0	29.1	0.6	0.51
4BC-477-1	104.3	61.0	31.6	0.8	0.54
4BC-477-3	128.6	64.9	34.6	1.1	0.57
4BC-477-4	135.0	78.3	40.6	1.7	0.62
4BC-477-5	114.9	73.6	37.4	1.3	0.59
4BC-477-6	110.7	76.4	38.2	1.3	0.60
5BC-306-1	169.3	103.0	53.0	3.7	0.70
5BC-306-2	125.9	82.1	41.6	1.8	0.63
5BC-306-3	152.0	102.5	51.5	3.3	0.69
5BC-306-4	122.7	79.6	40.4	1.6	0.62
5BC-306-5	134.0	77.2	40.1	1.7	0.61
5BC-306-6	152.5	93.0	47.8	2.7	0.67
5BC-474-1	143.9	78.3	59.0	1.8	0.63
5BC-474-2	125.3	95.3	64.2	2.4	0.67
5BC-474-3	146.5	75.2	57.8	1.7	0.62
5BC-474-4	124.5	89.7	61.6	2.1	0.65
5BC-474-5	137.6	99.2	68.0	2.8	0.68
5BC-474-6	163.8	108.5	76.6	4.0	0.71

Appendix C cont.

Sample	Length (µm)	Width (µm)	Equivalent sphere radius (µm)	Mass (µg)	Ft correction
Book Cliffs cores cont.					
GC1-54-1	128.4	90.2	44.9	2.2	0.65
GC1-54-2	135.9	91.9	46.2	2.4	0.66
GC1-54-3	119.7	79.6	40.1	1.6	0.62
GC1-54-4	114.6	78.1	39.2	1.4	0.61
GC1-54-5	114.0	75.6	38.1	1.3	0.61
GC1-54-6	118.0	69.2	35.8	1.2	0.58
GC1-153-1	167.2	75.6	41.1	2.0	0.63
GC1-153-2	121.9	71.3	37.0	1.3	0.58
GC1-153-3	150.5	89.9	46.4	2.5	0.66
GC1-153-4	117.9	87.1	42.9	1.9	0.64
GC1-153-5	119.1	86.1	42.6	1.8	0.63
GC1-153-6	94.6	73.2	35.6	1.1	0.57
GC1-288-1	110.6	67.1	34.5	1.0	0.56
GC1-288-2	106.2	80.5	39.3	1.4	0.61
GC1-288-3	150.5	69.0	37.4	1.5	0.59
GC1-288-4	88.2	57.3	29.0	0.6	0.49
GC1-288-5	109.8	73.3	36.9	1.2	0.59
GC1-288-6	85.7	58.8	29.4	0.6	0.50
GC1-445-1	91.8	75.6	36.2	1.1	0.58
GC1-445-2	119.2	88.7	43.6	1.9	0.65
GC1-445-3	110.2	80.1	39.6	1.5	0.61
GC1-445-4	119.6	62.5	33.1	1.0	0.56
GC1-445-5	150.2	77.1	41.0	1.9	0.62
GC1-445-6	118.1	63.1	33.3	1.0	0.55
GC1-609-1	104.4	63.8	32.7	0.9	0.54
GC1-609-2	96.5	59.5	30.5	0.7	0.52
GC1-609-3	105.8	58.2	30.5	0.7	0.51
GC1-609-4	104.3	66.6	33.9	1.0	0.55
GC1-609-5	106.0	66.9	34.1	1.0	0.56
GC1-609-6	109.5	70.2	35.7	1.1	0.58
GC1-749-1	127.7	66.8	35.4	1.2	0.57
GC1-749-2	112.5	65.5	34.0	1.0	0.56
GC1-749-3	115.4	65.0	33.9	1.0	0.55
GC1-749-4	109.4	57.5	30.4	0.7	0.51
GC1-749-5	77.3	56.5	27.9	0.5	0.47
GC1-749-6	88.6	71.8	34.5	0.9	0.56

Appendix C cont.

Sample	Length (µm)	Width (µm)	Equivalent sphere radius (µm)	Mass (µg)	Ft correction
Book Cliffs cores cont.					
GC1-1006-1	95.0	80.6	38.3	1.3	0.60
GC1-1006-2	99.3	69.5	34.6	1.0	0.58
GC1-1006-3	121.3	60.5	32.3	0.9	0.54
GC1-1006-4	92.9	58.4	29.8	0.7	0.51
GC1-1006-5	87.1	61.2	30.5	0.7	0.51
GC1-1006-6	114.0	62.1	32.6	0.9	0.54
3FED335-1	109.4	57.8	30.6	0.8	0.54
3FED335-2	85.6	80.3	37.1	1.1	0.60
3FED335-3	110.1	72.7	36.7	1.2	0.58
1AFED258-1†	140.0	98.3	68.0	2.8	0.69
	150.2	102.5	71.6	3.3	
	179.8	99.4	74.5	3.7	
	164.8	92.9	69.2	2.9	
	220.7	106.6	83.5	5.2	
	173.6	87.8	67.8	2.8	
1AFED258-2†	144.8	95.1	67.3	2.7	0.73
	159.3	120.5	81.3	4.8	
	157.6	106.7	74.8	3.7	
	177.9	136.4	91.7	6.9	
	217.7	119.6	89.8	6.5	
	172.8	114.9	81.0	4.7	
1AFED258-3†	124.3	78.0	56.0	1.6	0.63
	142.0	87.0	63.0	2.2	
	138.8	79.1	58.7	1.8	
	127.6	102.3	67.7	2.8	
	126.2	70.0	52.4	1.3	
	123.1	80.8	57.2	1.7	
PH-4669-1	104.5	67.8	34.4	1.0	0.56
PH-4669-2	93.2	62.4	31.4	0.8	0.53
PH-4669-3	79.5	69.8	32.9	0.8	0.54
PH-4669-4	86.3	68.5	33.1	0.8	0.55
PH-4669-5	87.1	62.2	30.9	0.7	0.52
RGU1-1751-1	93.6	58.7	30.0	0.7	0.51
RGU1-1751-2	91.6	58.0	29.6	0.6	0.50
RGU1-1751-3	94.8	55.3	28.7	0.6	0.48
RGU1-1751-4	104.5	62.3	32.1	0.8	0.53
RGU1-1751-5	100.2	63.1	32.2	0.8	0.54
RGU1-1751-6	76.7	60.9	29.4	0.6	0.49

Appendix C cont.

Sample	Length (µm)	Width (µm)	Equivalent sphere radius (µm)	Mass (µg)	Ft correction
Book Cliffs cores cont.					
Ppt-2499-1	104.0	66.0	33.6	0.9	0.55
Ppt-2499-2	118.9	67.1	35.0	1.1	0.58
Ppt-2499-3	113.1	70.1	35.9	1.2	0.58
Ppt-2499-4	125.1	74.1	38.3	1.4	0.61
Ppt-2499-5	103.0	66.6	33.8	0.9	0.57
Ppt-2499-6	101.8	68.8	34.6	1.0	0.57
Canyonlands cores					
LLE-2656-1	107.9	61.9	32.2	0.9	0.54
LLE-2656-2	72.6	61.2	29.1	0.6	0.51
LLE-2656-3	130.9	56.9	31.1	0.9	0.52
LLE-2656-4	70.3	66.4	30.6	0.6	0.52
LLE-2797-1†	128.0	77.4	56.3	1.6	0.60
	117.7	79.7	55.8	1.5	
	111.2	63.6	47.1	0.9	
	107.5	83.0	55.6	1.5	
	127.7	65.7	50.4	1.1	
LLE-2797-3†	128.9	90.7	62.7	2.2	0.68
	110.7	86.1	57.6	1.7	
	143.2	88.6	64.0	2.3	
	150.6	100.4	70.7	3.1	
	153.4	104.8	73.2	3.5	
	147.9	91.6	66.1	2.6	
SM-3032-1	101.4	75.9	37.2	1.2	0.59
SM-3032-2	92.6	59.2	30.1	0.7	0.53
SM-3032-3	87.6	56.2	28.6	0.6	0.50
SM-3032-4	98.2	55.8	29.1	0.6	0.50
SM-3032-5	79.7	60.2	29.5	0.6	0.50
SM-3032-6	61.6	53.7	25.3	0.4	0.43
Monument Uplift cores					
DC-212-1	114.4	71.3	36.5	1.2	0.60
DC-212-2	114.6	61.4	32.4	0.9	0.54
DC-212-3	137.9	78.2	40.8	1.7	0.62
DC-212-4	99.8	71.2	35.3	1.0	0.57
DC-282-1	136.2	67.5	36.1	1.3	0.59
DC-282-2	88.6	64.0	31.6	0.8	0.53
DC-282-3	116.6	62.0	32.7	0.9	0.54
DC-282-4	110.0	79.8	39.4	1.5	0.61

Appendix C cont.

Sample	Length (µm)	Width (µm)	Equivalent sphere radius (µm)	Mass (µg)	Ft correction
Monument Uplift cores cont.					
DC-282-5	117.0	87.5	42.9	1.9	0.64
DC-282-6	150.0	76.1	40.5	1.8	0.62
DC-430-1	212.7	110.1	58.4	5.3	0.74
DC-430-2	157.6	98.1	50.2	3.1	0.69
DC-430-3	217.5	97.0	52.8	4.2	0.71
DC-430-4	229.3	82.3	46.3	3.2	0.68
DC-655-1	157.5	95.2	49.0	3.0	0.68
DC-655-2	169.4	94.5	49.4	3.1	0.71
DC-655-3	124.8	62.0	33.1	1.0	0.55
DC-655-4	129.5	100.2	48.7	2.7	0.69
DC-655-5	108.5	67.6	34.6	1.0	0.58
DC-655-6	141.8	63.3	34.4	1.2	0.56
DC-1896-1	153.0	111.6	55.1	4.0	0.71
DC-1896-2	150.4	63.9	35.1	1.3	0.57
DC-1896-3	71.4	65.4	30.4	0.6	0.52
DC-2006-1	143.7	94.2	47.6	2.6	0.67
DC-2006-2	109.1	100.8	46.8	2.3	0.67
DC-2006-3	138.8	76.5	40.1	1.7	0.62
DC-2006-4	227.8	102.4	55.7	5.0	0.73
DC-2006-5	111.5	70.1	35.8	1.1	0.59
DC-2006-6	141.6	101.5	50.3	3.0	0.69

† Multigrain aliquots with inclusions

APPENDIX D

Photographs of core samples collected from the USGS Core Research Center. Photographs show core before approximately 30% was sliced off and collected. Photographs were not available for cores collected from collaborators on this project.

Core sample FMF-6351

Core sample FMF-6480

Core sample FMF-6686

Core sample FMF-7289

Core sample NB-4412

Core sample NB-7468

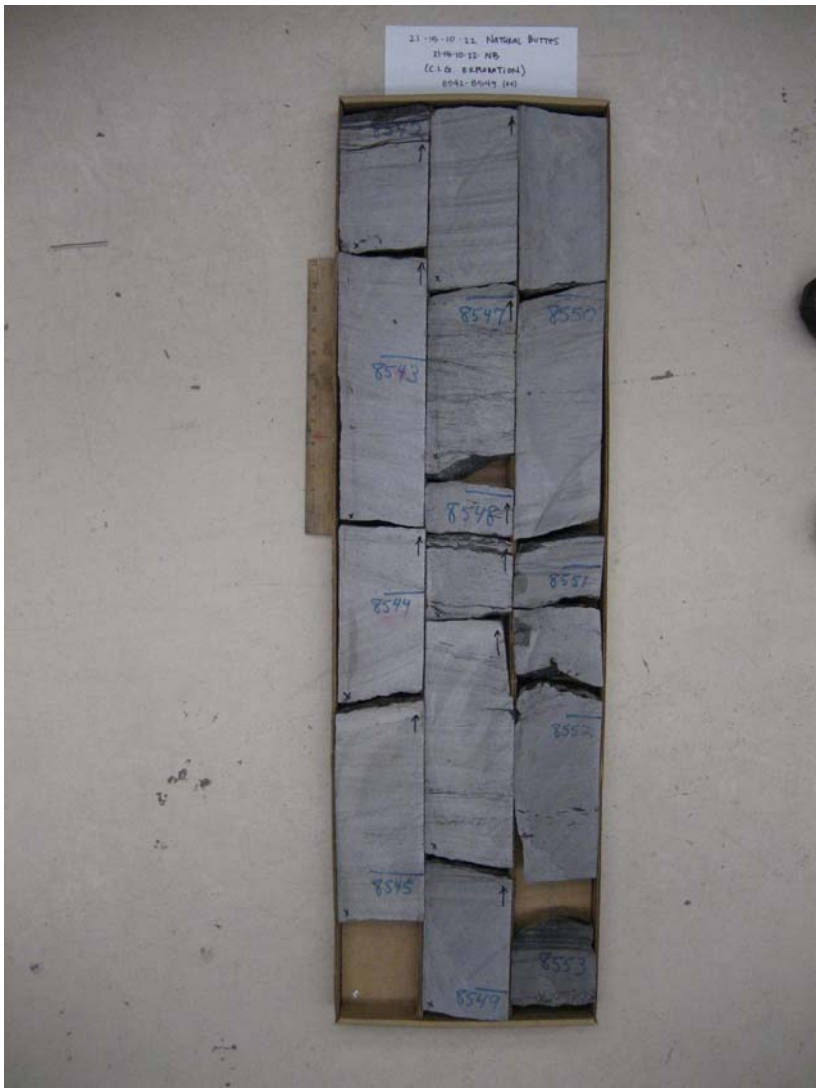

Core sample NB-8542

Core sample TS-8799

Core sample 2BC-67

Core sample 2BC-181

Core sample 2BC-248

Core sample 2BC-305

Core sample 2BC-469

Core sample 2BC-591

Core sample 2BC-675

Core sample 3BC-120

Core sample 4BC-187

Core sample 4BC-340

Core sample 4BC-477

Core sample 5BC-306

Core sample 5BC-474

Core sample GC-1-54

Core sample GC-1-153

Core sample GC-1-288

Core sample GC-1-445

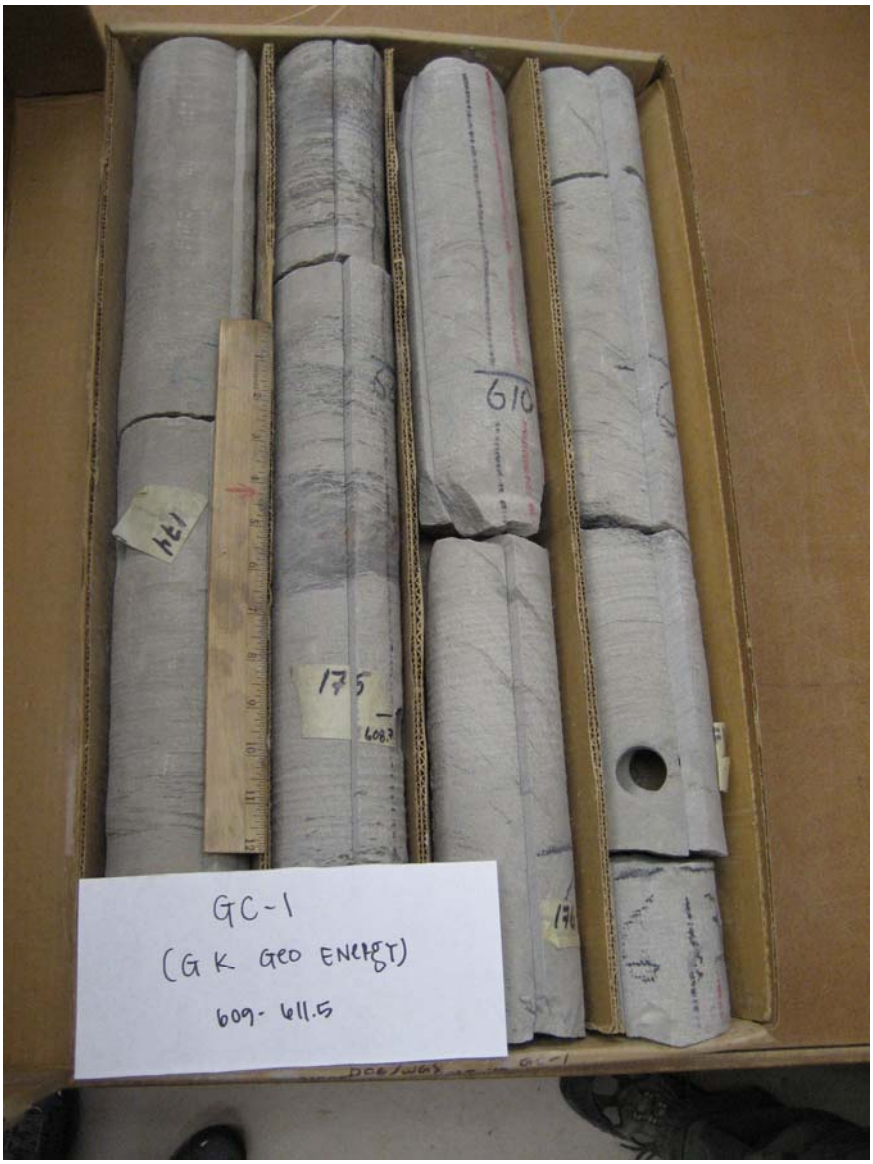

Core sample GC-1-609

Core sample GC-1-749

Core sample GC-1-1006

Core sample 3FED335

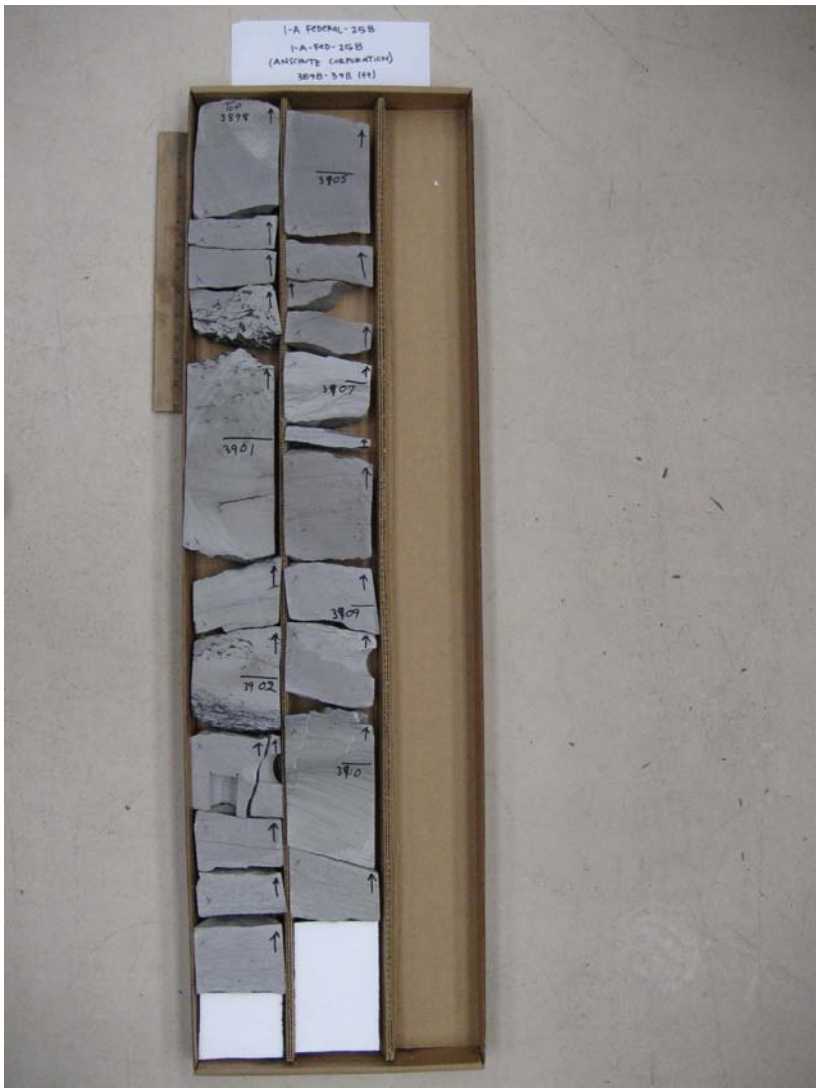

Core sample 1AFED258

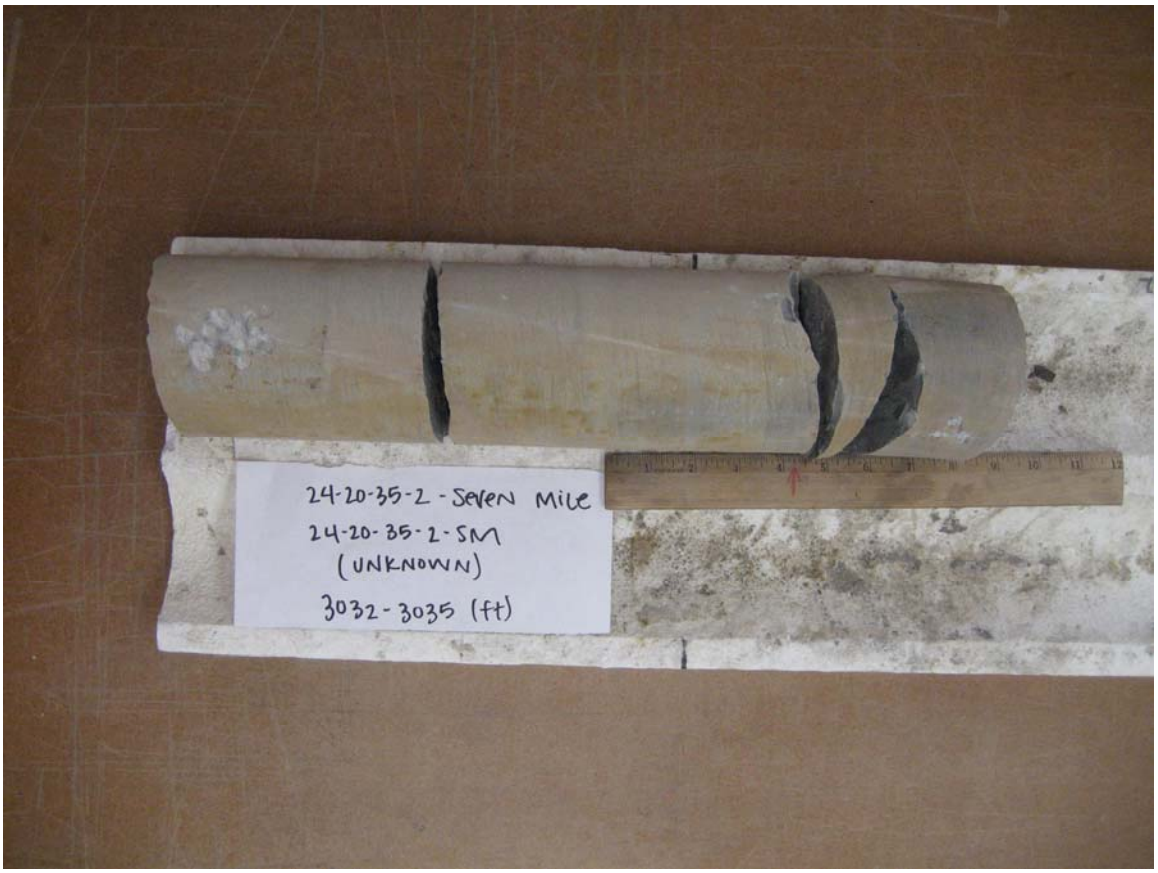

Core sample SM-3032